Delft University of Technology

Citation (APA)
Madzarevic, Z. (2017). *Tailoring the free volume of all-aromatic polyimide membranes for CO2/CH4 gas separation*. [Dissertation (TU Delft), Delft University of Technology]. https://doi.org/10.4233/uuid:a2289118-0909-49be-8071-ea062bf26adc

Important note
To cite this publication, please use the final published version (if applicable).
Please check the document version above.

Copyright
In case the licence states "Dutch Copyright Act (Article 25fa)", this publication was made available Green Open Access via the TU Delft Institutional Repository pursuant to Dutch Copyright Act (Article 25fa, the Taverne amendment). This provision does not affect copyright ownership.
Unless copyright is transferred by contract or statute, it remains with the copyright holder.

Sharing and reuse
Other than for strictly personal use, it is not permitted to download, forward or distribute the text or part of it, without the consent of the author(s) and/or copyright holder(s), unless the work is under an open content license such as Creative Commons.

Takedown policy
Please contact us and provide details if you believe this document breaches copyrights.
We will remove access to the work immediately and investigate your claim.

This work is downloaded from Delft University of Technology.

Tailoring the free volume of all-aromatic polyimide membranes for CO_2/CH_4 gas separation

Proefschrift

ter verkrijging van de graad van doctor
aan de Technische Universiteit Delft,
op gezag van de Rector Magnificus prof.ir. K. C. A. M. Luyben,
voorzitter van het College voor Promoties,
in het openbaar te verdedigen op
17 november 2017 om 10 uur
door

Željka MADŽAREVIĆ

Master of Science in Chemical Engineering
University of Belgrade, Serbia
geboren te Belgrado, Servië

This thesis has been approved by the promotor:

Prof.dr. T. J. Dingemans

Composition of the doctoral committee:

Rector Magnificus	chairman
Prof.dr. T. J. Dingemans	Delft University of Technology, promotor
Independent members:	
Prof.dr. S. J. Picken	Delft University of Technology
Prof.dr.ir. S. van der Zwaag	Delft University of Technology
Prof.dr. B. D. Freeman	The University of Texas at Austin, USA
Prof.dr.ir. I. Vankelecom	Katholieke Universiteit Leuven, Belgium
Prof.dr. A. P. H. J. Schenning	Eindhoven University of Technology
Prof.dr. F. M. Mulder	Delft University of Technology, reserve
Other members:	
Prof.dr.ir. N. E. Benes	University of Twente

The research carried out in this thesis is funded by the Dutch Polymer Institute (DPI), postbus 902, 5600 AX Eindhoven, Project #715.

ISBN: 978-94-6186-854-1

Copyright © 2017 by Željka Madžarević
madzarevic.zeljka@gmail.com

Published by: Gildeprint

All rights reserved. No part of the material protected by this copyright notice may be reproduced or utilized in any from or by any means, electronically or mechanically, including photocopying, recording or by any information storage and retrieval system, without written permission from the author.

An electronic version of this dissertation is available at:
http://repository.tudelft.nl/

Mom Bošku

Contents

Chapter 1: Introduction **1**

1.1 Introduction to membrane technology 2

1.2 Gas transport through dense glassy polymers 3

1.3 Polyimides as membrane materials 6

1.4 Structural backbone modifications 9

1.5 Emerging new generation polymer membranes for CO_2/CH_4 separation 10

1.6 Characterizing free volume in polymer membranes 12

1.7 Scope and outline of the thesis 12

1.8 References 15

Chapter 2: Systematic changes in the backbone structure of a series poly(etherimide)s and the effects on CO_2/CH_4 gas separation performance **19**

2.1 Introduction 20

2.2 Design 22

2.3 Gas permeation 23

2.4 Experimental 24

2.4.1 Materials 24

2.4.2 Characterization 24

2.4.3 Monomer synthesis 26

2.4.4 Polymer synthesis 27

2.4.5 Gas permeation measurements 28

2.5 Results 30

2.5.1 Viscosity and gel permeation chromatography measurements 30

2.5.2 Dynamic thermogravimetric analysis (TGA) 32

2.5.3 Differential scanning calorimetry (DSC) 33

2.5.4 Dynamic mechanical thermal analysis (DMTA) 35

2.5.5 Film morphology, X-ray diffraction (XRD) 37

2.5.6 Gas separation membranes 38

2.6 Conclusions 42

2.7 Appendix: GPC curves 43

2.8 References 44

Chapter 3: Free volume in PEI membranes measured by positron annihilation lifetime spectroscopy (PALS) and positron annihilation Doppler broadening (PADB) 47

3.1 Introduction 48

3.2 Theory behind positron annihilation techniques 49

3.3 Experimental 52

3.3.1 Positron annihilation Doppler broadening (PADB) 52

3.3.2 Positron annihilation lifetime spectroscopy (PALS) 53

3.3.3 Materials 54

3.4 Results 55

3.4.1 Positron annihilation Doppler broadening 55

3.4.2 Positron annihilation lifetime spectroscopy 58

3.5 Conclusions 62

3.6 References 63

Chapter 4: High-pressure sorption of carbon dioxide and methane in all-aromatic polyetherimide membranes 65

4.1 Introduction 66

4.2 Sorption 68

4.3 Ellipsometry 69

4.4 Experimental 70

4.4.1 Materials 70

4.4.2 Spin coating procedure 70
4.4.3 Thermo-ellipsometric analysis 70
4.4.4 *In situ* spectroscopic ellipsometry using a high-pressure cell 71
4.4.5 Spectroscopic ellipsometry data analysis 71
4.5 Results 72
4.5.1 Thermo-ellipsometric analysis 72
4.5.2 High-pressure gas sorption: swelling and isotherms 74
4.5.3 High-pressure gas sorption: sorbed gas molar volume 77
4.5.4 High-pressure gas sorption: gas solubility selectivities 78
4.5.5 High-pressure gas sorption: penetrant-induced relaxations 79
4.6 Conclusions 81
4.7 Appendix: TEA results 83
4.8 References 85
Chapter 5: Oxadiazole-based PI membranes for separating CO_2/CH_4 gas mixtures 87
5.1 Introduction 88
5.2 Polymer design 90
5.3 Gas permeation 92
5.4 Experimental 92
5.4.1 Materials 92
5.4.2 Characterization 93
5.4.3 Monomer synthesis 94
5.4.4 Polymer synthesis 96
5.4.5 Gas permeation measurements 98
5.5 Results 100
5.5.1 Gel permeation chromatography measurements 100
5.5.2 Dynamic thermogravimetric analysis 101

5.5.3 Differential scanning calorimetry (DSC) 102

5.5.4 Dynamic mechanical thermal analysis (DMTA) 104

5.5.5 Film morphology, X-ray diffraction (XRD) 106

5.5.6 Gas separation membranes 107

5.6 Conclusions 111

5.7 Appendix: GPC curves 113

5.8 References 114

Chapter 6: Free volume in oxadiazole-based polyimides measured by positron annihilation Doppler broadening (PADB) 117

6.1 Introduction 118

6.2 Experimental 121

6.2.1 Materials 121

6.2.2 PADB measurements 121

6.3 Results 122

6.4 Conclusions 127

6.5 Appendix: Extrapolation 129

6.6 References 130

Summary 133

Samenvatting 135

Curriculum Vitae 139

Acknowledgements 141

List of publications 145

CHAPTER 1

Introduction

1.1 Introduction to membrane technology

The principles of gas diffusion through polymer films have been known for over a century, nevertheless only in the last 40 years membranes have been used in industrial gas separating processes. This application was launched in 1980 with the success of the first effective gas separating membrane systems built by Monsanto to separate and recover H_2 from the purge gas of their ammonia synthesis plants. Since then this industry has grown exponentially and expanded into different demanding areas.[1–4]

The global demand for cleaner energy sources has resulted in a massive increase in the consumption of natural gas. The worldwide consumption of natural gas is projected to increase from 120 trillion cubic feet in 2012 to 203 trillion cubic feet in 2040.[5] Additionally, methane (main component of natural gas) is a major chemical feedstock used in the chemical industry. As methane-rich sources with little impurities are becoming scarce, the oil and gas industry has begun to exploit methane sources that that contain high concentrations of impurities. These impurities include H_2O and acid gases like CO_2 and H_2S. These acid gases need to be removed in order to increase the fuel heating value, prevent atmospheric pollution with SO_2, decrease the amount of gas for transport by pipelines and reduce corrosion of said pipelines.[6,7]

Methods of conventional natural gas "sweetening" (*i.e.* the removal of acid gases) entail absorption of acid gases in solvents (such as amine or hot potassium scrubbing), they incur significant costs as high amounts of energy are needed for a gas-liquid phase change that these processes require. These high energy costs and environmental impact can be reduced with the use of membrane-based gas separation technology. This technology offers compactness and lacks mechanical complexity. For commercial/economical success, membranes of high productivity need to be developed.

Membranes are selective semipermeable barriers that allow different gases to move across them at different rates (or not at all). Membrane materials used for gas separation are often polymer-based. They can be processed into hollow fibers, providing large contact areas at low manufacturing costs, and these hollow fibers are packed into suitable permeation modules.[3] For natural gas cleaning on offshore platforms this is very attractive as the commonly used amine treatment units are large, heavy and costly. For example natural gas streams are available in pressures ranging from 28 to 83 bar [8] meaning that the

CO_2/CH_4 separating process conditions are harsh and membranes need to be developed to withstand these operating conditions.

Commercialization and the economical value of gas separation membrane processes depends on the development of membranes with sufficient separating ability and productivity. Regardless of designing and assessing thousands of new membrane materials,[9–11] fewer than 10 polymer membranes have dominated the industry for the past four decades.[1]

1.2 Gas transport through dense glassy polymers

Gas diffusion through dense membranes is described by the *solution-diffusion model*, in which permeants dissolve in the membrane material at the feed side, diffuse through the membrane down a pressure gradient and then desorb at the permeate side. This is explained in more detail in Chapter 2. Operating conditions include three steady-state streams. The incoming feed stream is separated into a permeate stream and a retentate stream (Figure 1.1). In CO_2/CH_4 gas separation the permeate stream is CO_2 rich while the retentate stream is CH_4 rich. A pressure difference across the membrane is the driving force for the permeation. A "sweep" gas is often used to help move the permeate.

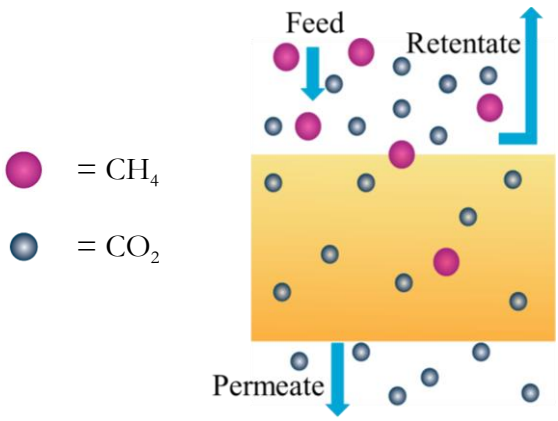

Figure 1.1. A typical membrane system separates the mixed feed stream into the retentate and the permeate streams. In this example CH_4 (●) is separated from CO_2 (●).

A membrane's gas separating ability is described by two characteristic transport properties: permeability and selectivity. These allow membranes to be compared.

Permeability is the flux of molecules through a membrane, *i.e.* the amount of gas permeating the membrane per unit of time and unit of surface area, normalized to the pressure gradient. The equation for permeability is given in Chapter 2, Eq. (2.1), this equation describes the mechanism of permeation in the solution-diffusion model.

The solubility parameter is dependent on the condensability of penetrating gas, which is determined by the critical temperature (T_c) of a gas. The critical temperature is the temperature at which the gas molecules can not be liquefied regardless of the pressure. The gas solubility is higher for gases with higher T_c, with CO_2 being higher than CH_4 (Table 1.1). Also worth noting is the fact that polar gases have higher polymer solubilities.[9]

Table 1.1. General properties of gases CO_2 and CH_4.[12]

Gas	Molecular mass (g/mol)	Kinetic diameter (Å)	T_c (K)
CO_2	44	3.3	304
CH_4	16	3.8	190

On the other hand, the diffusivity parameter is a kinetic parameter predominantly determined by the size and the shape of the penetrant.[13] Smaller and linear molecules can diffuse faster because of their small diameter and ability to diffuse along their smallest dimension.

In CO_2/CH_4 gas separation, CO_2 is more condensable (has a higher T_c) and more mobile (has a smaller kinetic diameter) than CH_4.[11,14] Since both CO_2 solubility and diffusivity are higher than that of CH_4, polymer membranes favor CO_2 permeation over CH_4.

Membrane technology employs a non-SI unit for gas permeability, the Barrer, named after Richard Barrer. Units of permeability "explain" the mechanism.

SI unit:

$$\frac{cm^3(273.15K; 1.013 \times 10^5 Pa) \times cm}{cm^2 \times s \times Pa}$$

1 Barrer, the non-SI unit:

$$\frac{10^{-10}(cm^3 STP) \times cm}{cm^2 \times s \times cmHg}$$

Selectivity for separating one component (CO_2) over another component (CH_4) can be expressed as the ratio of permeabilities of the two pure gas species measured separately. This is called the ideal selectivity and this parameter is most often reported in scientific publications in the field of polymer membrane design. Unfortunately, this does not correlate with conditions encountered in industrial processes where mixed-gas streams are treated. In binary mixtures one gas can influence the permeability of the other, which is the reason why the test results are disappointing when materials with a high ideal selectivity are tested with a CO_2/CH_4 gas mixture. The actual measure of a membrane's ability to separate a mixture of two gases is the selectivity of gas *i* to gas *j*, $\boldsymbol{\alpha_{i/j}}$ (a separating factor obtained from mixed gas experiments), which is explained in more detail later on in Chapter 2 (Eq. (2.3)). Pure-gas measurements should be replaced with appropriate CO_2/CH_4 mixture measurements to partially address this common problem.

Preferably, membranes should have both high permeability and high selectivity. However, in essentially all membranes a **trade-off** relationship is observed. A more permeable membrane is less selective and *vice versa*.[15] This major limitation in membrane design was validated empirically by Robeson[16,17] and modeled by Freeman[18].

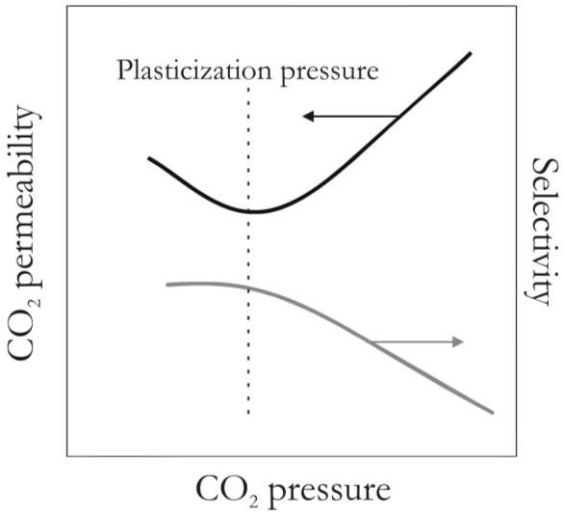

Figure 1.2. CO_2 induced plasticization behavior in polymer membranes.

After exposure to relatively low pressures of condensable gases, such as CO_2, the distance between polymer chains tends to increase. The polymer membrane swells, the permeability of both gas species increases with increasing pressure

and this results in a decreased separating ability *i.e.* low selectivity. This phenomenon results in loss of performance and is called **plasticization** and is schematically presented in Figure 1.2. When a membrane is vulnerable to plasticization, the permeability will reach a minimum as a function of pressure (at a value called plasticization pressure), and then rises sharply with increased pressure.[19] Penetrant induced plasticization is found to be most severe in natural gas separation where condensable gases such as CO_2, H_2O and H_2S are present.[20–22]

Membranes for gas separation offer:

- ✓ high energy efficiency
- ✓ easy scale-up
- ✓ high area to volume ratio
- × permeability-selectivity trade-off
- × plasticization in presence of CO_2.

Most widely used membranes in natural gas processing plants are cellulose acetate. They possess acceptable gas separating properties and processability. Under regular operating conditions these membranes display CO_2/CH_4 selectivity around 12–15.[23] They are notorious for their plasticization susceptibility, limiting the operating conditions to low feed pressures. Fortunately, other polymers, most prominently polyimides and perfluoropolymers, have been developed over the years and are making inroads in a variety of gas separating processes.[24–29]

1.3 Polyimides as membrane materials

Polyimides are rigid glassy polymers that rely on high selectivity coming from high diffusivity selectivity (when the diffusivity coefficient of carbon dioxide, D_{CO2}, is significantly greater than that of methane, D_{CH4}, Chapter 2, Eq. (2.2)).[14] This inherently means the permeability values are low due to the trade-off relationship.

All-aromatic polyimides and poly(etherimide)s are high-performance materials recognized for their high thermal stability, good mechanical properties, in addition it has been demonstrated that they remain relatively stable in the presence of compressed CO_2.[30]

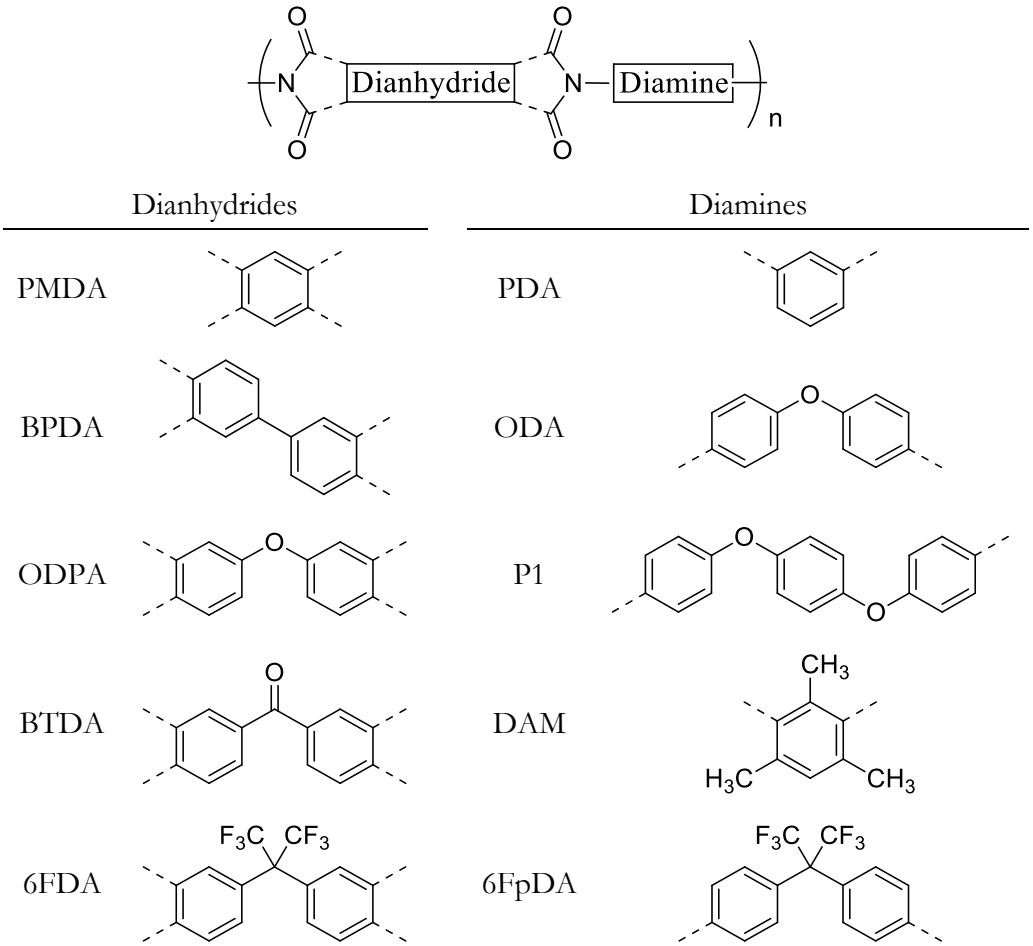

Figure 1.3. General chemical structure of polyimides and poly(etherimide)s with a selection of the most commonly encountered dianhydride and diamine monomers.

Aromatic polyimides are synthesized using a two-step polycondensation route starting from a dianhydride and a diamine. During the first step the diamine is dissolved at room temperature (commonly in a polar aprotic solvent such as N-methyl-2-pyrrolidinone (NMP) or N,N-dimethylacetamide (DMAc)). The dianhydride is then added, which results in the formation of a polyamic acid. In the second step, imidization (cyclodehydration) takes place either by extended heating (*i.e.* thermal imidization) or by chemical dehydration (*i.e.* chemical imidization). The general chemical structure of a polyimide/polyetherimide is shown in Figure 1.3 with a selection of several commonly used dianhydride and

diamine monomers. Polyimides are usually identified by the acronyms of their constituent monomers, first the dianhydride moiety followed by the diamine moiety (*e.g.* ODPA-P1).

Polymer chain rigidity has a significant effect on the selectivity, while chain mobility, inter-chain spacing and free volume (polymer's unoccupied volume, its "elbow room")[31] govern the permeability.[6] Gases can diffuse through non-porous polymers due to the presence of free volume.[32,33]

Starting in 2002, polyimide membranes were used for various gas separation applications by Air Liquide, Praxair and Ube Industries.[23,24] Commercial polyimide membranes such as Upilex®, Ultem® and Matrimid® (Figure 1.4) were included in many studies.[24,34,35] Upilex® (BPDA-ODA) has high thermal resistance (T_g = 285 °C)[24] meaning that it can be used at operating temperatures of up to 100 °C. It also shows low permeability and plasticization in presence of CO_2 above 30 bar.[34]

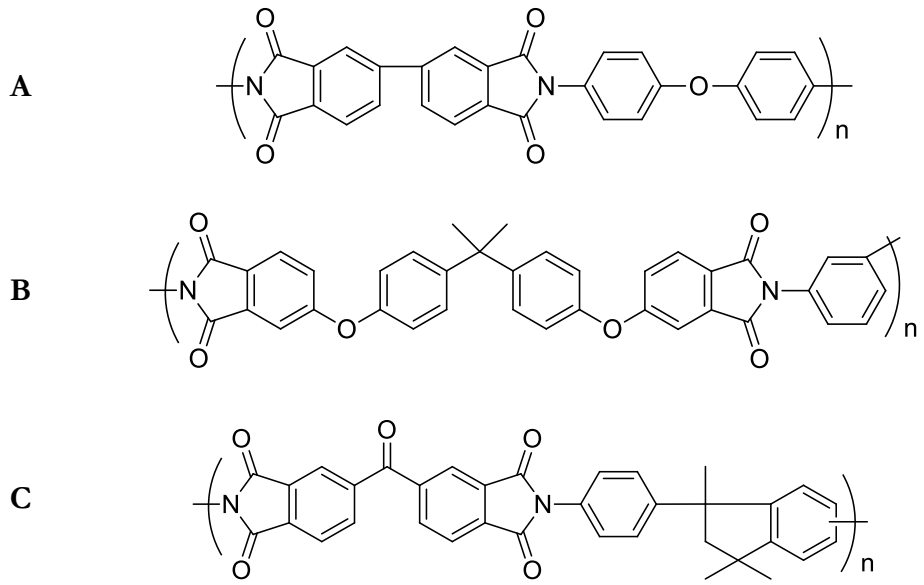

Figure 1.4. Chemical structures of commercial polyimide membranes. **A**- Upilex®, **B**- Ultem® and **C**- Matrimid®.

Today Matrimid® (shown in Figure 1.4) is the most relevant polyimide membrane used industrially for natural gas processing.[30,36] Therefore research on new polyimide architectures mainly refer to Matrimid's® performance. Matrimid® consists of 3,3',4,4'-benzophenonetetracarboxylic

dianhydride (BTDA) and diaminophenylindane (DAPI). Its bulky groups stretch out of the plane, make the polymer backbone rigid (T_g > 300 °C), and disrupt efficient chain packing. Because of this, Matrimid® and polyimides containing bulky -CF_3 groups, were one of the first aromatic polyimides truly soluble in common organic solvents.[37] Since Matrimid® is a soluble polyimide it is a more suitable choice for fabricating gas separation membranes as it can be solution processed. It shows a pure gas CO_2 permeability of 10 Barrer and an ideal CO_2/CH_4 selectivity of 36. Matrimid® outperforms cellulose acetate (P_{CO2} ~ 5 Barrer, α ~ 30).[24,38] The most important drawback of Matrimid® is that it is susceptible to plasticization in the presence of condensable CO_2, just like cellulose acetate. There have been efforts to reduce the plasticization sensitivity via annealing [39–41] or chemical cross-linking[35,42,43], but these efforts have usually resulted in lowering of the CO_2 permeabilities.

As for PEIs, a start towards understanding how subtle backbone changes affect membrane performance (tested at relevant conditions) was made by Simons *et al.* [30]. They showed that, under conditions where commercial membranes suffer from plasticization, ODPA based PEIs are promising membranes that show increasing CO_2 sorption with increasing T_g. The low extent of swelling for ODPA-based PEIs, between 3 and 4% measured up to 50 bar, as well as high CO_2/CH_4 selectivities of between 40 and 60 for at mixed feed pressure of 40 bar, show that these materials can possibly be useful in applications of CO_2 removal at elevated pressures.

1.4 Structural backbone modifications

The chemical structure of polyimides can be systematically altered by selecting, designing or substituting functional groups on the polyimide backbone. Pioneer work in defining the criteria for the polyimide chain structure were made by Koros *et al.* in 1988. They established that higher selectivities could be achieved by inhibition of intersegmental mobility (introducing molecular sieving) and higher permeabilities could be achieved by inhibiting the chain packing density (increasing free volume).

For instance, inclusion of a 6FDA dianhydride in the polymer backbone can result in both of these desirable effects. The bulky -CF_3 groups inhibit chain packing and increase free volume in the polymers, making 6FDA-based membranes more permeable and more selective. 6FDA-based polyimides have

been a major component of this work, their gas separating properties and free volume characteristics are discussed in great detail later on in Chapters 5 and 6.

Another example of structural modifications are the inclusions of ether linkages (–O–), they interact with quadrupolar CO_2 more favorably than with CH_4 leading to high solubility selectivity as demonstrated in Chapter 4 (Figure 4.5) of this thesis. These linkages are present in poly(etherimide)s, which are thoroughly investigated throughout this thesis, in chapters 2 through 4.

In 1991 Robeson presented an "upper bound" relationship of the permeability-selectivity trade-off, where the logarithm of the selectivity versus the logarithm of the permeability reaches a limit.[16] This upper bound relationship is valid for many gas pairs including CO_2/CH_4, O_2/N_2, H_2/N_2 and it was updated in 2008 to include more recent insights.[17]

Recently, series of unique rigid ladder-like polymers with molecular-sieving properties have been shown to perform above the 2008 upper bound. They will be discussed in the following section.

What seems to be missing in the field of PI/PEI-based membranes is a clear understanding of how subtle structural changes in the PEI or PI backbone affect the gas separation performance.

1.5 Emerging new generation polymer membranes for CO_2/CH_4 separation

Recent studies show significant development in high-performance membrane polymers, most were focused on increasing the free volume and diffusivity in membranes (thus improving permeability while maintaining high selectivity).[1] Among new generation polymers that are emerging we can recognize three classes: polymers of intrinsic microporosity (PIMs), thermally rearranged (TR) polymers and amorphous fluoropolymers. The first two exhibit a pore-diffusion molecular-sieving type of transport mechanism. Meaning that they are not solution-diffusion membranes.[1] Specifically TR polymers can reach performances above the 2008 upper bound, however this bound refers to solution-diffusion polymeric membranes.[17]

Polymers of microporosity were synthesized by Budd and McKeown[44,45] and have a stiff ladder-like structure connected by contortion sites that create kinks in the polymer chain. First in the PIM family, PIM-1 is shown in Figure 1.5A. Their kinked chain and highly constrained rotational movement are their most

important features. Many PIMs with varying backbones and pendant groups have been reported, however only PIM-1 and PIM-7 can be obtained in form of films for membrane testing. They exhibit high permeabilities, but low selectivities. For PIM-1 the permeability of pure CO_2 is reported as 2300 Barrer and 125 Barrer for CH_4 is.[45,46] The main drawback of PIMs is their ageing, as their permeability declines overtime.

Another approach towards the design of high diffusivity membranes was introduced in 2010 by Park *et al.*[47] They demonstrated that certain polyimide precursors can undergo structural rearrangement at high temperatures and form pores in thick membrane films. This chemistry is based on aromatic polyimides with hydroxyl groups in the *ortho*-position (polyhydroxyimide) and when heated above 400 °C these polymers thermally rearrange to form a polybenzoxazole backbone structure. The transformation of the 6FDA-HBA bisphenol precursor to the polybenzoxazole is illustrated in Figure 1.5B. This conversion results in a more rigid structure and an increase in fractional free volume, therefore enabling high permeability and selectivity. These membranes exhibit excellent separation performance well above the 2008 trade-off line[17] but they involve complicated synthetic and processing conditions.[48]

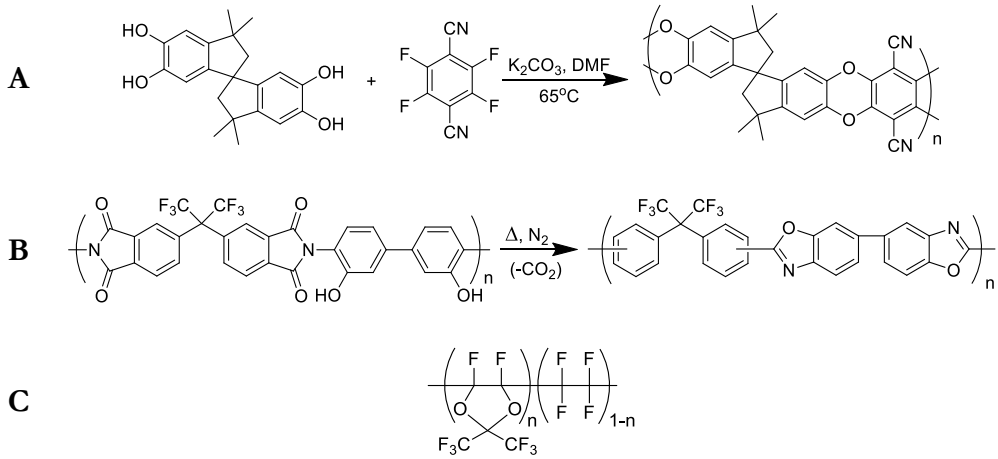

Figure 1.5. Selected examples of several new generation polymer structures for gas separation applications. **A**- PIM-1 is a polymer of intrinsic microporosity, **B**- TR(6FDA-HAB) is a thermally rearranged 6FDA-based polyimide membrane and **C**- Teflon® AF1600 (n = 0.65) or AF2400 (n = 0.87) are commercially available amorphous fluoropolymers.

However, so far when these materials are measured as actually thin membranes with mixed feeds at industrially relevant operating conditions of temperature and pressure, then we see their separation performances decline. Further studies into their ageing processes need to be performed.[49]

Since fluoropolymers already exhibit thermal and chemical stability,[50] further modifications to reduce the crystallinity and increase the free volume were of interest and amorphous fluoropolymers (AF) were the result.[51,52] DuPont introduced commercial Teflon® AF1600 and AF2400 (shown in Figure 1.5C). The later of which showed CO_2 permeabilities of 3900 Barrer.[53] The bulky hexafluoro dioxole group disrupts chain packing making this polymer amorphous. They are of interest for challenging N_2/CH_4 separation applications, more than for CO_2/CH_4 separation.[24,26]

1.6 Characterizing free volume in polymer membranes

In this thesis we often put emphasis on the free volume characterization. Since the fraction of unoccupied volume in a glassy polymer cannot be directly measured it is estimated. Because of this, the notion that free volume can be used to explain polymer membrane performance is still considered controversial.[31] Fortunately, the field of membrane technology is actively searching for methods to more accurately characterize the free volume in polymeric membrane materials.

Data collected with positron annihilation lifetime spectroscopy (PALS) techniques have been successfully correlated with gas transport properties of polymeric membranes.[54–58] Both PALS and positron annihilation Doppler broadening (PADB) techniques enable monitoring, in a non-destructive way and at the atomic level, of the free volume in polymers.[59–62] These techniques will be explained and discussed in Chapter 3 of this thesis.

1.7 Scope and outline of the thesis

The research described in this thesis is focused on understanding the structure-property relationship of polyimide- and polyetherimide-based gas separation membranes. In the previous sections we motivated why there is a need for new generation P(E)I-based polymer membranes. A proper systematic approach towards the design of suitable P(E)I chemistries is lacking and will slow down

the industrial adaptation of high-performance polymer gas separation membranes.

In the subsequent chapters we will present new dianhydride and diamine chemistries that enable us to induce subtle changes in the final P(E)I-backbone structure and by doing so, allow us to extract crucial design parameters. We will use PALS and PADB as tools to investigate the free volume of our new polymers and we will demonstrate that PADB can be used as a fast and convenient screen tool.

In **Chapter 2** we describe a homologous series of 12 PEIs based on 4 different aromatic dianhydrides and 3 aromatic diamines. The aim is to understand the relationships between subtle modifications of the PEI backbone structure and their performance as gas separation membranes. The monomer and polymer synthesis and characterization will be described together with the morphological, thermal and mechanical properties. All PEI films were tested using a CO_2/CH_4 mixed feed at different feed pressures.

Free volume characteristics of the PEI series presented in Chapter 2 are discussed in **Chapter 3**. We will utilize two non-destructive positron annihilation characterization techniques, *i.e.* positron annihilation lifetime spectroscopy (PALS) and positron annihilation Doppler broadening (PADB) in order to address one of the most difficult challenges of membrane design – assessing the polymer free volume. The pros and cons of both techniques will be addressed.

From the 12 PEIs discussed in **Chapter 3**, four backbones have been selected for a more in-depth study. The subtle changes in polymer backbone flexibility make them ideal candidates for a gas sorption study. In **Chapter 4** we report on the sorption of compressed CO_2 and CH_4 in thin PEI films using spectroscopic ellipsometry. The excess free volume, gas sorption capacities, and sorption- and temperature-induced dynamic changes in film thickness and refractive index will be discussed.

In **Chapter 5** we will present a novel series glassy polyimides based on non-linear diamines. The use of oxadiazole heterocycles allows us to introduce strong transverse dipole moments (~3 D) and increase free volume without significant polymer crystallization. We disrupt chain packing even further by inclusion of bulky groups using 6FDA, aiming to increase the free volume

content and CO_2 diffusivity. The permeability and selectivity of this new series will be discussed.

The free volume of the novel series PI membranes described in **Chapter 5** was investigated using PADB and the results are discussed in **Chapter 6**. We will demonstrate that PADB is a suitable technique for quick assessments of free volume characteristics of polymer membranes through interpretation of the *S* and *W* parameters.

1.8 References

[1] R. W. Baker, B. T. Low, *Macromolecules* **2014**, *47*, 6999.

[2] W. J. Koros, G. K. Fleming, *J. Membr. Sci.* **1993**, *83*, 1.

[3] S. A. Stern, *J. Membr. Sci.* **1994**, *94*, 1.

[4] L. M. Robeson, Z. P. Smith, B. D. Freeman, D. R. Paul, *J. Membr. Sci.* **2014**, *453*, 71.

[5] Energy information administration of US Department of Energy, *International Energy Outlook 2016*, **2016**.

[6] Y. Xiao, B. T. Low, S. S. Hosseini, T. S. Chung, D. R. Paul, *Prog. Polym. Sci.* **2009**, *34*, 561.

[7] B. D. Bhide, A. Voskericyan, S.A. Stern, *J. Membr. Sci.* **1998**, *140*, 27.

[8] B. D. Bhide, S. A. Stern, *J. Membr. Sci.* **1993**, *81*, 209.

[9] S. Kanehashi, S. Sato, Chapter 1 in: Y. Yampolskii, B. D. Freeman (Eds.), *Membrane Gas Separation*, John Wiley & Sons, Chichester, UK, **2010**, 3.

[10] Y. Yampolskii, *Macromolecules* **2012**, *45*, 3298.

[11] B. D. Freeman, I. Pinnau, Chapter 1 in: B. D. Freeman, I. Pinnau (Eds.), *Polymer Membranes for Gas and Vapor Separation*, ACS Symposium Series; American Chemical Society, Washington DC, USA, **1999**, *733*, 1.

[12] *CRC Handbook of Chemistry and Physics*, CRC Press, Boca Raton, FL, USA, **2003**.

[13] M. Mulder, *Basic Principles of Membrane Technology*, Kluwer Academic Publishers, Dordrecht, The Netherlands, **1996**.

[14] H. Lin, E. Van Wagner, R. Raharjo, B. D. Freeman, I. Roman, *Adv. Mater.* **2006**, *18*, 39.

[15] M. Wessling, M. L. Lopez, H. Strathmann, *Sep. Purif. Technol.* **2001**, *24*, 223.

[16] L. M. Robeson, *J. Membr. Sci.* **1991**, *62*, 165.

[17] L. M. Robeson, *J. Membr. Sci.* **2008**, *320*, 390.

[18] B. D. Freeman, *Macromolecules* **1999**, *32*, 375.

[19] C. E. Powell, G. G. Qiao, *J. Membr. Sci.* **2006**, *279*, 1.

[20] E. S. Sanders, *J. Membr. Sci.* **1988**, *37*, 63.

[21] R. G. Wissinger, M. E. Paulaitis, *J. Polym. Sci. Part B Polym. Phys.* **1991**, *29*, 631.

[22] J. S. Chiou, J. W. Barlow, D. R. Paul, *J. Appl. Polym. Sci.* **1985**, *30*, 2633.

[23] R. W. Baker, *Ind. Eng. Chem. Res.* **2002**, *41*, 1393.

[24] D. F. Sanders, Z. P. Smith, R. Guo, L. M. Robeson, J. E. McGrath, D. R. Paul, B. D. Freeman, *Polymer* **2013**, *54*, 4729.

[25] R. W. Baker, K. Lokhandwala, *Ind. Eng. Chem. Res.* **2008**, *47*, 2109.

[26] T. C. Merkel, I. Pinnau, R. Prabhakar, B. D. Freeman, Chapter 9 in: Y. Yampolskii, B. D. Freeman, I. Pinnau (Eds.), *Materials Science of Membranes for Gas and Vapor Separation*, John Wiley & Sons, Chichester, UK, **2006**, 251.

[27] R. W. Baker, I. Pinnau, H. Zhenjie, K. D. Amo, A. R. Da Costa, R. Daniels, US Patent No.: 6572680B2, **2003**.

[28] R. W. Baker, I. Pinnau, H. Zhenjie, A. R. Da Costa, R. Daniels, US Patent No.: 6579342B2, **2003**.

[29] J. W. Simmons, S. Kulkarni, O. M. Ekiner, US Patent No.: 20040159233A1, **2004**.

[30] K. Simons, K. Nijmeijer, J. G. Sala, H. van der Werf, N. E. Benes, T. J. Dingemans, M. Wessling, *Polymer* **2010**, *51*, 3907.

[31] R. P. White, J. E. G. Lipson, *Macromolecules* **2016**, *49*, 3987.

[32] D. W. van Krevelen, *Properties of Polymers*, Elsevier, Oxford, UK, **2009**.

[33] L. H. Sperling, *Introduction to Physical Polymer Science*, John Wiley & Sons, Inc, Hoboken, NJ, USA, **2006**.

[34] E. Sada, H. Kumazawa, P. Xu, *J. Appl. Polym. Sci.* **1988**, *35*, 1497.

[35] A. Bos, I. G. M. Pünt, M. Wessling, H. Strathmann, *Sep. Purif. Technol.* **1998**, *14*, 27.

[36] T. Visser, N. Masetto, M. Wessling, *J. Membr. Sci.* **2007**, *306*, 16.

[37] J Bateman, D. Gordon, US Patent No.: 3856752, **1974**.

[38] D. Q. Vu, W. J. Koros, S. J. Miller, *J. Membr. Sci.* **2003**, *211*, 311.

[39] J. S. Lee, W. Madden, W. J. Koros, *J. Membr. Sci.* **2010**, *350*, 242.

[40] X. J. Duthie, S. E. Kentish, C. E. Powell, G. G. Qiao, K. Nagai, G. W. Stevens, *Ind. Eng. Chem. Res.* **2007**, *46*, 8183.

[41] A. Bos, I. G. M. Pünt, M. Wessling, H. Strathmann, *J. Polym. Sci. Part B Polym. Phys.* **1998**, *36*, 1547.

[42] P. Tin, *J. Membr. Sci.* **2003**, *225*, 77.

[43] H. Y. Zhao, Y. M. Cao, X. L. Ding, M. Q. Zhou, J. H. Liu, Q. Yuan, *J. Memb. Sci.* **2008**, *320*, 179.

[44] N. B. McKeown, P. M. Budd, *Chem. Soc. Rev.* **2006**, *35*, 675.

[45] P. M. Budd, B. S. Ghanem, S. Makhseed, N. B. McKeown, K. J. Msayib, C. E. Tattershall, *Chem. Commun.* **2004**, 230.

[46] P. Budd, K. Msayib, C. Tattershall, B. Ghanem, K. Reynolds, N. Mckeown, D. Fritsch, *J. Membr. Sci.* **2005**, *251*, 263.

[47] H. B. Park, C. H. Jung, Y. M. Lee, A. J. Hill, S. J. Pas, S. T. Mudie, E. Van Wagner, B. D. Freeman, D. J. Cookson, *Science* **2007**, *318*, 254.

[48] H. B. Park, S. H. Han, C. H. Jung, Y. M. Lee, A. J. Hill, *J. Membr. Sci.* **2010**, *359*, 11.

[49] K. Pilnáček, O. Vopička, M. Lanč, M. Dendisová, M. Zgažar, P. M. Budd, M. Carta, R. Malpass-Evans, N. B. McKeown, K. Friess., *J. Membr. Sci.* **2016**, *520*, 895.

[50] V. Arcella, P. Colaianna, P. Maccone, A. Sanguineti, A. Gordano, G. Clarizia, E. Drioli, *J. Membr. Sci.* **1999**, *163*, 203.

[51] E. N. Squire, US Patent No.: 5006382A, **1990**.

[52] E. N. Squire, US Patent No.: 4754009, **1988**.

[53] S. Kim, Y. M. Lee, *Curr. Opin. Chem. Eng.* **2013**, *2*, 238.

[54] W. Xie, H. Ju, G. M. Geise, B. D. Freeman, J. I. Mardel, A. J. Hill, J. E. McGrath, *Macromolecules* **2011**, *44*, 4428.

[55] A. Pethrick, *Prog. Poly. Sci.* **1997**, *22*, 1.

[56] G. M. Geise, C. M. Doherty, A. J. Hill, B. D. Freeman, D. R. Paul, *J. Membr. Sci.* **2014**, *453*, 425.

[57] H. Ju, A. C. Sagle, B. D. Freeman, J. I. Mardel, A. J. Hill, *J. Membr.*

Sci. **2010**, *358*, 131.

[58] A. J. Hill, B. D. Freeman, M. Jaffe, T. C. Merkel, I. Pinnau, *J. Mol. Struct.* **2005**, *739*, 173.

[59] R. Zhang, J. Robles, J. Kang, H. Samha, H. M. Chen, Y. C. Jean, *Macromolecules* **2012**, *45*, 2434.

[60] C. A. Quarles, J. R. Klaehn, E. S. Peterson, J. M. Urban-Klaehn, F. D. McDaniel, B. L. Doyle, **2011**, *513*, 513.

[61] G. C. Eastmond, J. H. Daly, A. S. Mckinnon, R. A. Pethrick, *Polymer* **1999**, *40*, 3605.

[62] B. W. Rowe, S. J. Pas, A. J. Hill, R. Suzuki, B. D. Freeman, D. R. Paul, *Polymer* **2009**, *50*, 6149.

CHAPTER 2

Systematic changes in the backbone structure of a series poly(etherimide)s and the effects on CO_2/CH_4 gas separation performance

In this chapter a homologous series of 12 all-aromatic polyetherimide membranes was investigated with the aim to understand how subtle changes in the polyetherimide (PEI) backbone geometry affect the gas separation (CH_4/CO_2) performance. In ODPA-based membranes CO_2 permeability decreases in the order P1>O1>M1 and remains steady throughout the measurements with the mixed feed pressure increase up to 40 bar, however selectivity decreases for ODPA-O1 and ODPA-M1. All three M1-based membranes suffer from plasticization. For high-pressure applications OPDA-P1 membrane is a good candidate with selectivity of 48 and resistance to plasticization up to 40 bar. Alternatively, for applications up to 10 bar of mixed feed, BPDA-O1 is a promising candidate because it displays a high selectivity of 70 and permeability of 1.3 Barrer.

2.1 Introduction

Membrane-based gas separation is an important unit operation in many industrial processes; such as natural gas upgrading [1], carbon dioxide removal from flue gas [2], biogas [3] and landfill gas. While the majority of global carbon dioxide (CO_2) emission comes from fossil fuel combustion and cement making processes, there is a substantial increase in CO_2 emission associated with the exploration of natural gas. Sources of natural gas with higher concentrations of CO_2 are being explored since the sources of low CO_2 containing natural gas are limited and all but exhausted. CO_2 reduces the heating value of methane gas streams and causes corrosion in pipelines and equipment, so it must be removed prior to use. Separation of CO_2 using membranes is a competitive alternative to conventional absorption technology (traditional method is amine scrubbing [4]) owing to its high energy efficiency, simple design (easy scale-up), and high area-to-volume ratio (compactness).[5] In order to have the desired robustness and membrane lifetime, these materials need to meet the following requirements: chemical and thermal resistance, good mechanical properties, plasticization resistance and physical aging tolerance.[2]

A great deal of research has been done on the control of gas permeability and selectivity for polymer membranes separating gases, with the main focus being on the relationship between the polymer structure and gas separation properties. The gas permeation properties of glassy polymers are much more sensitive to the chemical structure of the repeat units than that of rubbers [6], and their chains have restricted mobility. It has been shown that an increase in backbone rigidity improves selectivity since it helps molecular sieving of gases with similar solubility coefficients.[7] Most of the polymers that have been investigated typically show the general trend that highly permeable polymers possess rather low selectivity and *vice versa*, named permeability/selectivity trade-off relationship.[8,9] The most studied class of polymers for membrane materials are polyimides.[10]

Commercial polyimides (PIs) for gas separation are known under trade names such as Upilex® and Matrimid®. The later has been a target of considerable research owing to a great combination of properties and one major flaw: for CO_2/CH_4 gas separation at 10 bar, it shows a selectivity of 34 and permeability of CO_2 of 6.5 Barrer [11], however, the downside is that Matrimid® is known to exhibit strong plasticization in the presence of CO_2 [12,13]. Plasticization is a

common problem in polyimide- and polyetherimide-based membranes. If this issue could be resolved, PIs and PEIs could become potential candidates for high-pressure CO_2/CH_4 gas separation.

Park *et al.*[14] reported a new family of thermally rearranged membranes. This modification is established when an aromatic polyhydroxyimide with hydroxyl groups in the *ortho*-position is heated to high temperatures (above 400 °C) at which point the polymer precursor thermally rearranges to a polybenzoxazole. This conversion results in a more rigid structure and an increase in fractional free volume, therefore it combines excellent permeability and selectivity, well above the 2008 CO_2/CH_4 bound.[8] Cross-linking has been shown to be an effective method to improve membrane stability, specifically referring to plasticization and physical aging.[15,16] Bulky groups in the backbone help to disrupt the chain packing leading to an increase in free volume, that is why 6FDA-durene has very high permeability values (678 Barrer), but values of selectivity are around 20.[17] It is clear that major backbone modifications in polymer membranes have been explored. However, what seems to be missing is a detailed study towards designing, investigating and understanding the effects of subtle structural changes in the PEI or PI backbone and what the effects are on the gas separation performance.

A start was made by Simons *et al.* [18], they showed that, under conditions where commercial membranes suffer from plasticization, 3,3',4,4'-oxydiphthalic dianhydride (ODPA) based poly(etherimide)s (PEIs) are promising membranes that show increasing CO_2 sorption with increasing T_g. The low extent of swelling for ODPA-based PEIs, between 3 and 4 % measured up to 50 bar, as well as high CO_2/CH_4 selectivities of between 40 and 60 for at mixed feed pressure of 40 bar, show that these materials can possibly be useful in applications of CO_2 removal at elevated pressures. ODPA-P1, see Figure 2.1, showed a decrease in CH_4 permeability with increasing pressure, a desirable property indicating that the selectivity for separation increased with increasing pressure. Increasing the number of arylether units in the diamine moiety reduced the CO_2/CH_4 selectivity. This polymer motivated us to look into more detail at how small changes in the PEI backbone affect gas transport properties and CO_2 swelling behavior. The role of the dianhydride structure, *i.e.* rigid versus flexible, will be investigated as well as the aryloxy-substitution pattern (*para*, *meta* or *ortho*) of the diamine moiety.

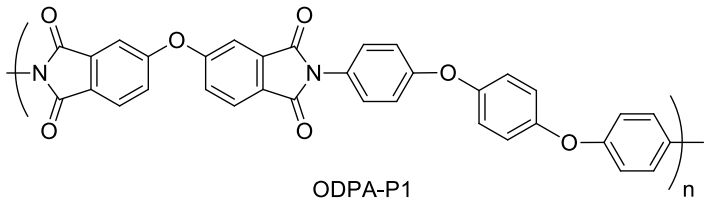

Figure 2.1. Structure of ODPA-P1 polyetherimide.[18]

2.2 Design

In order to understand the relationship between the polyetherimide backbone structure and the membrane gas separation (CO_2/CH_4) performance we have synthesized a systematic series of 12 PEIs. Structures of the diamines were based on *para*-, *meta*-, or *ortho*-based aryl ether units, which act as "flexible" spacer units between the terminal *para*-phenylamine functionalities (Figure 2.2). Three diamines chosen for this study are 1,4-bis(4-aminophenoxy)benzene (P1), 1,3-bis(4-aminophenoxy)benzene (M1) and 1,2-bis(4-aminophenoxy)benzene (O1). Changing the exocyclic bond angle in this 3-ring diamine changes the backbone from a more linear to a more bend or kinked conformation. In addition, the (local) electrostatic dipole moment changes as the oxygen atoms move closer to one another when moving from a *para*- to an *ortho*-substitution pattern.

Additionally, four different dianhydride moieties have been selected to systematically change the flexibility of the polymer backbone, to tailor the segmental mobility, and the non-equilibrium excess free volume of the polyetherimide. Selected dianhydrides include: pyromellitic dianhydride (PMDA), 3,3',4,4'-biphenyltetracarboxylic dianhydride (BPDA), 3,3',4,4'-benzophenonetetracarboxylic dianhydride (BTDA) and 3,3',4,4'-oxydiphthalic dianhydride (ODPA), as shown in Figure 2.2.

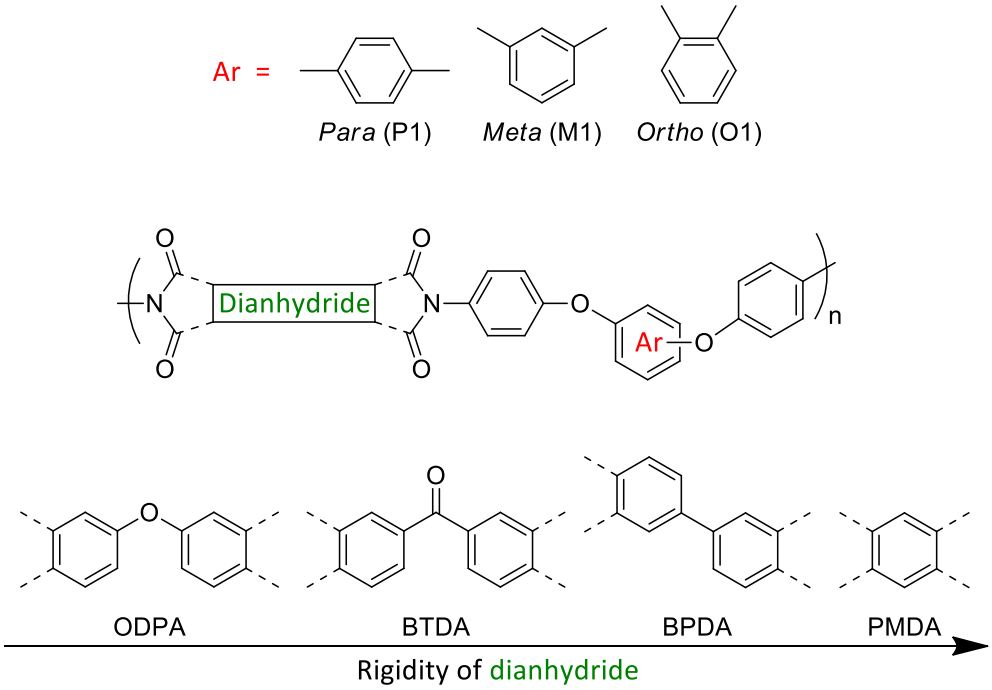

Figure 2.2. Chemical structures of PEI membranes used for this study.

2.3 Gas permeation

In order to be useful for gas separation applications a membrane must be able to control the permeation of different species. The permeation of gases through polymer membranes is often described by the solution-diffusion model, in which the permeability coefficient is the product of a solubility coefficient (S_i) and a diffusivity coefficient (D_i) (Eq. (2.1)).[19]

$$P_i = S_i \times D_i \tag{2.1}$$

Selectivity of a membrane for one gas over the other will arise due to differences either in the solubility coefficient (S_i/S_j) or in the diffusivity coefficient (D_i/D_j). Therefore the ability of a polymer membrane to separate two gases (*e.g.*, i and j) is the ideal selectivity $\alpha^*_{i/j}$ (Eq. (2.2)).

$$\alpha^*{}_{i/j} = \frac{P_i}{P_j} = \left(\frac{D_i}{D_j}\right) \times \left(\frac{S_i}{S_j}\right) \tag{2.2}$$

For a binary gas mixture, the actual measure of a membrane's ability to separate a mixture of two gases is the selectivity of gas i to gas j, $\alpha_{i/j}$, a value that is less commonly reported as this is not a material property since it depends on operating conditions, such as the feed composition. This gas selectivity of a membrane is expressed by the following relationship:

$$\alpha_{i/j} = \frac{y_i \,/\, y_j}{x_i \,/\, x_j} \tag{2.3}$$

where y_i and y_j are the mole fractions of the components i and j in the permeate, while x_i and x_j are their corresponding mole fractions in the feed.[20]

2.4 Experimental

2.4.1 Materials

1,2-bis(4-aminophenoxy)benzene (O1) was synthesized according to a literature procedure [21], shown in Scheme 2.1, and described in detail in the following section. All other start materials were purchased from commercial sources and used as received unless stated otherwise. Dianhydrides ODPA, BTDA, BPDA and PMDA were purchased from TCI Co. Ltd. and dried prior to use overnight in a vacuum oven at 60 °C. Diamine P1 was purchased from ABCR, diamine M1 from TCI and N-Methyl-2-pyrrolidinone (NMP) was obtained from Acros Organics.

2.4.2 Characterization

The chemical structure of O1 diamine was confirmed by ^{1}H NMR (Bruker WM-400, 400 MHz) and ^{13}C NMR (Bruker WM-400, 100 MHz). All samples were dissolved in deuterated chloroform and the recorded spectra were referenced to the solvent ($CDCl_3$: ^{1}H 7.26 and ^{13}C 77.0 ppm) relative to TMS. For GC/MS analysis of O1, a Shimadzu GCMS-QP2010S gas chromatograph mass spectrometer was used coupled with the GL Sciences Optic 3 high-performance injector. Separation of the evolved gases was achieved using a 30 m × 0.025 mm SGE forte BPX-5 capillary column operated at a He flow rate of about 1 ml/min. Software ATAS Evolution Workstation (ATAS GL International) controlled heating of the injection port of the GC from 50 °C to 300 °C in 5 min. The GC column oven was programmed from 50 °C, with a heating rate of 20 °C/min, to 300 °C (held for 30 min). LabSolutions data system,

GCMSsolutions (Shimadzu) Postrun analysis software was used to integrate the peaks. Melting point of O1 was determined using a Leica DM LM optical microscope equipped with a Linkam TMS94 hot stage; heating rate was 5 °C/min.

Gel permeation chromatography (GPC) measurements of polyamic acids were performed on a Shimadzu Prominence GPC system equipped with two Shodex LF-804 columns. N-Methyl-2-pyrrolidone (NMP) with 5 mM of LiBr was used as eluent at a flow rate of 0.5 mL/min at 60 °C. Data analyses were performed with LabSolutions software using the refractive index detector data. Quantification was made based on polystyrene standard calibration. All polyamic solutions were filtered through a 0.45 μm PTFE filter prior to a GPC run.

The thermal properties of the PEI films were determined by differential scanning calorimetry (DSC) using a PerkinElmer Sapphire DSC. Samples were heated at a rate of 20 °C/min under a nitrogen atmosphere. Thermogravimetric analysis (TGA) was performed on a Perkin Elmer Pyris diamond TG/DTA under a nitrogen atmosphere and a scan rate of 10 °C/min. Polymer thin films were investigated using a dynamic mechanical thermal analyzer (DMTA) in the temperature range -100 °C to 400 °C, at a heating rate of 2.5 °C/min and at a frequency of 1 Hz under a nitrogen atmosphere. Approximate dimensions of films were 20 × 4 × 0.03 mm. All samples were dried in a vacuum oven at 60 °C for 1 h prior to testing.

To investigate the morphology of the PEI films (15–35 μm), wide-angle XRD experiments were conducted using a Bruker AXS D8 Discover X-ray diffractometer in transmission mode with Cu Kα as the radiation source. For every PEI film, four layers were fixed onto a support, with the film surface perpendicular to the beam direction. All experiments were performed at room temperature, the sample–detector distance was set at 6 cm and the exposure time was set to 10 min.

2.4.3 Monomer synthesis

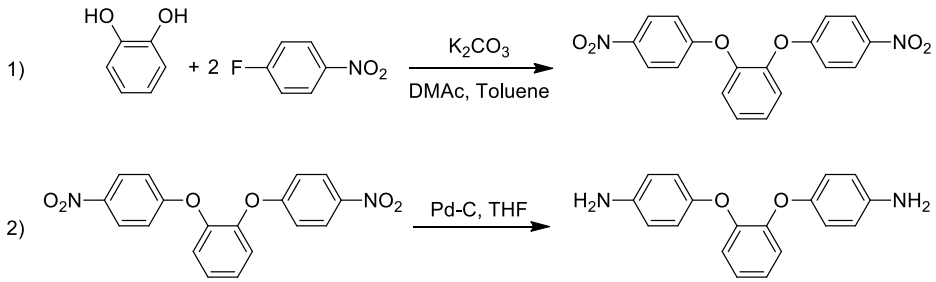

Scheme 2.1. Synthesis of 1,2-bis(4-aminophenoxy)benzene (O1).

1,2-bis(4-nitrophenoxy)benzene: A dried 1000 mL three-neck flask, equipped with a nitrogen inlet, a mechanical overhead stirrer and a Dean–Stark trap with reflux condenser, was charged with 9.38 g (0.085 mol) of 1,2-dihydroxybenzene (catechol), 23.54 g (0.170 mol) of finely ground K_2CO_3, 160 ml of toluene and 200 ml of dimethylacetamide. This mixture was heated and stirred at 135 °C for 1.5 h, after which the temperature was increased to 175 °C. The theoretical amount of water was collected in the Dean–Stark trap and removed together with the toluene. The reaction mixture, now dark colored, was cooled to room temperature and 24.03 g (0.170 mol) of 1-fluoro-4-nitrobenzene was added. This mixture was heated at 160 °C overnight. The reaction mixture was cooled to room temperature and precipitated in 600 mL of ice water. The solids were collected by filtration, washed with water and recrystallized twice from 96% ethanol. Yield 24.32 g (81%); mp: T_{onset} = 134 °C, T_{max} = 136 °C (135–136 °C).[22] TLC: (9/1 hexane/ethyl acetate) t_r = 0.134 (one spot).

1,2-bis(4-aminophenoxy)benzene (O1). A 250 mL hydrogenation bottle was charged with 12 g (0.034 mol) of 1,2-bis(4-nitrophenoxy)benzene, 100 mL of dry THF, and 1.2 g of 10% palladium on carbon. After degassing with nitrogen for 20 minutes, the bottle was placed in a Parr hydrogenator, and the nitro group was reduced under hydrogen atmosphere at 50 psi for 5 h at room temperature, then the shaker was turned off and the mixture was left under the same conditions (pressure and temperature) overnight. The solution was filtered over silica gel and celite, and the THF was removed by rotary evaporation. Pure O1 was obtained after two recrystallizations from ethanol/water (90/10) as pale brown crystals. Yield: 7 g (71%); mp: T_{onset} = 132 °C, T_{max} = 136 °C (135–136 °C)[21]. TLC (9/1 hexane/ethyl acetate) t_r = 0 (one spot). ^{1}H NMR ($CDCl_3$, 400 MHz) δ (ppm): 3.46 (s, 4H), 6.63 (d, 4H, J = 8.4 Hz), 6.83 (d, 4H, J = 8 Hz), 6.89–6.96

(m, 4H); ^{13}C NMR ($CDCl_3$, 400MHz) δ (ppm): 116.1, 119.2, 119.9, 123.1, 142.1, 148.7, 149.3.

2.4.4 Polymer synthesis

Polyamic acids of high molecular weight were prepared from the dianhydride and diamine monomers, in equimolar quantities, as 15 wt.% solutions in NMP at 25 °C.

Preparation of ODPA-P1 15 wt.% polymer film (representative procedure, Scheme 2.2): A dry 50 mL one-neck round-bottom flask was charged with 1.498 g (5.12 mmol) of 1,4-bis(4-aminophenoxy)benzene (P1) and 18 mL of dry NMP (water content <0.005 %) was added. This solution was then stirred for 5 min, under a dry nitrogen flow, at room temperature with a magnetic stirrer at 120 rpm until the diamine monomer was dissolved. After this step the polymerization was initiated by adding 1.589 g (5.12 mmol, an equimolar amount) of 3,3',4,4'-oxydiphthalic dianhydride (ODPA), and the walls of the flask were washed with 2 mL of NMP. Polymerization was allowed to continue for 24 h. under a nitrogen atmosphere, stirring at 90 rpm.

Film preparation. In order to remove any present solids, the polyamic acid solution was filtered using a Sartorius pressure filter. The resulting filtered solution was degassed to remove bubbles and then cast with a doctor-blade onto a clean, dry glass plate (film thickness ~ 0.6 mm) and placed in a clean vacuum oven at 60 °C for 1.5 h. Films were thermally imidized by heating to 100 °C for 1 h, 200 °C for 1 h, and 300 °C for 1 h. After an overnight cooling to 25 °C, the film was released from the glass plate by placing it in lukewarm water. All PEIs were obtained as free-standing films using this procedure.

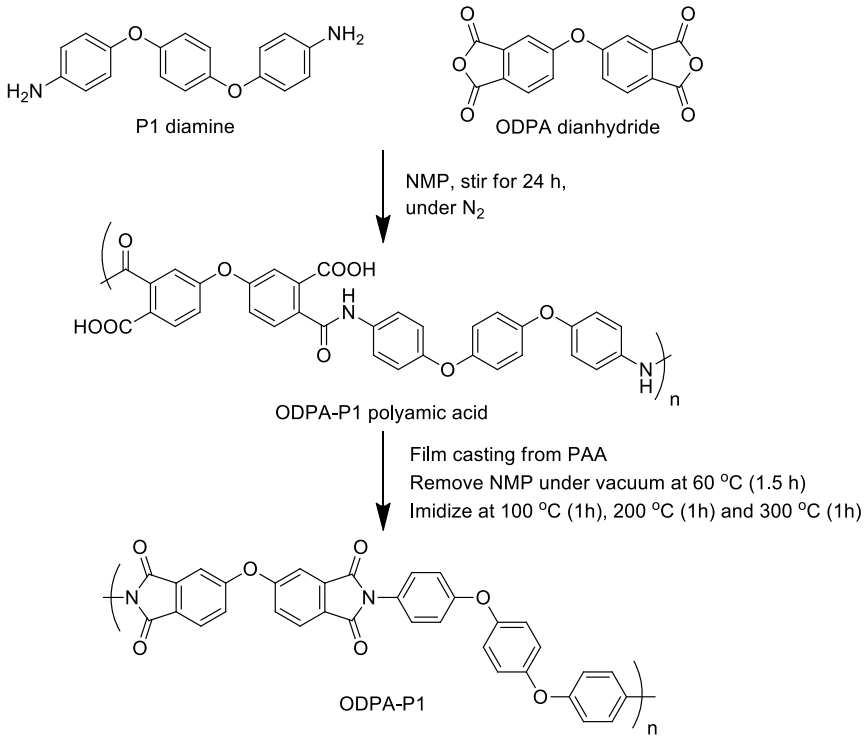

Scheme 2.2. Polymerization procedure used to prepare an ODPA-P1 free-standing membrane.

2.4.5 Gas permeation measurements

Gas permeation experiments were performed to evaluate the CO_2/CH_4 separating ability of our PEI membranes using the constant volume variable pressure method with vacuum at the permeate side. The N_2, CO_2, and CH_4 permeability coefficients of the PEI films, as well as the separation performance of a CO_2/CH_4 (50/50) mixture, were measured as function of feed temperature and feed pressure. Experiments were performed in two different permeation units, both operating at four different pressures (10, 20, 30 and 40 bar). Permeability coefficients were calculated from the steady-state pressure increase $\Delta P_p/\Delta t$ in a calibrated volume at the permeate side with Eq. (2.4):

$$\frac{P}{l} = \frac{V_c \cdot 273.15 \cdot \left(P_{pt} - P_{p0}\right)}{A \cdot T \cdot \frac{\left(P_{ft} - P_{f0}\right)}{2} \cdot 76 \cdot t} \tag{2.4}$$

where the ideal gas law is assumed to be valid and t (s) is the time, P_{pt} (bar) the pressure at the permeate side at time t, P_{p0} the permeate pressure at $t = 0$, T (K) the temperature, V_c (cm^3) the calibrated permeate volume, and A (cm^2) the total membrane area. The gas permeance P/l is expressed in gas permeation unit, GPU, *i.e.* $10^{-6} cm^3/cm^2$ s cmHg. Multiplying the gas permeance with the membrane thickness, l (μm), gives the permeability coefficient in Barrer units. As a correction for non-ideal behavior, partial pressures were replaced by their corresponding fugacities.

Alternating nitrogen and CO_2/CH_4 gas permeation measurements were performed on the same membrane samples. The pressure of the nitrogen feed was kept constant at 5 bar to investigate plasticization effects. The pressure of the CO_2/CH_4 feed was increased from 10 to 20, 30 and 40 bar, for these mixed gas experiments, both feed and permeate were analyzed using a Varian 3900GC gas chromatograph equipped with an Alltech Alumina F-1 60/80 packed bed column at 150 °C. In experiments with the CO_2/CH_4 (50/50) binary mixture, for each feed pressure, flow rate of the retentate was kept constant and equal to 30 cm^3 (STP)/min in order to achieve a uniform feed composition across the membranes. Sufficient permeate was collected to reach a signal/noise (S/N) ratio of at least 10. Mixed gas selectivity was calculated with Eq. (2.5):

$$\alpha_{CO_2/CH_4} = \frac{y_{CO_2} / y_{CH_4}}{x_{CO_2} / x_{CH_4}} \tag{2.5}$$

where y and x are the concentrations of components in the permeate stream and feed stream, respectively.

For gas permeation experiments, the detailed experimental protocol consisted of the following steps:

1. Determine pure N_2 permeability at 5 bar;
2. Switch to mix feed of 10 bar, followed by overnight membrane degassing with N_2 (5 bar);
3. Repeat Step 2 with increased feed pressure by 10 bar.

The high-pressure permeation unit was fully automated and controlled by means of Lab View Software. The temperature was kept constant at 35 °C.

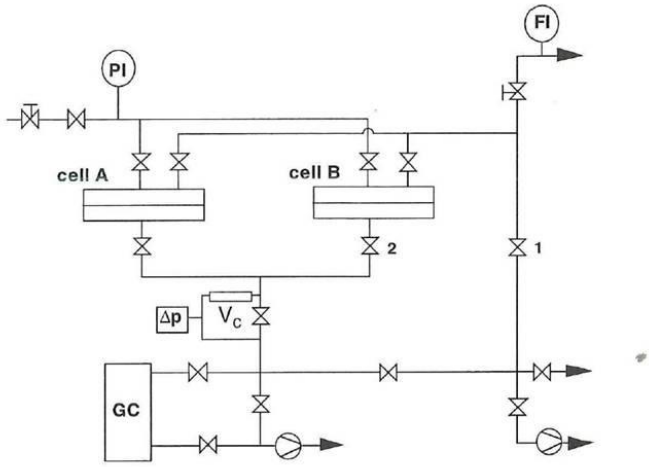

Scheme 2.3. Gas permeation set-up. FI is a flow meter, PI is a pressure indicator, Δp is a differential pressure indicator, V_c is the calibrated volume and GC is the gas chromatograph.[23]

The high-pressure gas permeation set-up used is schematically given in Scheme 2.3. The setup consists of two double-walled permeation cells, which allow permeation at elevated temperatures. A feed pressure is applied on top of the film; a pressure difference across the film is maintained by keeping the permeate side at vacuum. Two membranes were measured simultaneously and their permeabilities were determined separately by GC. In V_c the pressure increases with time due to the permeating gas build-up.

2.5 Results

2.5.1 Viscosity and gel permeation chromatography measurements

The molecular weights of the polyamic acid intermediates, measured using GPC, are listed in Table 2.1. The actual GPC curves are shown in Appendix A. High molecular weight polyamic acids could be prepared without difficulties, with number average molecular weights in the range of ~ 60,000 to ~ 120,000 g/mol. With the exception of PMDA-M1 (Figure A2), PMDA-O1 and BPDA-O1 (Figure A3), all GPC curves show a unimodal molecular weight distribution. All P1-based polyamic acids show unimodal molecular weight distribution (Figure A1) and the highest number average molecular weights (Table 2.1).

Table 2.1. Molecular Weight data as determined by GPC and Inherent viscosities of the polyamic acids.

Polymer	M_n (g/mol)	M_w (g/mol)	PDI=M_w/M_n	η_{inh}[a] (dL/g)
ODPA-P1	64,000	119,000	1.9	0.78
BTDA-P1	109,000	212,000	2.0	0.89
BPDA-P1	102,000	191,000	1.9	1.11
PMDA-P1	108,000	154,000	1.4	2.00
ODPA-M1	63,000	152,000	2.4	0.98
BTDA-M1	87,000	169,000	1.9	0.89
BPDA-M1	59,000	153,000	2.6	1.09
PMDA-M1	69,000	174,000	2.5	1.70
ODPA-O1	53,000	104,000	2.0	0.72
BTDA-O1	119,000	331,000	2.8	1.03
BPDA-O1	84,000	364,000	4.3	1.15
PMDA-O1	97,000	296,000	3.1	1.03

[a] Inherent viscosities of the polyamic acids were measured by an Ubbelohde viscometer at room temperature, at a concentration of 0.5 g/dL in NMP.

Inherent viscosities of the polyamic acids were between 0.7 and 2.0 dL/g. Tough, flexible and easy-to-handle films were obtained after thermal imidization. All polyamic acids were prepared at 15 wt.% solids, however this concentration proved to be difficult for casting a useful PMDA-P1 film. Polymerization of the other dianhydrides with all three diamines went without difficulty. The polymerization of PMDA with the P1 diamine, on the other hand, resulted in gel-like polyamic acid, which could not be solution processed. The polyamic acid was prepared at 10 wt.% solids in order to cast a useful amic acid film; the viscosity of this solution was 2.0 dL/g. Although the other two PMDA-based polyamic acids exhibited inherent viscosities of 1.7 and 1.03 dL/g, respectively, the fully imidized PMDA-M1 and PMDA-O1 films appeared highly crystalline and very brittle in nature. The films had to be handled with care and did not make good membranes. The polymerization of ODPA with all three diamines resulted in polyamic acids with the lowest inherent viscosity. None of the fully imidized films were soluble in NMP at 25 °C (10 mg polymer/mL).

2.5.2 Dynamic thermogravimetric analysis (TGA)

The thermal stability of the polyetherimide films was investigated by dynamic thermogravimetric analysis. Sample films were cleaned and degreased with ethanol and dried at 60 °C for 2 hours. All films were investigated under inert (nitrogen) conditions using a heating rate of 10 °C/min. This provides information with respect to the polymer decomposition temperature, the temperature at which a weight loss of 5% occurs ($T_{5\%}$). The resulting thermograms, showing polymer weight as a function of temperature, are shown in Figure 2.3 and the values for $T_{5\%}$ and char yield are listed in Table 2.2.

In Figure 2.3 it is shown that all 12 PEIs show a gradual decrease in weight as a function of temperature up to ~ 500 °C. The weight loss below 500 °C is due to outgassing of low molecular weight species such as solvent (NMP). Above 500 °C, the PEI films degrade due to thermal decomposition. The values reported here are typical for all-aromatic PEIs.[21] As the PEI-based membranes will operate at or slightly above 25 °C the thermal stability of this PEI-series will not be an issue.

Table 2.2. Dynamic thermogravimetric analysis results of the polyetherimide films. Heating rate 10 °C/min and nitrogen atmosphere.

Polymer	TGA	
	5% weight loss (°C)	char yield at 595 °C (%)
ODPA-P1	531	70
BTDA-P1	509	71
BPDA-P1	542	76
PMDA-P1	533	70
ODPA-M1	530	71
BTDA-M1	510	71
BPDA-M1	549	81
PMDA-M1	540	72
ODPA-O1	508	73
BTDA-O1	504	70
BPDA-O1	520	73
PMDA-O1	509	74

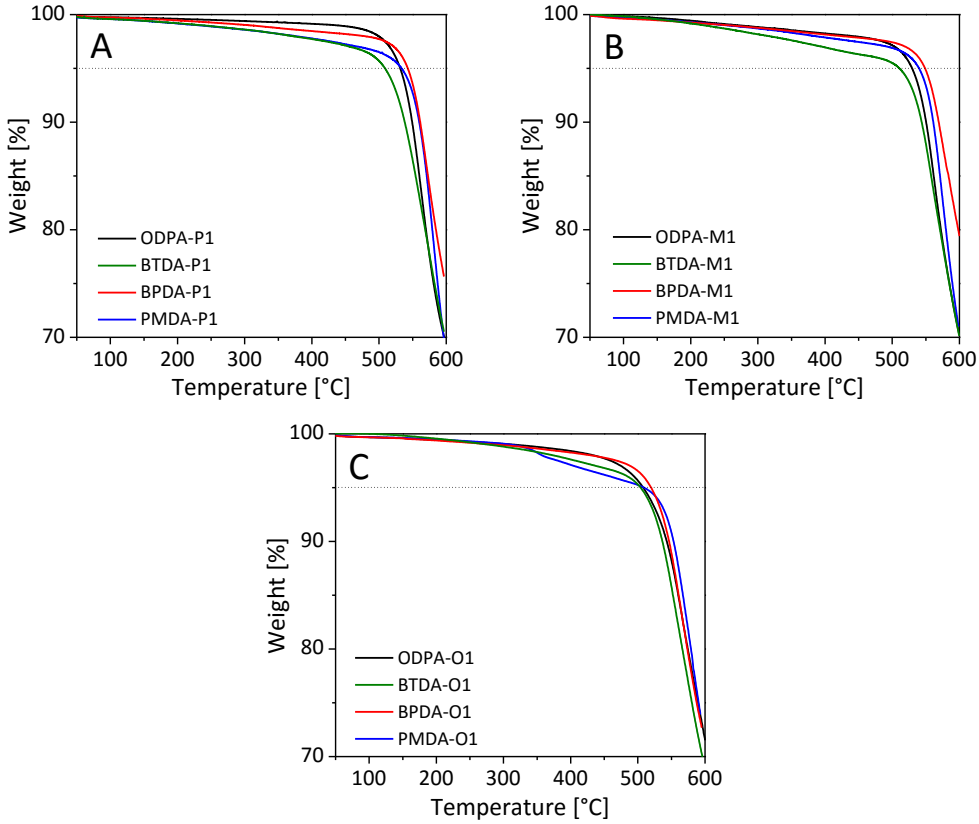

Figure 2.3. TGA thermograms of the PEI films **A**- P1-series, **B**- M1-series and **C**- O1-series; heating rate 10 °C/min (N_2 atmosphere). The dotted line marks the 5% weight loss point.

2.5.3 Differential scanning calorimetry (DSC)

The thermal properties of the PEI films were determined by DSC using a PerkinElmer Sapphire DSC. Samples were heated at a rate of 20 °C/min under a nitrogen atmosphere to ~ 450 °C, depending on the samples thermal stability range as determined by TGA. The DSC curves, second heats only, are shown in Figure 2.4 and the T_g and T_m data are summarized in Table 2.3.

Both P1- and M1-series (Figure 2.4A and 2.4B, respectively) gave three semi-crystalline and one amorphous polymer film, while the O1-series gave one semi-crystalline film. However, since the DSC measurements were performed up to a temperature limit determined by the thermal stability of each polymer as determined by TGA measurements, not all of the melting endotherms are

observable by DSC as they may overlap with the polymer degradation temperature. We were unable to detect a T_g for the PMDA-based films by DSC.

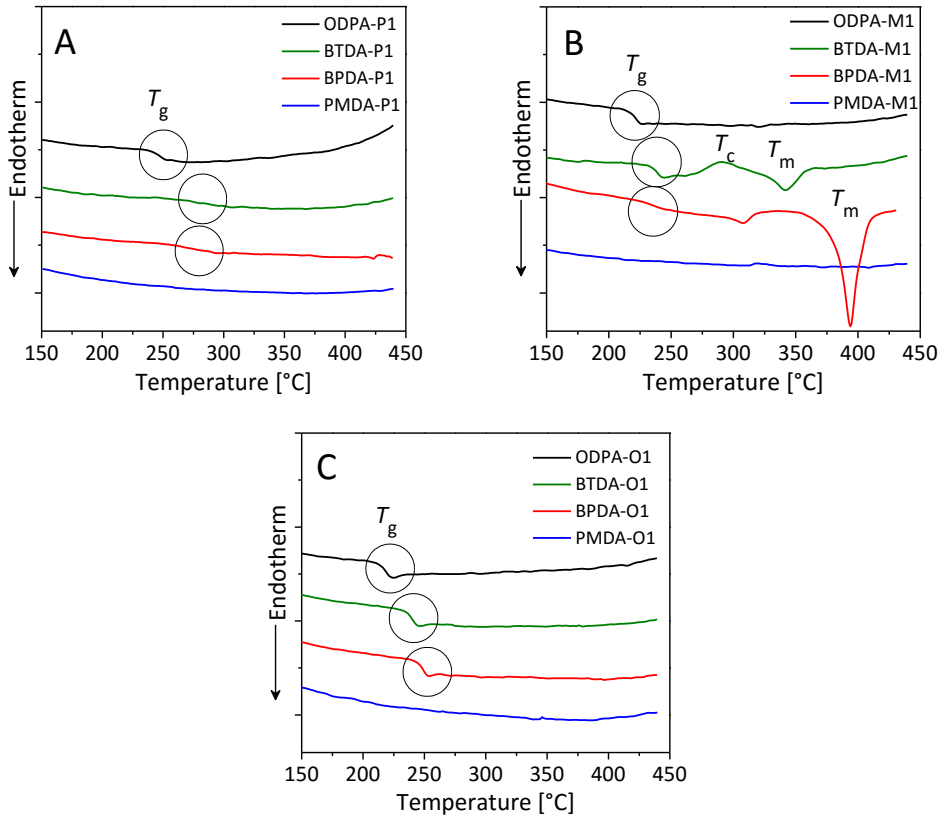

Figure 2.4. DSC curves showing the T_g and T_m events as a function of temperature. **A**- P1-series, **B**- M1-series and **C**- the O1-series. Second heat, recorded in N_2 atmosphere at 20 °C/min. All curves have been normalized to sample weight and translated vertically for sake of clarity.

For the P1- and M1-based PEI films we observed the following trend in T_g: PMDA>BTDA>BPDA>ODPA. The trend for the O1-based PEIs is similar except for the fact that the T_g of BPDA-O1>BTDA-O1. As anticipated, the more rigid PMDA-based PEIs exhibit the highest T_g values and the flexible ODPA-based PEIs display the lowest T_g values. BPDA-P1, BTDA-M1 and BPDA-M1 are the only 3 films exhibiting an accessible melting point. The melting points for semi-crystalline BPDA-P1, BTDA-M1 and BPDA-M1 are 457 °C, 342 °C and 394 °C respectively, and these results are in agreement with previously reported T_m values.[21] It has to be noted that the onset of the melting endotherm of BPDA-P1 is observed at ~ 450 °C. However, due to

restrictions of the upper temperature limit, (determined by TGA) the melt event could not be recorded.

Table 2.3. Morphology and (thermo)mechanical properties of the polyetherimide films.[a]

Polymer	XRD		DSC		DMTA	
	morphology[b]	ϕc (%)[c]	T_g (°C)[d] DSC	T_m(°C)[e] DSC	T_g (°C)[f] DMTA	*E'* (GPa, 30 °C)
ODPA-P1	Am		248		248	4.5
BTDA-P1	SC	18	286		302	6.5
BPDA-P1	SC	6	272	457	276	5.4
PMDA-P1	SC	19			321	4.8
ODPA-M1	Am		221		221	8.1
BTDA-M1	SC	6	238	342	261	6.6
BPDA-M1	SC	3	236	394	242	4.0
PMDA-M1[g]	SC	11			318	4.7
ODPA-O1	Am		217		226	4.9
BTDA-O1	Am		239		238	5.2
BPDA-O1	Am		248		248	4.9
PMDA-O1[g]	SC	4			302	4.1

[a] DSC (second heating) and DMTA data were collected using a heating rate of 20 and 2.5 °C/min, respectively. [b] Morphology: SC = semi-crystalline; Am = amorphous. [c] ϕc is the degree of crystallinity determined by XRD. [d] T_g is reported at the inflection point. [e] T_m is reported as the peak temperature. [f] T_g is determined at the maximum of the loss modulus (E''). [g] brittle film

2.5.4 Dynamic mechanical thermal analysis (DMTA)

The DMTA results show the values for the storage modulus (E') and T_g as determined at the maximum of the loss modulus (E'') (Table 2.3). All PEI membrane films show storage moduli (E') of 4-8 GPa, which is typical for all-aromatic PEIs. The T_g values determined by DMTA correspond well with ones observed by DSC. All DMTA curves are shown in Figure 2.5. With the exception of the PMDA-based PEIs, all films show clear T_g events (as determined at the max of E''). The same is true for the β-transitions, which can clearly be observed between 80 and 110 °C for all films with the exception of the PMDA-based films.

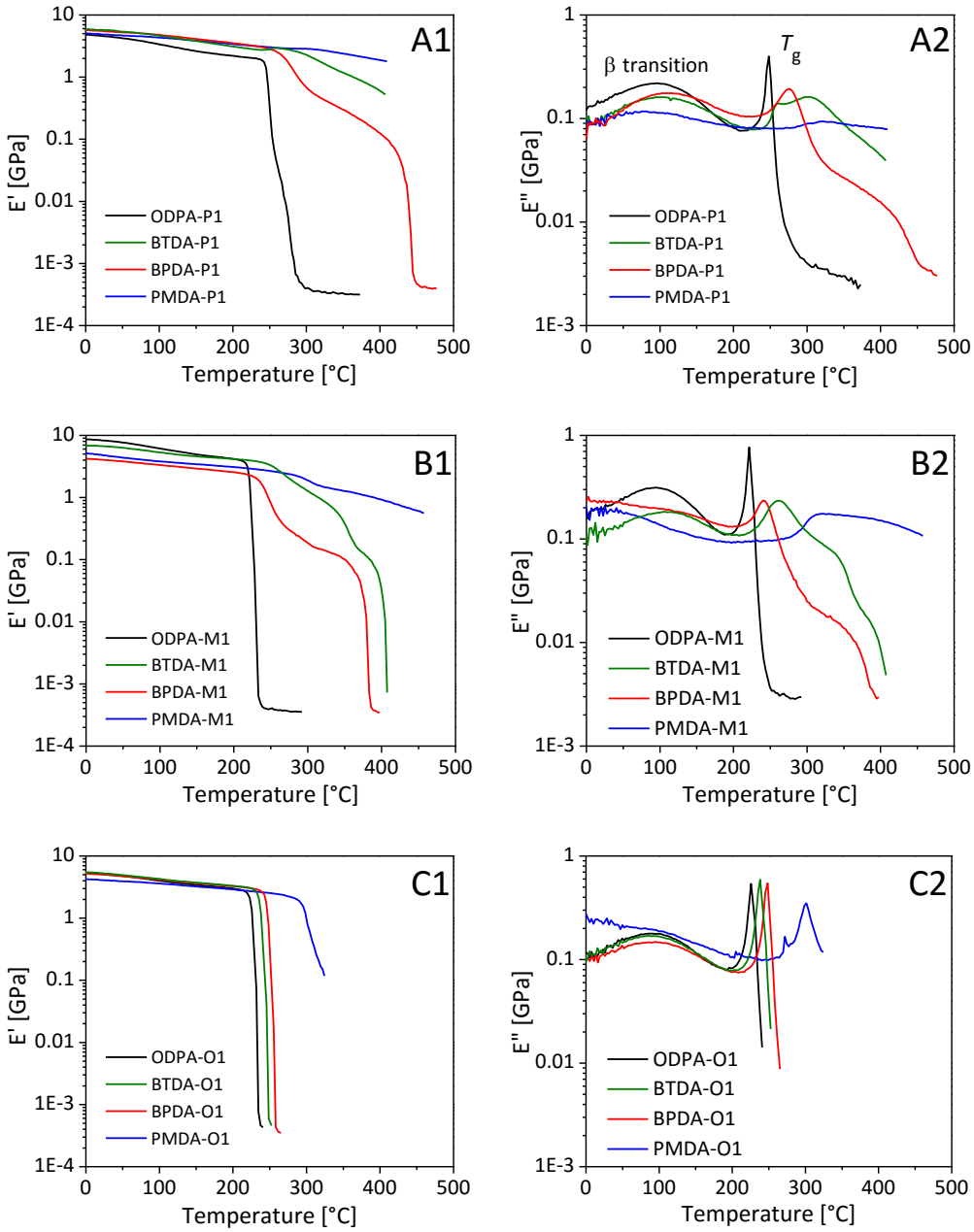

Figure 2.5. DMTA results for the PEI films. The storage modulus (E') and loss modulus (E'') were recorded as a function of temperature (N_2 atmosphere at a frequency of 1 Hz and a heating rate of 2.5 °C/min). **A**- P1-series, **B**- M1-series, and **C**- O1-series.

2.5.5 Film morphology, X-ray diffraction (XRD)

Wide-angle XRD analysis was performed on all 12 PEI films (15–35 μm) and the results are shown in Figure 2.6 while the values for the degree of crystallinity are presented in Table 2.3.

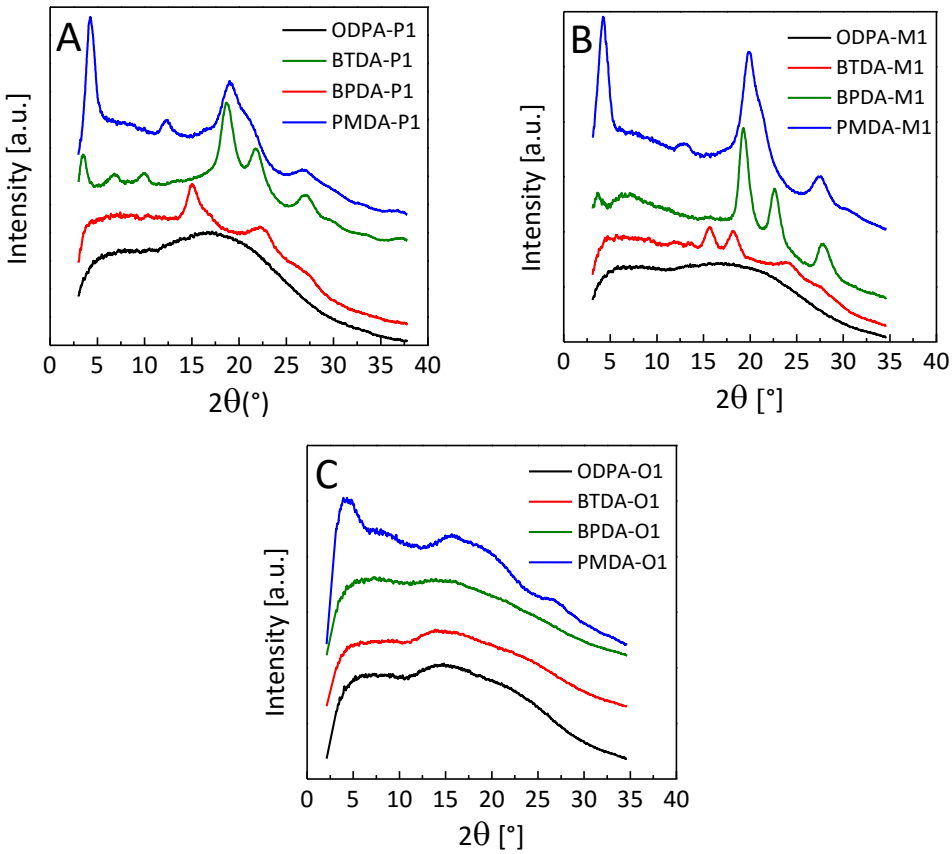

Figure 2.6. Wide angle XRD results of the fully imidized PEI films. The intensity is plotted as a function of the scattering angle. All curves have been normalized to sample thickness and translated vertically for sake of clarity. **A**- P1-series, **B**- M1-series and **C**- O1-series.

All three ODPA-based films are fully amorphous and all three PMDA-based films are semi-crystalline, with the degree of crystallinity decreasing in the order P1>M1>O1. This indicates that the more linear structures pack better, with the kinked structure of O1 only allowing a small degree of crystallinity (4%) in PMDA-O1. Figure 2.6A shows the XRD spectra of all P1-based films. By comparing the ratio of the area under the crystalline peaks to the total area of the curve, the degree of crystallinity in the films was quantified. PMDA-P1

shows the highest degree of crystallinity of 19%, followed by BTDA-P1 and BPDA-P1 with values of 18% and 6%, respectively.

XRD analysis of the M1-based films shows an identical trend in crystallinity (Figure 2.6B), with PMDA-M1 displaying the highest degree of crystallinity (11%), followed by BTDA-M1 (6%) and BPDA-M1 (3%). Within the O1-based series, Figure 2.6C, only PMDA-O1 shows a small degree of crystallinity (4%).

Characteristic peaks corresponding to the lengths of polymer repeating units are observed for all three PMDA-based films and two BTDA-based ones. In the XRD spectrum for PMDA-P1 (Figure 2.6A), the diffraction peak at $2\theta = 4.25°$ corresponds to the repeat unit length of 20.8 Å, and for BTDA-P1 (Figure 2.6A) the diffraction peak at $2\theta = 3.49°$ agrees with the length of repeat unit of 25.3 Å. For PMDA-M1 (Figure 2.6B) a diffraction peak at $2\theta = 4.21°$ corresponds to the length of 21 Å and for BTDA-M1 (Figure 2.6B) the peak at $2\theta = 3.61°$ corresponds to a repeat unit length of 24.5 Å. In case of PMDA-O1 (Figure 2.6C) the peak is not sharp enough for determining the length of the repeat unit.

2.5.6 Gas separation membranes

Polymers PMDA-M1 and PMDA-O1 were too brittle to handle and therefore they could not be tested as gas separation membranes. Attempts were made but significant leaks were observed and therefore the results were omitted.

The permeability of CO_2 is greater than that of CH_4 due to its significantly higher solubility in the polymer.[24] In this series the CH_4 permeability is very low, therefore the focus will be on the CO_2 permeabilities. Figure 2.7 shows the CO_2 permeabilities of 10 PEI membranes as a function of the gas partial pressure at 35 °C, grouped by the diamine moiety for the sake of clarity.

In Figure 2.7A three membranes, ODPA-P1, BTDA-P1 and BPDA-P1, show a very slight decrease in CO_2 permeability with increasing feed pressure. The highest permeability is observed for the PMDA-P1 membrane, going from 1.6 to 1.9 Barrer in the applied pressure range, twice as high as for the other three PEI membranes. The shape of the curve for CO_2 permeability unfortunately indicates plasticization behavior of this polymer. Of the other three polymers not showing plasticization, the ODPA-P1 membrane shows the best performance with an average CO_2 permeability around 0.6 Barrer over the applied pressure range. Performance of BTDA-M1 and BPDA-M1 membranes

appears to be identical, with overlapping low values for CO_2 permeability around 0.1 Barrer (Figure 2.7B). ODPA-M1 shows a slightly higher CO_2 permeability value of 0.3 Barrer. However, this membrane also suffers from plasticization. Same behavior is observed for ODPA-O1 and BTDA-O1. Both polymers appear to be resistant to CO_2 plasticization and show permeabilities of 0.5 and 0.32 Barrer respectively. Interestingly, BPDA-O1 shows a high initial permeability of 1.3 Barrer but this drops rapidly to 0.7 Barrer due to plasticization.

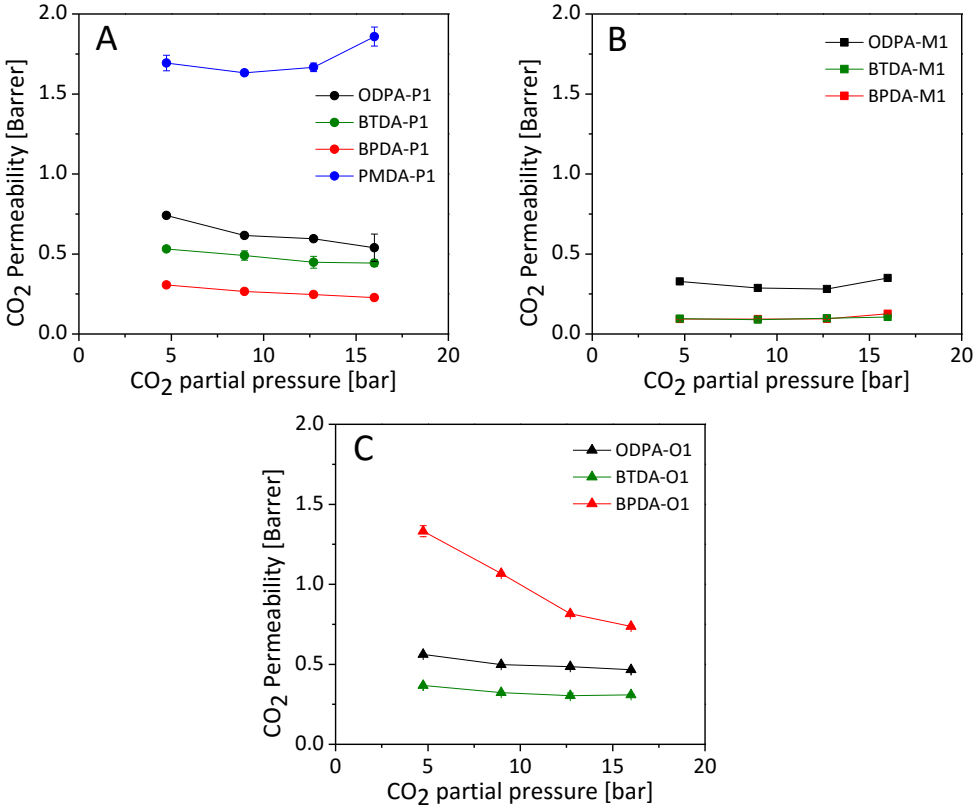

Figure 2.7. CO_2 permeability as a function of gas partial pressure at 35 °C. **A**- P1-series, **B**- M1-series and **C**- O1-based membrane series. Feed mixed gas: CO_2/CH_4 (50/50 vol.%). All measurements were performed *in duplo*.

In both ODPA- and BTDA-based membranes a trend is detected. Permeability of CO_2 for ODPA- and BTDA-based membranes decreases slightly in the order P1>O1>M1 and remains steady throughout the measurements with the mixed feed pressure increase up to 40 bar (17 bar of CO_2 partial pressure). Therefore, if only looking at permeability, up to 40 bar, these six ODPA- and BTDA-based membranes show indication of resistance to plasticization, with CO_2

permeabilities remaining steady when CO_2 pressure increases. High-pressure resistance of all-aromatic PEIs would be one of their most interesting aspects for gas separation applications.

In gas separation, the phenomenon of penetrant induced plasticization is an undesirable feature. Since the transport of the "slow" penetrant, CH_4 in our case, is being more affected, an overall loss in separation performance is observed. The BPDA-O1 membrane displays typical plasticization behavior, indicated by the drop in permeability at increasing pressure. The permeability reaches a minimum and it is assumed that it would increase again with further pressure increase, making the typical plasticization shape of the curve with the lowest value in permeability as a function of CO_2 partial pressure around 17 bar of CO_2. Interestingly, it is only when BPDA is paired with O1 that this plasticization behavior is observed; with permeability dropping from 1.3 to 0.7 Barrer. With the other two diamines the permeability is low and remains stable up to 40 bar. The semi-crystalline BTDA-M1 and BPDA-M1 membranes show the lowest CO_2 permeabilities indicating the more crystalline polymers and are the least permeating of the 10 membranes reported here.

The gas separating abilities of these 10 PEI membranes are shown in Figure 2.8. The values of CO_2/CH_4 selectivities as a function of gas partial pressure are presented as grouped by the diamine moiety.

With increasing pressure, we do not observe large differences in selectivity for the P1-based membranes, as shown in Figure 2.8A. Three membranes show very similar values for selectivity at a feed pressure of 10 bar, selectivity of approximately 47. PMDA-P1 selectivity values are significantly lower than for the other three films at any point. Having the highest value for permeability, it is expected for PMDA-P1 membrane to have the lowest selectivity, due to the trade-off relationship between permeability and selectivity. The selectivities of ODPA-P1, BTDA-P1 and BPDA-P1 remain relatively constant at all feed pressures, with values between 42 and 48. Regardless of the slight decrease in selectivity for BTDA-P1 and BPDA-P1, these materials still have selectivity of around 42 at total feed pressure of 40 bar, which is much higher than the selectivity of the commercially available polyimide Matrimid®, which is reported to be approximately 30 at 35 bar at same temperature and a similar feed composition[23].

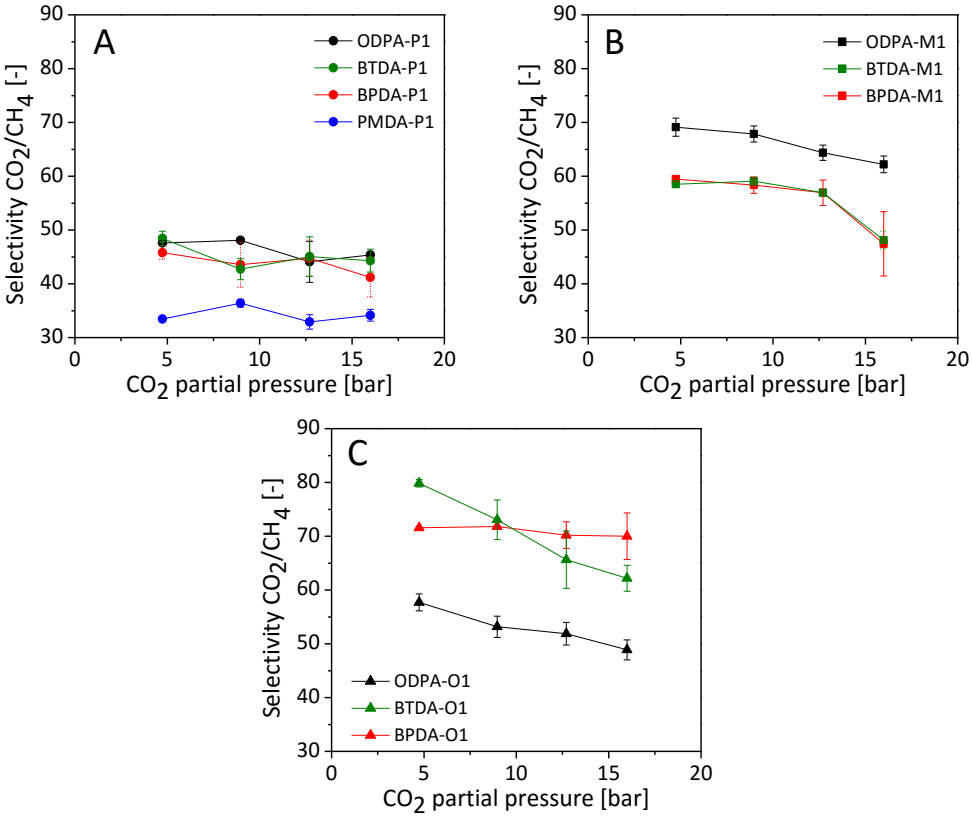

Figure 2.8. CO_2/CH_4 selectivity as a function of CO_2 gas partial pressure. **A**- P1-series, **B**- M1-series and **C**- the O1-based membrane series. Feed mixed gas: CO_2/CH_4 (50/50 vol.%). All measurements were performed *in duplo*.

All three M1-based membranes show higher selectivity values than the P1-based membranes, again an example of the permeability/selectivity trade-off (Figure 2.8B). With increased pressure however, all three membranes show a drop in selectivity (from 58 to 48), indicating plasticization not observable solely by interpreting the permeability values.

ODPA-O1 and BTDA-O1 display the same undesirable plasticization behavior as the M1-based membranes, with their quite high values of permeability dropping significantly as the feed pressure is increased to 20 bar. Selectivity values of BPDA-O1 membrane remain high at 70 regardless of the pressure increase, however, CO_2 permeability drops significantly after the feed pressure is increased signifying plasticization phenomena. This high selectivity value and permeability of 1.3 Barrer would make BPDA-O1 and interesting membrane for applications up to 10 bar and should be subjected to additional ageing studies.

2.6 Conclusions

A homologous series of 12 poly(etherimide)s based on 4 different aromatic dianhydrides and 3 aromatic diamines was prepared with the aim to understand the relationships between the backbone structure of the polyetherimide and their performance as gas separation membranes. These high T_g polymers are characterized by their high thermal stability ($T_{5\%}$ > 500 °C) and excellent mechanical properties (E' = 4-8 GPa at 30 °C). As gas separation membranes, these materials have shown low values for permeability, high selectivity and resistance to plasticization and stable high-pressure performance. The highest permeability was observed for the PMDA-P1 membrane, going up to ~2 Barrer in the applied pressure range, which is twice as high as for the other P1-based membranes. Unfortunately, the CO_2 permeability curve of PMDA-P1 indicates plasticization behavior. Of the other P1 membranes not suffering from plasticization, ODPA-P1 shows the best performance with an average CO_2 permeability around 0.6 Barrer throughout the applied pressure range. The selectivities of ODPA-P1, BTDA-P1 and BPDA-P1 membranes remain relatively constant at all feed pressures, with values between 42 and 48, making them attractive candidates for further high-pressure application studies. All M1-based membranes show CO_2 induced plasticization, which drops selectivity values from 58 to 48. For all ODPA- and BTDA-based membranes a trend is identified in which the permeability increasing slightly in the order P1>O1>M1. The permeability remains stable up to 40 bar, which is evidence that ODPA- and BTDA-based membranes do not suffer from plasticization. This study has yielded two interesting PEI membranes that need to be investigated in more detail. The OPDA-P1 membrane, which exhibits high selectivity and resistance to plasticization up to 40 bar and the BPDA-O1 membrane. The latter is of interest because of its high selectivity (70) and permeability (1.3 Barrer). For both polymers additional gas permeation experiments using different feed compositions and ageing studies are required.

2.7 Appendix A: GPC curves

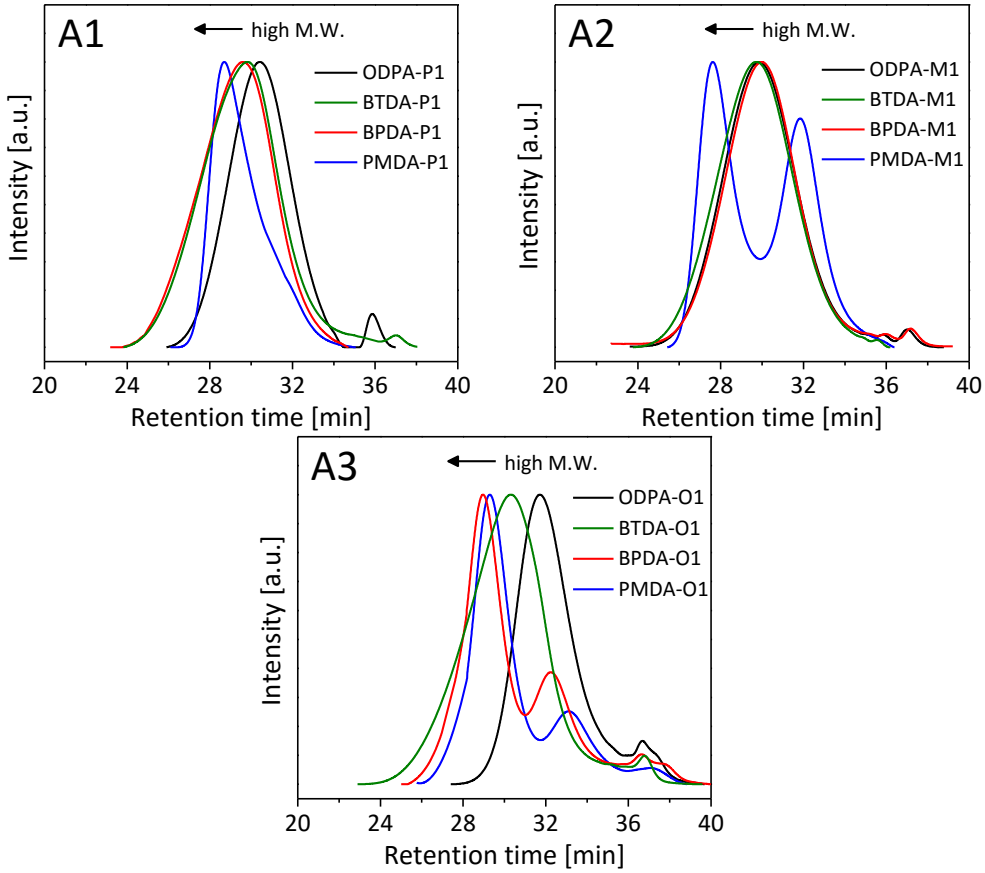

Figure A. GPC curves obtained for polyamic acid intermediates of series based on **A1**- P1, **A2**- M1 and **A3**- O1. The removal of any possible solids in the polyamic acids, prior to a GPC run, is done by filtration of the solution through a 0.45 μm PTFE filter.

2.8 References

[1] W. J. Koros, G. K. Fleming, *J. Membr. Sci.* **1993**, *83*, 1.

[2] C. E. Powell, G. G. Qiao, *J. Membr. Sci.* **2006**, *279*, 1.

[3] S. Basu, A. L. Khan, A. Cano-Odena, C. Liu, I. F. J. Vankelecom, *Chem. Soc. Rev.* **2010**, *39*, 750.

[4] G. T. Rochelle, *Science* **2009**, *325*, 1652.

[5] K. Simons, PhD Thesis, *Membrane Technologies for CO_2 Capture*, University of Twente, **2010**, 12.

[6] S. Matteucci, Y. Yampolskii, I. Pinnau, B.D. Freeman, Chapter 1 in: Y. Yampolskii, I. Pinnau, B.D. Freeman (Eds.), *Materials Science of Membranes for Gas and Vapor Separation*, John Wiley & Sons, Chichester, UK, **2006**, 2.

[7] I. Rose, M. Carta, R. Malpass-Evans, M. Ferrari, P. Bernardo, G. Clarizia, J. C. Jansen, N. B. McKeown, *ACS Macro Lett.* **2015**, 4.

[8] L. M. Robeson, *J. Membr. Sci.* **2008**, *320*, 390.

[9] L. M. Robeson, *J. Membr. Sci.* **1991**, *62*, 165.

[10] A. Y. Alentiev, K. A. Loza, Y. P. Yampolskii, *J. Membr. Sci.* **2000**, *167*, 91.

[11] P. Tin, *J. Memb. Sci.* **2003**, *225*, 77.

[12] T. Visser, N. Masetto, M. Wessling, *J. Membr. Sci.* **2007**, *306*, 16.

[13] J. Xia, T. Chung, D. R. Paul, *J. Membr. Sci.* **2014**, *450*, 457.

[14] H. B. Park, C. H. Jung, Y. M. Lee, A. J. Hill, S. J. Pas, S. T. Mudie, E. Van Wagner, B. D. Freeman, D. J. Cookson, *Science* **2007**, *318*, 254.

[15] C. Staudt-Bickel, W. J. Koros, *J. Membr. Sci.* **1999**, *155*, 145.

[16] J. D. Wind, C. Staudt-Bickel, D. R. Paul, W. J. Koros, *Macromolecules* **2003**, *36*, 1882.

[17] Y. Liu, R. Wang, T. Chung, *J. Membr. Sci.* **2001**, *189*, 231.

[18] K. Simons, K. Nijmeijer, J. G. Sala, H. van der Werf, N. E. Benes, T. J. Dingemans, M. Wessling, *Polymer* **2010**, *51*, 3907.

[19] J. G. Wijmans, R. W. Baker, *J. Membr. Sci.* **1995**, *107*, 1.

[20] B. D. Freeman, H. Q. Lin, *Permeation and Diffusion* in: H. Czichos, T. Saito, L. Smith (Eds.), *Springer Handbook for Materials Measurement Methdods*, Springer, New York, New York, USA, **2006**, 371.

[21] T. J. Dingemans, E. Mendes, J. J. Hinkley, E. S. Weiser, T. L. StClair, *Macromolecules* **2008**, 2474.

[22] G. C. Eastmond, J. Paprotny, *Synthesis* **1998**, *6*, 894.

[23] A. Bos, PhD Thesis, *High Pressure CO_2/CH_4 Separation With Glassy Polymer Membranes*, University of Twente, **1996**, 25.

[24] S. A. Stern, *J. Membr. Sci.* **1994**, *94*, 1.

CHAPTER 3

Free volume in PEI membranes measured by positron annihilation lifetime spectroscopy (PALS) and positron annihilation Doppler broadening (PADB)

In order to characterize the free volume of our all-aromatic PEI membrane series we utilized two positron annihilation techniques, positron annihilation lifetime spectroscopy (PALS) and positron annihilation Doppler broadening (PADB). First PADB, a fast and convenient method, indicated differences in free volume of all PEIs investigated, whereas PALS experiments gave more quantitative information with respect to the size and distribution of the voids. PADB results show that *S*, *W* pairs for this PEI-series tend to group according to their dianhydride moiety, meaning that in this series dianhydrides govern the differences in *S* parameter, indicating more free volume. The semi-crystalline PMDA-based PEI samples exhibit the lowest *S* parameter, while the amorphous ODPA-based samples all lie on the higher *S* side of the *S*-*W* plot, with ODPA-P1 really standing out with the highest *S* parameter. The same could be confirmed and quantified by PALS, where ODPA-P1 is the only membrane in this series with its free volume described by both smaller and larger free volume elements. The larger voids in ODPA-P1 can be characterized as having a radius *R* of 3.3 Å, which is 5 times larger than the lowest measured free volume content in this series observed for BPDA-M1, which has voids with a radius *R* ≈ 0.7 Å. When comparing results obtained by PADB and PALS a very good correlation is observed between the *S* parameter (determined by PADB) and the free volume content (quantified by PALS).

3.1 Introduction

Glassy polymers are inherently non-equilibrium systems where excess free volume exists.[1] This excess free volume is kinetically confined within the polymer matrix due to a rapid increase in the polymer chain relaxation upon vitrification. Essentially, because of the excess free volume, the polymer effectively becomes a two-component system; an equilibrium polymer matrix containing an additional void fraction.[2]

While the relaxation behavior of polymers is well understood [3], only limited information is available about the free volume. What are the dimensions of the voids? What is their distribution in terms of size and shape?[4] This is primarily due to a lack of suitable techniques to probe open volumes of such dimensions. In this chapter we will report on the free volume of the polyetherimide (PEI) series presented in Chapter 2, as measured using 2 different positron annihilation techniques. The techniques are positron annihilation lifetime spectroscopy (PALS) and positron annihilation Doppler broadening (PADB). Both techniques enable monitoring, in a non-destructive way and at the atomic level, of the free volume in polymers.[5–12] Free volume data obtained by PALS have been effectively linked with transport properties of polymer membranes.[10–14]

In particular PALS has developed into a very powerful technique for studying free volume in polymers.[5–8] In work by G. Dlubek *et al.* polyimides and poly(etherimide)s were studied using a variable-energy positron beam in combination with a Doppler broadened annihilation radiation technique.[15] The polymers were irradiated with boron ions, which causes changes in structure and composition. With this method they could profile the modification-depth or damage-depth, since penetration depth of positrons can be controlled. Inhibition of positronium formation by polar groups in Kapton® and PMMA was studied by Shantarovich *et al.* [16] using coincidence Doppler broadening (CDB) and the results were compared to PMMA. Polyimide Kapton® has a higher permeability for oxygen and a higher free volume. On the CDB ratio curve Kapton® shows a high momentum component typical for positron annihilation on oxygen. Recently Chung and Le [17] characterized the mean depth profiles of dual-layer hollow fibers by by $2\gamma/3\gamma$ ratio measurements. This polymer blend of polyimide and sulfonated polyimide has been investigated as a layer for ethanol dehydration and this method was used to

validate the change in the structure of the water-selective layer. A paper by Eastmond *et al.*[7] reports that there is a correlation between the void structure measured by PALS and the gas permeability of poly(etherimide)s. Positron lifetimes and intensities differ systematically with variations in polymer backbone structure and composition, and is therefore ideal to study the relationship between permeability and separation of CO_2 and CH_4 in polymer-based membranes. The experimentally measured lifetimes represent the average of spherical free volume elements, where the larger lifetime values correspond to a larger free volume elements.[10] Although a good deal of PALS experiments have been reported on PEIs, thus far a methodical study on a systematic series of all-aromatic PEI-based membranes is lacking. In this chapter we report the results of a comparative PADB and PALS study. Both techniques were used to probe the free volume of a homologous PEI-based membrane series as discussed in Chapter 2.

3.2 Theory behind positron annihilation techniques

The antimatter counterpart of an electron, a *positron*, is generated by positron emission radioactive decay from a radioactive source. In polymers, a positron may form a system called *positronium* (Ps), which is a bound state comprised of an electron and a positron bound together in an exotic atom. Ps is formed in two states in a 3:1 ratio, consisting of *ortho*-positronium (o-Ps, a parallel spin complex of a positron and an electron) and *para*-positronium (p-Ps, an antiparallel spin complex), shown in Figure 3.1. The intrinsic lifetimes of o-Ps and p-Ps (*i.e.* vacuum lifetimes) are 142 ns and 125 ps, respectively.

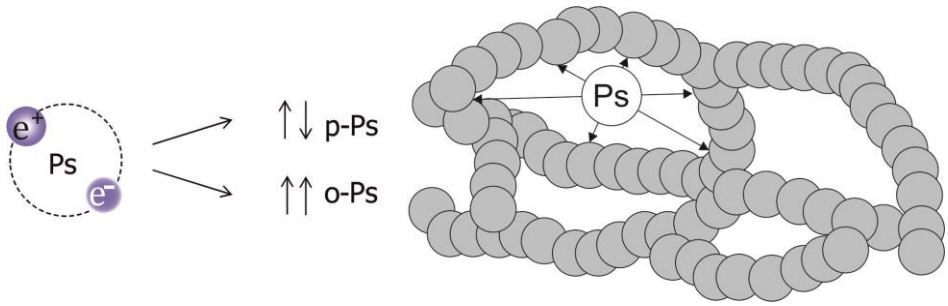

Figure 3.1. Positronium formation and localization in a void of the polymer's free volume: when an electron and a positron have parallel spin-states they can combine to form *ortho*-positronium, and o-Ps can have a lifetime on the order of nanoseconds in electron deficient regions of a polymer (*i.e.* free volume elements).[4,18]

Para-Ps decays into two 511 keV annihilation photons (γ), while o-Ps intrinsically decays into three annihilation photons with energies distributed from 0 to 511 keV. However, during the many collisions that o-Ps undergoes with the surrounding polymer, it has a finite probability of annihilating with an opposite spin electron from the surrounding polymer (not its bound partner), a process generally known as the *pick-off*.[4] This pick-off reaction competes with the o-Ps self-annihilation and sharply reduces the long o-Ps lifetime to typically 1-3 ns, depending on the collision frequency.[18]

Because of the change in electron spin, two 511 keV photons are emitted. A third o-Ps annihilation mode is by conversion into p-Ps through exchange of the parallel spin electron of o-Ps with an anti-parallel spin electron from the surrounding polymer. This p-Ps then self-decays within 125 ps by two photon emission. Positrons that do not form a positronium annihilate with an electron of the atoms of the polymer molecules. In polymers the lifetime component associated with this direct two photon annihilation mode lies between 200–400 ps. The collision frequency of the Ps with the surrounding polymer molecules will depend on the dimensions of the confining volume because the local electron density is lower in larger holes. This results in a highly sensitive correspondence of the o-Ps pick-off rate (and thus the lifetime) to the free volume hole size [19–22].

In a so-called delayed coincidence PALS experiment (Figure 3.2) we measure a pair of "start" and "stop" signals. This corresponds to the time interval between the detection of the 1.27 MeV photon, emitted by ^{22}Na almost simultaneously with the positron, and the 511 keV annihilation photon. By accumulating many coincidence events (typically > 10^6) a *lifetime spectrum* is obtained, which consists of several exponentially decaying lifetime components with corresponding intensities.[19,20]

As a result of momentum conservation during the above-mentioned two photon annihilation processes (positrons that do not form positronium), the measured energy of annihilation photons is shifted (according to equation 3.1.) by an amount of

$$\Delta E = \pm\, p \cdot c/2 \tag{3.1}$$

where c is the speed of light and p the momentum component of the *electron* in the direction of photon emission. In an annihilation photon energy spectrum

these shifts give rise to a *Doppler broadening* of the 511 keV photo peak. In case of localization (or trapping) of positrons in open-volume defects the fraction of low momentum valence electrons taking part in the direct annihilation process is larger compared to (higher momentum) core electrons. In particular in crystalline solids (such as metals) this introduction of open-volume defects leads to a narrower annihilation photo peak in comparison to the same but defect-free material. In addition, in polymers the decay of p-Ps exhibits an even narrower energy distribution because of its intrinsic zero electron-positron momentum. Since in regions with low electron density Ps is formed more readily such a narrow distribution can hint at the presence of open volume.[23–25]

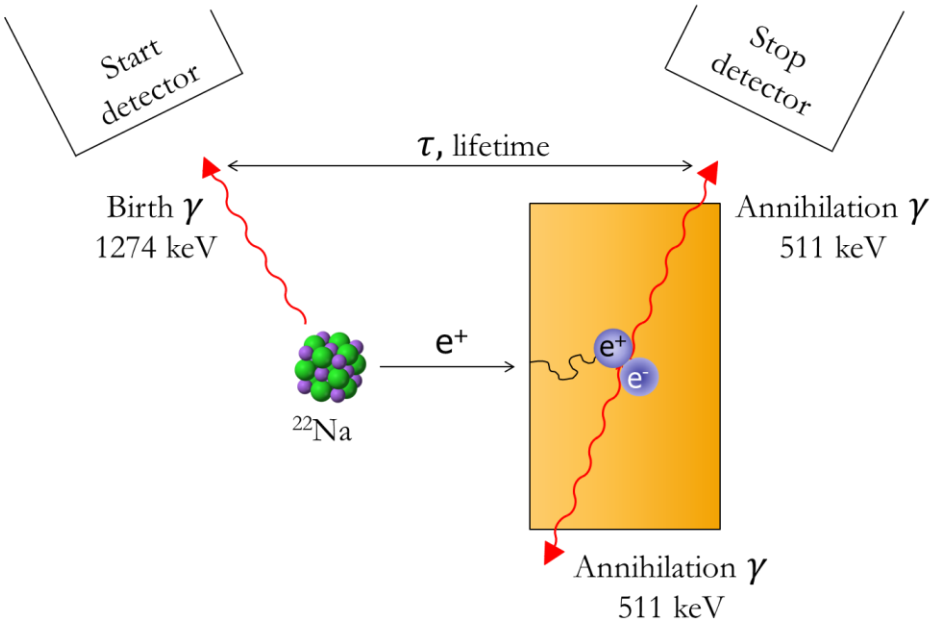

Figure 3.2. Schematic overview of a PALS experiment. The time between detecting a pair of signals from the emission of a positron, emanating from a radioactive source (^{22}Na), and the detection of annihilation gammas corresponds to the *lifetime* of a positronium (τ).

The Doppler broadening of the 511 keV photo peak is quantified by two specific line shape parameters *S* and *W* (shown in Figure 3.3). The *S* (sharpness) parameter describing the area under the curve immediately around the peak (A_S) and the *W* (wing) parameter describing the area under the left and right wings of the curve (W_L + W_R), both normalized over the total area (A_T). The higher the

S/*W* ratio, the larger the number of the free volume voids within a polymeric material.[25]

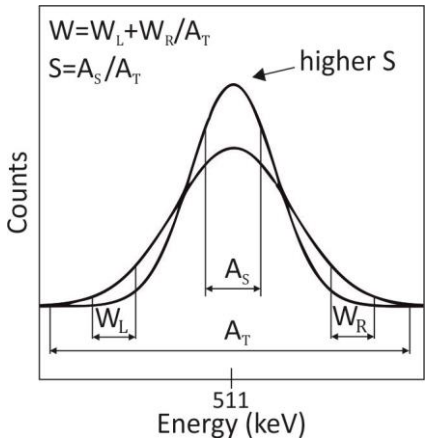

Figure 3.3. Doppler broadening of the 511 keV photo peak. The *S* parameter is defined as the ratio of the central peak area (A_S) to the total area (A_T) while the *W* parameter is defined as the ratio of the tail areas (W_L + W_R) to the total peak area.[25]

3.3 Experimental

3.3.1 Positron annihilation Doppler broadening (PADB)

In this study the PADB experiments were performed with the Delft Variable Energy Positron beam (VEP). Positrons emitted from a radioactive ^{22}Na source are, after moderation to thermal energies and subsequent acceleration, injected in the PEI films with a kinetic energy ranging from 100 eV to 25 keV. The beam intensity is about 10^4 positrons per second and the beam diameter at target is about 8 mm. The mean implantation depth of the positrons $\langle z \rangle$ scales with the implantation energy according to:

$$\langle z \rangle = \frac{A}{\rho} \cdot E^{1.62} \tag{3.2}$$

Here A is a material independent parameter (4.0 μg cm^{-1} keV$^{-1.62}$), ρ is the density of the polymer (g/cm^3) and E the positron implantation energy (keV). In the polymers with a density of about 1.4 g/cm^3 the maximum mean positron implantation depth is about 4 μm. As the thinnest sample had a thickness of 7 μm the Doppler data were taken at an implantation depth around 2 μm to avoid

contributions of positrons implanted in the vicinity of the front- or backside surface.

The *S* parameter was calculated as the ratio of the counts registered in a fixed central momentum window ($|p_{//}| < 3.5\times10^{-3}$ m_oc) to the total number of counts in the photo peak. This choice of the momentum window makes the *S* parameter sensitive to annihilations with low momentum valence electrons or as p-Ps. Similarly, the *W* parameter is obtained from the high momentum regions (W_{left} and W_{right}) (10×10^{-3} $m_oc < |p_{//}| < 26\times10^{-3}$ m_oc) and accounts for annihilations with high momentum core electrons. The energy resolution of the detector setup is 1.2 keV at 511 keV. PADB measurements were performed at 25 °C.

3.3.2 Positron annihilation lifetime spectroscopy (PALS)

Positron lifetime measurements were carried out with the digital positron lifetime spectrometer at Charles University in Prague, as described in detail elsewhere,[26] with a time resolution of 143 ps full width at half maximum (FWHM). The resolution function was obtained by fitting the positron lifetime spectrum of an annealed Mg reference sample. At least 10^7 annihilation events were accumulated in each positron lifetime spectrum measurement. PALS measurements were performed at 25 °C.

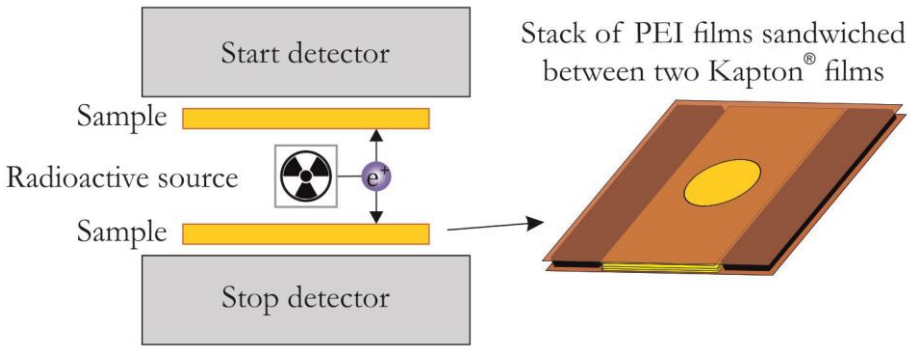

Figure 3.4. PALS was performed by sandwiching a radioactive source with stacks of polymer film samples from both sides and counting the positron formation (start) and annihilation (stop) events that occur within the analyte.

Sample preparation. A $^{22}Na_2CO_3$ positron source (2 mm in diameter) with an activity of ~1 MBq was deposited on a 2-μm thick Mylar® foil, sandwiched between two stacks of 20 mm × 20 mm polymer films (held together by a

Kapton® casing), each approximately 0.6 mm thick ensuring that a minimum of 93% of positrons from the source annihilate within the sample (Figure 3.4). Since our 12 PEI films have different thicknesses (varying from 10 μm to 35 μm) the number of films in the stacks varied between 18 and 50 to ensure a minimum thickness of 0.6 mm. The source contribution consists of two components: the positron annihilation within the $^{22}Na_2CO_3$ source itself and positron annihilation in the Mylar® foil, with lifetimes of 368 ps and 1 ns and relative intensities of 7.2% and 0.3%, respectively.

PALS spectra were collected and de-convoluted into 3 lifetimes and intensity components. From the o-Ps lifetime data an estimate of the average radius of free volume elements (R) in the polymer is obtained by using the Tao–Eldrup model:

$$\tau_{o-Ps} = \frac{1}{\lambda_A}\left(1 - \frac{R}{R+\Delta R} + \frac{1}{2\pi}\sin\left[2\pi\frac{R}{R+\Delta R}\right]\right)^{-1} \tag{3.3}$$

Here τ_{o-Ps} is the reduced o-Ps lifetime and ΔR is the empirical electron layer thickness of 1.66 Å. $\lambda_A = \frac{\lambda_{p-Ps}+3\,\lambda_{o-Ps}}{4} = 2\,ns^{-1}$ is the spin averaged Ps annihilation rate in vacuum with λ_{p-Ps} and λ_{o-Ps} the annihilation rates of the singlet and triples state, respectively.[27,28]

The average volume of the free volume elements, V_{FVE}, can be calculated using equation 3.4.[29]

$$V_{FVE} = \frac{4\pi}{3}R^3 \tag{3.4}$$

The fractional free volume (FFV) is then proportional to the product of V_{FVE} and I_{o-Ps}

$$FFV = kV_{FVE}I_{o-Ps} \tag{3.5}$$

where k is a scaling parameter whose value has been experimentally determined to be 0.018 nm^{-3} [11,18,30].

3.3.3 Materials

For this study we used a homologous series of 12 PEI membrane films, their synthesis and properties are introduced and described in Chapter 2. Our aim is

to understand the relationship between the backbone structure of the polyetherimide, the free volume characteristics and the gas permeating capability. Structures of the diamines were designed so that they have a *para*-, *meta*-, or *ortho*-based aryl ether "flexible" spacer unit between the two terminal phenylamine functionalities (Scheme 3.1). Three diamines chosen for this study are P1, M1 and O1. Four different dianhydride moieties have been selected to systematically change the flexibility of the PEI backbone, to tailor the segmental mobility, and the non-equilibrium excess free volume of the polymer (Scheme 3.1). All ODPA-based PEI membranes are amorphous, while all PMDA-based ones are semi-crystalline, the degrees of crystallinities can be found in Scheme 3.1 where the colored shading is used as a guide for the eye.

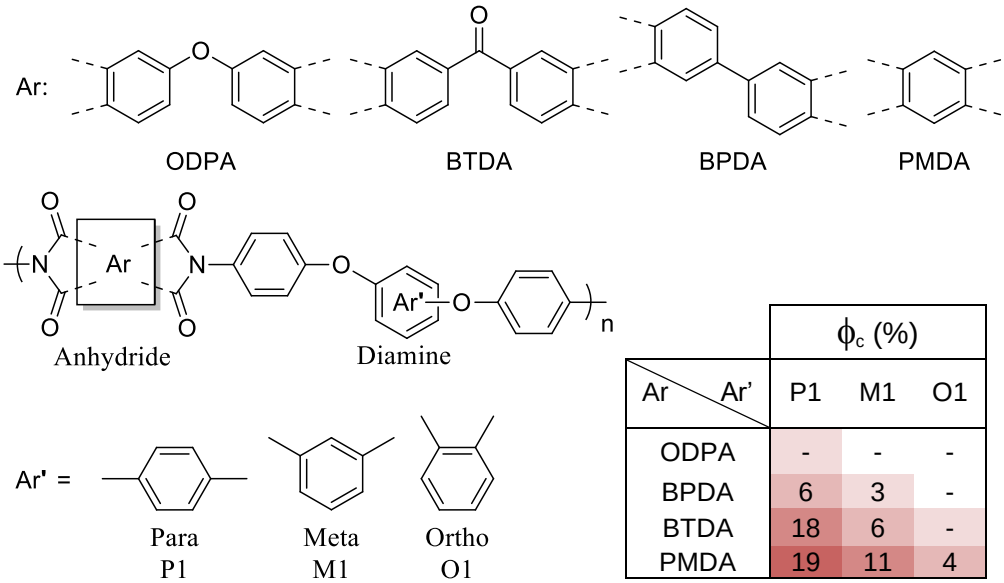

Ar \ Ar'	ϕ_c (%) P1	M1	O1
ODPA	-	-	-
BPDA	6	3	-
BTDA	18	6	-
PMDA	19	11	4

Scheme 3.1. Chemical structure of PEIs with different dianhydride and diamine moieties. Table insert shows the tailoring of the degree of crystallinity (ϕ_c in %) with the inclusion of more rigid monomers.

3.4 Results

3.4.1 Positron annihilation Doppler broadening

PADB measurements on our 12 PEI films were performed *in duplo* at the Delft Variable Energy Positron beam facility. After analysis, data are presented in an *S-W* map as shown in Figure 3.5. It is immediately clear from this plot that the

(*S*, *W*) pairs for these polymers group according to their chemical composition. Looking at the *S* parameter it seems that the major differentiator is the dianhydride moiety. The rigid PMDA-based PEI samples are located at the lower *S* and higher *W* side of the plot, while the flexible ODPA-based samples all lie on the higher *S*, lower *W* side; whereas the other two polymer groups (BPDA- and BTDA-based) are located in between.

The resulting *S* parameter values, from low to high, follow the sequence: PMDA~BTDA> BPDA>ODPA. Recall that a high *S* value is associated with a narrow momentum distribution (*i.e.* low momentum annihilations either via direct annihilation with valence electrons or through p-Ps decay) this sequence can be interpreted as reflecting an increase in free volume, either by size or by concentration.

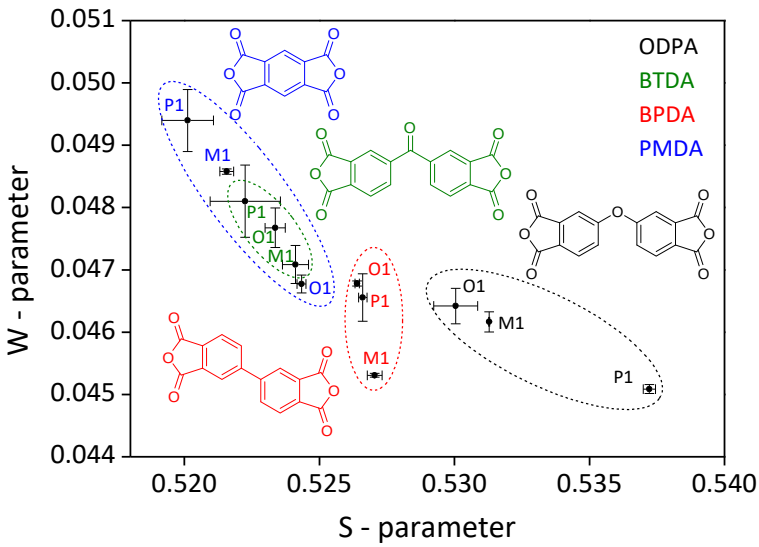

Figure 3.5. *S*-*W* plot from PADB measurements showing the Doppler broadening parameters of all 12 PEI film samples summarized in a single *S*-*W* map.

Gas permeation results, discussed in detail in Chapter 2, have shown that ODPA-P1 is the most permeable and plasticization-resistant membrane. The high permeability of this membrane is second to only the PMDA-P1 membrane. However, it has been found that the high permeability exhibited by PMDA-P1 stems from the sorption capacity of this membrane, not the free volume content. The high affinity of CO_2 towards the PMDA-P1 backbone (Chapter 4) results in plasticization and an increase in gas permeation (Chapter 2). This

correlates well with the PADB results, where we identified PMDA-P1 as the material with the least amount of free volume, *i.e.* similar to Kapton® [16], as was expected based on the backbone composition and chain packing ability. On the other end of the spectrum, within the ODPA-based membrane series, ODPA-P1 really stands out with the highest value of *S*, compared to ODPA-M1 and ODPA-O1. This indicates that in this group the kinked diamines, and the associated larger local dipole moments, do not have much of an effect on the free volume. The most rigid and symmetric analog within this group, ODPA-P1, does not crystalize and thus generates the most free volume. Generally, a more prominent and rigid kink in the polymer backbone is expected to create more free volume in the material by inhibiting efficient chain packing [8,31–33], however M1 and O1 are not as rigid as P1, whose linear backbone in combination with a flexible ODPA moiety causes packing in such a way that it creates more free volume.

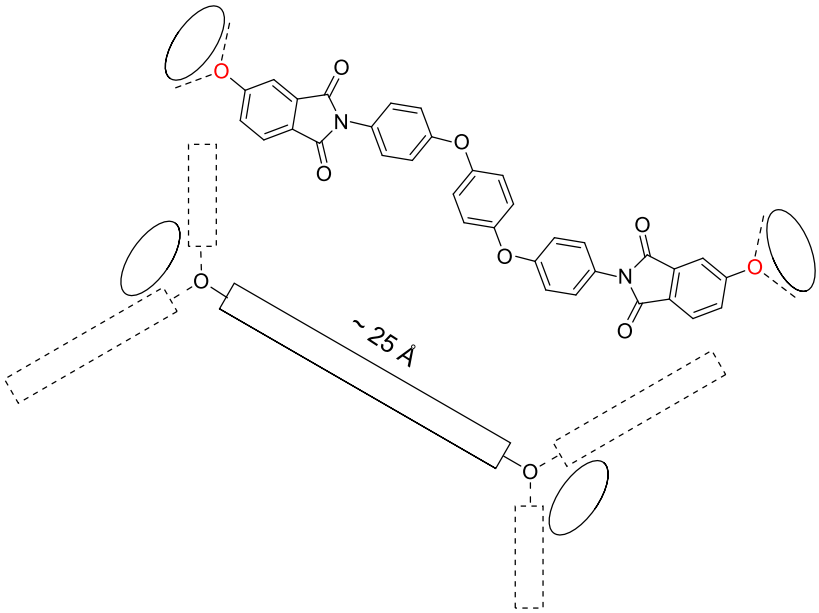

Scheme 3.2. Schematic representation of the structural rigidity of the ODPA-P1 repeating unit and rod-like depiction of the P1 moiety.

The P1 diamine generates the most free volume because rotation around the diamine Ar-O-Ar bonds does not change the overall shape of the moiety between the dianhydride oxygen bridges. In principle, an amorphous network is built using rigid rods of 25 Å (Scheme 3.2). The average length of the rods for M1 and O1 are shorter.

3.4.2 Positron annihilation lifetime spectroscopy

In order to quantify the free volume differences indicated by PADB and to gain more insight into the free volume size and distribution, lifetime experiments on selected samples have been carried out. Table 3.1 shows the PALS results for 10 PEI films. Polymers PMDA-M1 and PMDA-O1 are very brittle and difficult to handle, therefore it was not possible to stack enough defect-free films required for PALS experiments (unlike for PADB, where only one defect-free film is sufficient).

The shorter component with lifetime τ_1 and intensity I_1 represents a contribution from positrons annihilated as free particles while the long lived components τ_{o-Ps} are associated with the pick-up annihilation of ortho-Ps. The lifetime of p-Ps self-annihilation was fixed at 125 ps and the ratio of o-Ps to p-Ps contribution was kept at 3:1. In the table I_{Ps} denotes the total intensity of the Ps contribution (*i.e.* p-Ps plus o-Ps). The mean size (radius R) of free volumes can be estimated using the Tao-Eldrup equation (Equation 3.3) and is also given in the Table 3.1.

A first look at the P1-based series shows that in case of the ODPA-P1 membrane it was necessary to use two Ps components in order to achieve a good fit. Hence, the ODPA-P1 sample exhibits two distinguishable free volume elements:

(i) smaller ones characterized by o-Ps lifetime $\tau_{o-Ps-1} \approx 0.80$ ns and

(ii) larger ones characterized by o-Ps lifetime $\tau_{o-Ps-2} \approx 2.3$ ns

All other 9 PEIs contain only the smaller open volumes since the o-Ps component with lifetime 2.3 ns could not be detected.

Moreover, the mean size of the smaller volumes in ODPA-P1 is larger than in the other three P1-based samples. In particular PMDA-P1 sample exhibits the smallest free volume size among all P1-based samples studied ($\tau_{o-Ps-1} \approx 0.66$ ns corresponding to $R \approx 0.1$ nm).

Table 3.1. Summarized PALS results. The o-Ps lifetime and intensity, average radius of free volume elements, average volume of free volume elements and fractional free volume.

Polymer	τ_1 (ps)	I_1 (%)	τ_{o-Ps-1} (ns)	I_{Ps-1} (%)	R_1 (nm)	V_{FVE} (nm^3)	FFV (%)	τ_{o-Ps-2} (ns)	I_{Ps-2} (%)	R_2 (nm)	V_{FVE} (nm^3)	FFV (%)
ODPA-P1	363.3	88.7	0.80	8.8	0.13	0.009	0.15	2.3	2.5	0.33	0.151	0.68
BTDA-P1	361.4	94.7	0.71	5.3	0.11	0.006	0.05	-	-	-	-	-
BPDA-P1	362.7	95.5	0.72	4.5	0.11	0.006	0.05	-	-	-	-	-
PMDA-P1	371.5	95.8	0.66	4.2	0.10	0.004	0.03	-	-	-	-	-
ODPA-M1	366.4	96.0	1.10	4.0	0.18	0.025	0.18	-	-	-	-	-
BTDA-M1	369.8	100	-	-	-	-	-	-	-	-	-	-
BPDA-M1	352.6	89.9	0.57	10.1	0.07	0.001	0.03	-	-	-	-	-
ODPA-O1	368.6	96.1	1.15	3.9	0.19	0.029	0.20	-	-	-	-	-
BTDA-O1	374.4	100	-	-	-	-	-	-	-	-	-	-
BPDA-O1	367.0	95.5	0.77	4.5	0.12	0.007	0.06	-	-	-	-	-

In M1- and O1-based PEI membranes it was interesting to see that the BTDA-M1 and BTDA-O1 PEIs do not show any o-Ps formation, the intensities were below the detection limit, similar to what was observed for Kapton®[16] indicating poor membrane performance. In the M1- and O1-based series, the ODPA-based PEI membranes have the highest free volume, actually higher than that of the "smaller volumes" of ODPA-P1. However, unlike ODPA-P1, these two do not exhibit the "larger type" free volumes. BPDA-O1 shows similar values in free volume size to that of BPDA-P1 and BTDA-P1, while BPDA-M1 shows the lowest measurable free volume content in the whole series characterized with o-Ps lifetime of $\tau_{o-Ps-1} \approx 0.57$ ns corresponding to radius $R \approx 0.07$ nm. This is almost 5 times smaller than the radius of larger free volume voids observed for ODPA-P1 characterized with a radius of 0.33 nm (or 3.3 Å).

Analogous to the PADB measurements, we observed that the free volume content results for this PEI series can also be grouped according to dianhydride moiety. With ODPA-based materials exhibiting the highest free volume content, followed by significantly lower values for BPDA-based membranes and next to none for PMDA- and BTDA-based ones.

The relation between the PADB and PALS measurements is visualized in Figure 3.6 by indicating the values of radii of free volume voids R in the PADB *S-W* plot. For sake of clarity, we focused on the P1-based series. It shows a good correlation between *S* parameter obtained by PADB and free volume radius obtained by PALS, with the PADB component indicating what the PALS component is quantifying. The larger free volume void is indicated both with the *S*-parameter and the calculated radius.

By plotting the o-Ps lifetime components against the Doppler broadening *S* parameter a good agreement between PADB and PALS results was observed, as shown in Figure 3.7. The *S* parameter positively follows the trend of o-Ps lifetime, more so than the o-Ps intensity, and appears to be more affected by the amount of positronium formed.

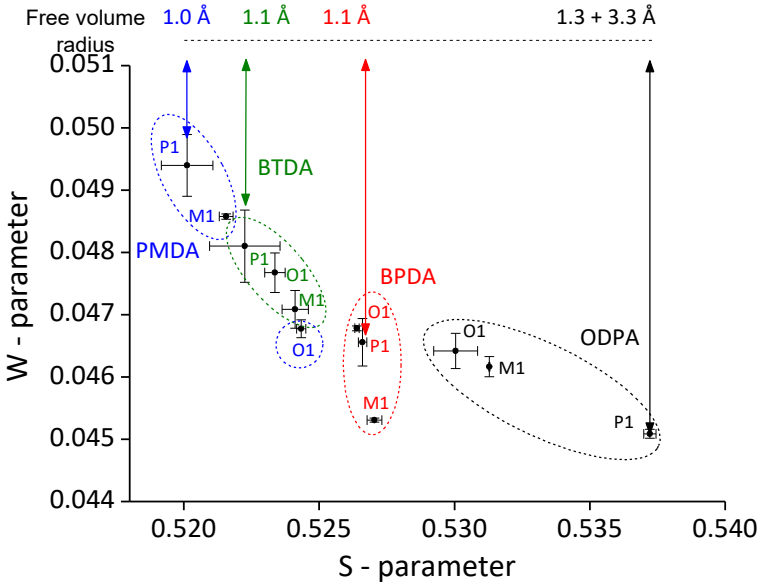

Figure 3.6. Free volume indicated by the PADB *S* parameter and quantified by PALS, focusing on P1-based PEIs with four distinctive dianhydride moieties.

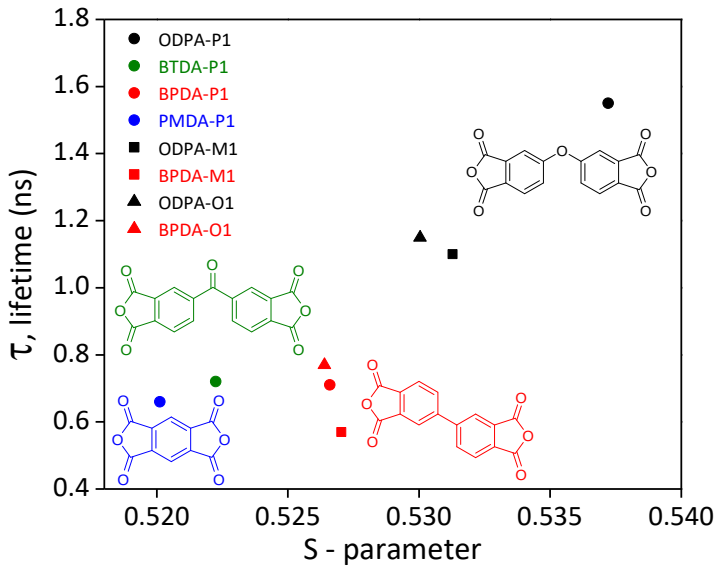

Figure 3.7. o-Ps Lifetime versus *S* parameter.

In polyimides, formation of positronium is strongly inhibited by oxygen atoms in the conjugated five member cycles, these are expected to be strong positron scavengers, reducing the chance of Ps formation.[16] A well-known example is Kapton®, in which Ps is not observed. Our polyetherimide PMDA-P1 has a

structure very similar to that of Kapton®, which is poly-oxydiphenylene-pyromellitimide (PMDA-ODA) and in our results PMDA-P1 has the lowest value for *S* parameter, confirming its similarity to Kapton®. These two materials are both closely packed and semi-crystalline and have poor membrane performances.

3.5 Conclusions

We have investigated the free volume of a homologous series of all-aromatic polyetherimide-based membranes using two positron annihilation techniques, PALS and PADB. Both techniques allowed us to monitor the free volume of this important class of membranes in a non-destructive manner and at the atomic level. PADB proved to be a fast and convenient method to assess differences in free volume of all-aromatic PEIs whereas PALS experiments gave more quantitative information with respect to the size and number of Angstrom-scale voids. In cases where a quick estimation of relative differences between the free volumes in PEIs is needed, PADB was demonstrated to be the preferred method.

From the PADB experiments the resulting *S, W* pairs for these polymers show a tendency to group according to their dianhydride composition, meaning that the dianhydride governs the differences in *S* parameter. The PMDA-based PEI samples are located at the lower *S* and higher *W* side of the plot, while the ODPA-based samples all lie on the higher *S*, lower *W* side with ODPA-P1 really standing out. The same trend was observed by PALS, where ODPA-P1 is the only polymer in the series with its free volume defined by both smaller and larger free volume elements. These characteristics are quantified with an o-Ps lifetime component that can estimate the radius of the free volume that the o-Ps resided in using the Tao-Eldrup model. In case of ODPA-P1, the larger voids have a radius of 3.3 Å, which is 5 times larger than the lowest measured free volume content in this series observed for BPDA-M1, which has a radius $R \approx$ 0.7 Å.

It is clear that the main factor for higher permeability of PMDA-P1 is not the free volume but rather the solubility of CO_2 in the membrane material. Membranes based on the other three dianhydrides have similar gas separation properties with the best performing one being the one with the largest free volume, ODPA-P1. Specifically this membrane shows potential for real application in high-pressure gas separation processes.

3.6 References

[1] M. R. Tant, G. L. Wilkes, *Polym. Eng. Sci.* **1981**, *21*, 874.

[2] W. Ogieglo, H. Wormeester, M. Wessling, N. E. Benes, *Polymer* **2014**, *55*, 1737.

[3] E. Donth, *The Glass Transition: Relaxation Dynamics in Liquids and Disordered Materials*, Springer-Verlag, Berlin, Germany, **2001**, 156.

[4] G. Dlubek, D. Kilburn, V. Bondarenko, J. Pionteck, R. Krause-Rehberg, M. A. Alam, *Macromol. Symp.* **2004**, *210*, 11.

[5] R. Zhang, J. Robles, J. Kang, H. Samha, H. M. Chen, Y. C. Jean, *Macromolecules* **2012**, *45*, 2434.

[6] C. A. Quarles, J. R. Klaehn, E. S. Peterson, J. M. Urban-Klaehn, F. D. McDaniel, B. L. Doyle, *AIP Conf. Proc.* **2011**, *1336*, 513.

[7] G. C. Eastmond, J. H. Daly, A. S. McKinnon, R. A. Pethrick, *Polymer* **1999**, *40*, 3605.

[8] M. Calle, C. M. Doherty, A. J. Hill, Y. M. Lee, *Macromolecules* **2013**, *46*, 8179.

[9] B. W. Rowe, S. J. Pas, A. J. Hill, R. Suzuki, B. D. Freeman, D. R. Paul, *Polymer* **2009**, *50*, 6149.

[10] A. J. Hill, B. D. Freeman, M. Jaffe, T. C. Merkel, I. Pinnau, *J. Mol. Struct.* **2005**, *739*, 173.

[11] H. Ju, A. C. Sagle, B. D. Freeman, J. I. Mardel, A. J. Hill, *J. Membr. Sci.* **2010**, *358*, 131.

[12] W. Xie, H. Ju, G. M. Geise, B. D. Freeman, J. I. Mardel, A. J. Hill, J. E. McGrath, *Macromolecules* **2011**, *44*, 4428.

[13] B. W. Rowe, B. D. Freeman, D. R. Paul, *Polymer* **2009**, *50*, 5565.

[14] R. A. Pethrick, F. Santamaria-Mendia, *J. Polym. Sci. Part B Polym. Phys.* **2015**, *53*, 1654.

[15] G. Dlubek, F. Börner, R. Buchhold, K. Sahre, R. Krause-Rehberg, K.-J. Eichhorn, *J. Polym. Sci. Part B Polym. Phys.* **2000**, *38*, 3062.

[16] V. P. Shantarovich, T. Suzuki, C. He, V. W. Gustov, *Radiat. Phys. Chem.* **2003**, *67*, 15.

[17] N. L. Le, T.-S. Chung, *J. Membr. Sci.* **2014**, *454*, 62.

[18] R. A. Pethrick, *Prog. Poly. Sci.* **1997**, *22*, 1.

[19] Y. C. Jean, P. E. Mallon, D. M. Schrader, (Eds.), *Principles and Applications of Positron and Positronium Chemistry*, World Scientific, Singapore, **2003**, 236.

[20] O. E. Mogensen, *Positron Annihilation Chemistry*, Springer-Verlag, Berlin, Germany, **1995**, 26.

[21] S. Vleeshouwers, J.-E. Kluin, J. D. McGervey, A. M. Jamieson, R. Simha, *J. Polym. Sci. Part B Polym. Phys.* **1992**, *30*, 1429.

[22] F. Müller-Plathe, H. Schmitz, *J. Chem. Phys.* **2000**, *112*, 1040.

[23] Y. Kobayashi, *Defect Diffus. Forum* **2012**, *331*, 253.

[24] M. L. Ruiz-Ripoll, H. Schut, N. H. Van Dijk, R. C. Alderliesten, S. van der Zwaag, R. Benedictus, *J. Phys. Conf. Ser.* **2011**, *262*, 12052.

[25] G. Choudalakis, A. D. Gotsis, H. Schut, S. J. Picken, *Eur. Polym. J.* **2011**, *47*, 264.

[26] F. Bečvář, J. Čížek, I. Procházka, J. Janotová, *Nucl. Instruments Methods Phys. Res. Sect. A Accel. Spectrometers, Detect. Assoc. Equip.* **2005**, *539*, 372.

[27] M. Eldrup, D. Lightbody, J. N. Sherwood, *Chem. Phys.* **1981**, *63*, 51.

[28] S. J. Tao, *J. Chem. Phys.* **1972**, *56*, 5499.

[29] Y. Yampolskii, V. Shantarovich, *Positron Annihilation Lifetime Spectroscopy and Other Methods for Free Volume Evaluation in Polymers*, in: Y. Yampolskii, I. Pinnau, B.D. Freeman (Eds.), *Materials Science of Membranes for Gas and Vapor Separation*, John Wiley & Sons, Chichester, UK, **2006**, 191.

[30] Y. C. Jean, *Microchem. J.* **1990**, *42*, 72.

[31] R. Mercado, Y. Wang, T. Flaim, W. Dimenna, U. Senapati, *Proc. SPIE: Organic Photonic Materials and Devices VI*, **2004**, *5351*, 276.

[32] N. Ritter, I. Senkovska, S. Kaskel, J. Weber, *Macromolecules* **2011**, *44*, 2025.

[33] B. S. Ghanem, N. B. McKeown, P. M. Budd, J. D. Selbie, D. Fritsch, *Adv. Mater.* **2008**, *20*, 2766.

CHAPTER 4

High-pressure sorption of carbon dioxide and methane in all-aromatic polyetherimide membranes

The sorption of compressed carbon dioxide and methane in a series of all-aromatic polyetherimide (PEI) thin films is presented in this chapter. The polymer films used for this study are based on the P1 diamine and four different dianhydrides, *i.e.* ODPA, BPDA, BTDA and PMDA (Chapter 2). The monomers have been selected to systematically change the flexibility of the polymer backbone, the segmental mobility, and the non-equilibrium excess free volume of the polymer. The excess free volume (EFV), gas sorption capacities, and sorption- and temperature-induced dynamic changes in film thickness and refractive index have been investigated by spectroscopic ellipsometry. The sorption capacity depends to a great extent on the PEI backbone composition. PMDA-P1 shows the highest carbon dioxide sorption, combined with the lowest sorption selectivity because of the predominant sorption of methane in the excess free volume. For ODPA-P1, the highest sorption selectivity is obtained, while it shows little long-term relaxations at carbon dioxide pressures up to 25 bar.

4.1 Introduction

Removal of carbon dioxide from natural gas with membrane technology has emerged as a viable alternative to traditional separation technologies. Traditional CO_2/CH_4 gas separation methods are associated with high capital costs and complex operation; in particular for smaller gas processing plants (< 1.5×10^5 $m^3 day^{-1}$) membrane technology is considered to be a more undemanding and energy-efficient alternative.[1] In addition, membrane design is more flexible and the equipment is more compact.[2] The first commercial polymer membranes were made from cellulose acetate but now predominantly polyimides with a high glass transition temperature (T_g) are used.[3,4] A drawback of these glassy polymer membranes is that at elevated pressures of sorbing gases, like CO_2, plasticization phenomena may occur.[5–7] In the presence of such penetrants, polymer networks experience enhanced segmental mobility, swelling stresses, and relaxation phenomena, resulting in higher permeabilities for all components.[3,7–9] This decreases the selectivity of a membrane and hence reduces its performance, in molecular separations. High-T_g glassy polymer membranes remain attractive candidates because of their rigid backbone structures and high selectivities.[10,11] If high-T_g glassy polymer membranes can be designed such that they become resistant to plasticization they will become more competitive.[1] In this context, poly(etherimide)s (PEIs) are an attractive class of polymers[12] that possess high CO_2/CH_4 selectivities, high thermal stability, good mechanical properties, and it has been demonstrated that they remain relatively stable in the presence of compressed CO_2.[11]

In situ ellipsometry (discussed in more detail later on) is proven to be very successful in fundamental studies on the nature of interactions of glassy and rubbery polymers with liquids and condensable gases.[13] It is a versatile tool for studying thin films exposed to compressed CO_2. The technique is nonintrusive, accurate, fast, and can be automated; nevertheless, there are not many studies of *in situ* ellipsometry with gases at high pressure. Virtually all of these studies focus on sorption of CO_2, mainly due to the importance of this gas in membrane separation applications. In membrane science, the sorption, relaxation, and plasticization in a compressed CO_2 environment has been investigated for various high-T_g polymers, including PEIs, polysulfones, polyphenylene oxide, and sulfonated-poly(etherketone)s.[8,11,14–16]

Plasticization phenomena in rigid polymers are dependent on the CO_2 concentration in the polymer network, which is directly related to the activity of the CO_2 in the gas phase.[6] Relaxation dynamics caused by CO_2 in thin and thick polyimide films have been studied by Wind *et al.*[8,14] Thin films have been shown to plasticize faster and at lower pressures than bulk films. Their study also shows a correlation between dynamics of sorption and diffusion of CO_2 in polyimide membrane materials with permeation measurements. Horn *et al.*[15] have investigated the relaxations and physical aging of ultra-thin polymer films induced by CO_2 sorption. They have systematically investigated various polymer membranes, including Matrimid®, and they have shown that sorption induced relaxations dominate the dynamics of diffusion since the evolution of CO_2 diffusivity is shown to be the main cause of changes in CO_2 permeability at constant pressure. Results published by Simons *et al.*[11] indicate that the affinity of CO_2 toward a series ODPA-based PEIs originates from the inherent chemical structure of the polymer backbone. High CO_2 affinity in PEIs is anticipated, due to the presence of two imide functionalities in the polymer main chain.[11,17] The low extent of swelling for these membranes, between 3 and 4% measured by spectroscopic ellipsometry at pressures up to 50 bar, as well as high CO_2/CH_4 selectivities of 40–60 at 40 bar of mixed feed, show that these materials have great potential in CO_2 removal applications at elevated pressures. ODPA-P1 (Figure 4.1, P1 indicates that there is one –O–Ar–O– group) has shown a decrease in CH_4 permeability with increasing pressure, which is manifested by an increase in selectivity with increasing pressure.[11] This polymer serves as the starting point of the work presented in this chapter.

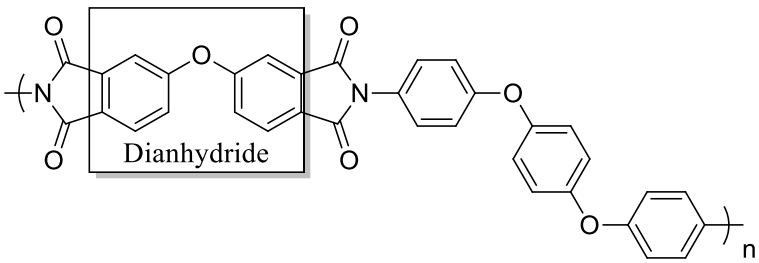

Figure 4.1. Structure of ODPA-P1 polyetherimide.

Herein, we systematically varied the backbone of a series of all-aromatic PEIs, derived from the reactions between the P1 diamine and a series of aromatic dianhydrides (Scheme 4.1). We have studied the influence of the dianhydride

precursor on free volume content, CO_2 and CH_4 sorption capacities, and (long-term) chain dynamics of the polymer.

Four different dianhydrides have been selected to systematically change the flexibility of the polymer backbone, to tailor the segmental mobility, and the non-equilibrium excess free volume (EFV) of the polymer. The sorption-induced changes in polymer film thickness (polymer swelling) and refractive index (mass uptake) have been investigated by spectroscopic ellipsometry.

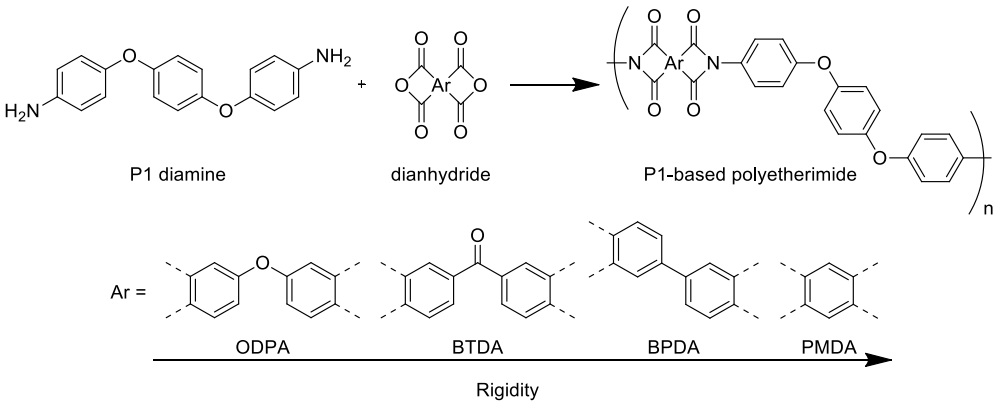

Scheme 4.1. Preparation of P1-based PEIs and structures of dianhydride moieties.

4.2 Sorption

The sorption of gases in glassy polymers is described by the "dual mode" sorption model (Equation 4.1).[18–20] This model describes gas sorption occurring in two different regions: within the dense polymer matrix (region of Henry's law) and in the microcavities (Langmuir region).[20] Microcavities correspond to the non-equilibrium excess free volume as fixed, independent sorption sites. Model for pure gas sorption is given by [18,19]:

$$C = C_D + C_H = k_D p + \frac{C'_H bp}{1 + bp} \tag{4.1}$$

Here C (cm^3 gas (STP)/cm^3 polymer) is the total concentration of the sorbed gas in the polymer, C_D and C_H are the concentrations of penetrant sorbed in the Henry's law and Langmuir regions, respectively; k_D (cm^3 gas (STP)/(cm^3 polymer bar)) is the Henry's law constant, p (bar) is the pressure of the gas phase, C'_H (cm^3 gas (STP)/cm^3 polymer) is the Langmuir sorption capacity,

parameter *b* (1/bar) is the Langmuir affinity, an equilibrium constant that describes penetrant's affinity for a Langmuir site.

4.3 Ellipsometry

Spectroscopic ellipsometry is a precise, non-destructive and contactless optical technique that uses polarized light to characterize thin films. The polarized light beam undergoes a change in polarization state as it interacts with the sample structure, and this reflected light beam is detected and analyzed (Scheme 4.2).

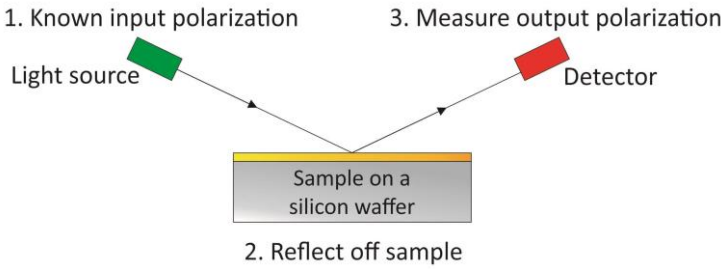

Scheme 4.2. Schematic representation of an ellipsometric experiment.

Experimental results are then fitted using an optical model in order to calculate quantities such as the thickness and the refractive index (dispersion) of the sample films.[21] Both the thin film and the glass substrate are dielectric materials, and dispersion of dielectrics is given by an empirical equation called Cauchy's equation [22]:

$$n = a + \frac{b}{\lambda^2} + \frac{c}{\lambda^4} \tag{4.2}$$

In Equation 4.2 *n* (-) is the refractive index, λ (nm) is the wavelength of the light and *a*, *b* and *c* are constants which depend on medium characteristics. Upon gas sorption, the mass concentrations, *C*, of the penetrant *e.g.* CO_2 and the polymer in the swollen film can be related to the film's refractive index and estimated by applying the Clausius-Mossotti equation [22,23]:

$$\frac{\langle n_f \rangle^2 - 1}{\langle n_f \rangle^2 + 2} = q_{CO_2} C_{CO_2} + q_{polymer} C_{polymer} \tag{4.3}$$

Here, $\langle n_f \rangle$ (-) is an averaged refractive index of the swollen film, as determined by Equation 4.2, C_{CO2} and $C_{polymer}$ (g/cm^3) are the mass based concentration of

the sorbed gas and the polymer, and q_{CO2} and $q_{polymer}$ (cm^3/g) are constants determined from pure component data.[22]

4.4 Experimental

4.4.1 Materials

For this study we used a series of 4 PEI membrane films introduced and described in detail in Chapter 2. With the goal of understanding the relationship between the backbone structure of the polyetherimide on one side and free volume characteristics and gas permeating capabilities on the other side, it was crucial to have a systematic approach in designing our PEIs. The diamine chosen for this study is P1 and four different dianhydride moieties have been selected to systematically change the flexibility of the PEI backbone, to tailor the segmental mobility, and the non-equilibrium excess free volume of the polymer (Scheme 4.1).

4.4.2 Spin coating procedure

Thin polymer films were prepared by spin-coating (WS-400B-6NPP/LITE, Laurell Technologies) of a polymer dope onto a silicon wafer under a nitrogen atmosphere. Polymer dope was prepared by diluting the four poly amic acids 1:5 with NMP before spin-coating. The general spinning procedure consisted of a spin-coating step at 600 rpm for 35 s, followed by a step at 1200 rpm for 10 min. Directly after spin coating, the samples were thermally imidized under a nitrogen atmosphere (N_2 flow of 0.5 L min^{-1}). The temperature program consisted of isothermal holds for 1.5 h at 60 °C, 1 h at 100 °C, 1 h at 200 °C, and 1 h at 300 °C. The heating rate between the isothermal hold steps was set at 5 °C min^{-1}. After imidization, the oven was switched off and the samples were allowed to cool to room temperature without controlling the cooling profile.

4.4.3 Thermo-ellipsometric analysis

Thermo-ellipsometric analysis (TEA measurements) was conducted with an M2000X spectroscopic ellipsometer (J. A. Woollam) equipped with a temperature-controlled hot-stage (HCS622, INSTEC). Spectroscopic ellipsometry measurements were conducted in the wavelength range of 210–1000 nm. The glass transition temperature (T_g), the EFV content and the linear coefficient of thermal expansion (CTE) were determined from the thickness and refractive index data as function of temperature. The Complete EASE v.4.86

software package (J. A. Woollam) was used both to control the instrument and for data analysis by resolving the optical models. Temperature-controlled experiments were performed at a fixed angle of incidence (70 °). During the experiments, the hot stage was continuously purged with ultrapure N_2. Temperature calibration was done using melting standards.[24]

4.4.4 *In situ* spectroscopic ellipsometry using a high-pressure cell

Spectroscopic ellipsometry measurements were conducted with an Alpha-SEVR ellipsometer (J. A. Woollam). All measurements were done at a fixed angle of incidence (70 °) in the wavelength range from 370 to 900 nm. Samples were placed in a home-built stainless steel cell (P_{max} = 20 MPa, T_{max} = 200 °C) equipped with a temperature and pressure control system. Accurate pressure and flow determination was assured by a syringe pump (Teledyne ISCO, 500D). The gas temperature was maintained at 35 °C by water baths connected to the stainless steel ellipsometry cell and the syringe pump, to correct temperature changes due to Joule-Thompson effects upon incremental pressure change. Light entered and exited the cell through 0.01 m thick quartz windows positioned perpendicular to the light beam. The PEI samples on silicon wafers were held under vacuum for several hours, followed by stepwise CO_2 or CH_4 pressure increments.

Important note: The risks of using high-pressure CO_2 and CH_4 was extensively assessed. A variety of safety measures were taken, including working in a fume hood, reducing volumes, and using equipment with a pressure rating (calculated and tested by the High Pressure Lab at the University of Twente) at least 1.43 × the maximum operating pressure equipped with appropriate pressure safety valves and pressure relief valves.[25]

4.4.5 Spectroscopic ellipsometry data analysis

CompleteEASE (v.4.86, J. A. Woollam) was used for the data analysis. For the TEA data analysis, the optical model used to model Psi (Ψ) and Delta (Δ) data consisted of a substrate with the temperature-dependent optical model for silicon, a 2 nm native oxide layer and a top layer that was fitted with a Cauchy dispersion model with uniaxial anisotropy with A_{xy}, A_z, $B_{xy} = B_z$, and k_z and k_{xy} as fit parameters. For the high pressure sorption experiments, the model consisted of a substrate with a fixed optical dispersion of crystalline silicon,[26] a 2 nm native oxide layer and a top layer that was fitted with a Cauchy dispersion

model with uniaxial anisotropy with A_{xy}, A_z, B_{xy} = B_z, and k_z and k_{xy} as fit parameters. Pressure induced birefringence of the cell windows was taken into account via a high-pressure helium calibration on a 25 nm SiO_2/Si wafer. This provides an appropriate Delta offset parameter that negates the pressure-induced birefringence. The optical dispersion of CO_2 and CH_4 were corrected for the pressure. All refractive index values reported in this chapter are obtained at 632.8 nm.

4.5 Results

4.5.1 Thermo-ellipsometric analysis

The EFV, T_g, and CTE of the PEIs prepared using P1 with PMDA, BPDA, ODPA, and BTDA have been measured using TEA. The thickness and refractive index as function of temperature derived from the TEA data are given in the Appendix. The CTE is obtained from the slope of the linear relation between the thickness and the temperature; CTE_{rubber} in the rubbery region and CTE_{glass} in the glassy region. The T_g is obtained from extrapolating the linear relations in the rubbery and glassy regions, and determining their intersection. The EFV value is calculated by extrapolating the refractive index of an equilibrium polymer film from above its glass transition temperature, and comparing the obtained hypothetical value (n_{eqliq}) with the experimentally found value (n_{glass}).[21] The CTE_{rubber}, CTE_{glass}, n_{eqliq}, n_{glass}, and EFV values are listed in Table 4.1.

The T_gs of BPDA-P1 and ODPA-P1 are similar to those measured by differential scanning calorimetry (DSC) and dynamic mechanical thermal analysis (DMTA). The T_g of BTDA P1 is 6 °C lower as determined by DSC measurements and the T_g of PMDA-P1 is about 15 °C lower as determined by DMTA (Chapter 2, Table 2.3). The difficulties in determining a clear T_g might be related to the semi-crystalline character of PMDA-P1, and is reflected by the absence of a T_g event in DSC measurements. All DSC and DMTA results are summarized in Table 4.1. Moreover, the degree of crystallinity of the thin films used for TEA may be different from bulk samples (with thickness ca. 30 mm) that are used for DSC and DMTA.

Table 4.1. EFV, T_g, and CTE of the PEIs prepared using PMDA, BPDA, BTDA, and ODPA, measured by TEA.

Polymer		ODPA-P1	BTDA-P1	BPDA-P1	PMDA-P1
T_g (°C)	TEA	250	254	273	306
	DSC[a]	248	286	272	-
	DMTA[b]	248	300	276	321
EFV (%)		8.7	9.3	7.8	6.7
n_{eqliq}[c] (-)		1.722	1.735	1.788	1.747
n_{glass}[c] (-)		1.674	1.683	1.740	1.714
CTE_{rubber}[d] (PPM °C^{-1})		473	470	414	367
CTE_{glass}[d] (PPM °C^{-1})		139	115	141	168

[a] DSC (second heating) data were collected using a heating rate of 20 °C min^{-1}; T_g is reported at the inflection point. [b] DMTA data were collected using a heating rate of 2.5 °C min^{-1}; T_g is determined at the maximum of the loss modulus (E"). [c] Relative index at 632.8 nm and at 25 °C. [d] The CTE reported here is the 1D CTE.

The EFV is in the order BTDA>ODPA>BPDA>PMDA. The lack of a clear T_g and the semi-crystalline character of the PMDA-P1 complicate the TEA analysis and therefore the PMDA-P1 results should be treated with caution. Experiments to determine the EFV for all four PEIs using Positron Annihilation Lifetime Spectroscopy and Doppler Broadening (PALS and PADB) are reported in Chapter 3. In the rubbery state, the values for linear thermal expansion coefficient follow a consistent trend: a more rigid precursor gives a lower CTE. For the glassy states, the non-equilibrium characteristics are different and no obvious trend is found.

4.5.2 High-pressure gas sorption: swelling and isotherms

Figure 4.2 shows the swelling, relative refractive index, and CO_2 concentration as function of CO_2 pressure. The swelling degrees for all PEIs increase with increasing CO_2 pressure. The hysteresis in the swelling degrees, manifested by the higher swelling degrees upon desorption, results from the slow polymer chain reorganizations in the time-scale of the pressure increments.

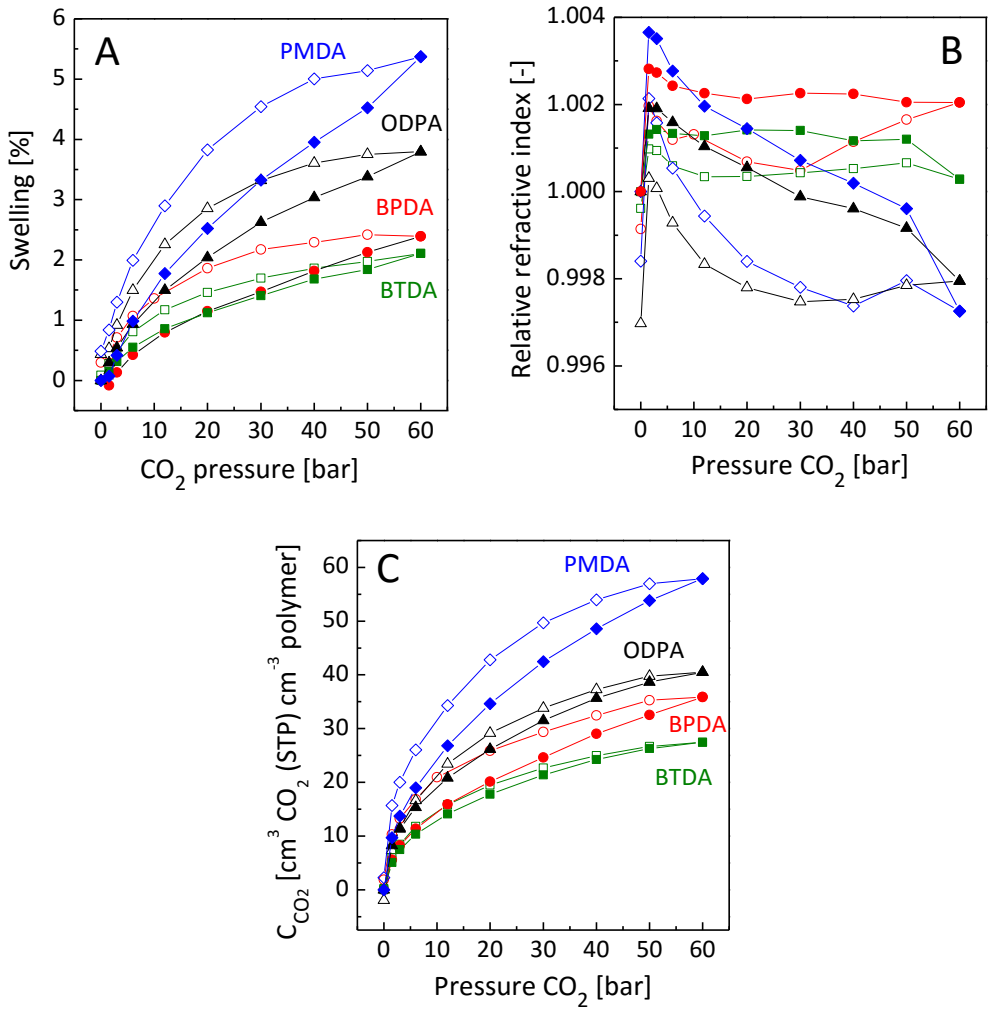

Figure 4.2. **A-** swelling, **B-** relative refractive index, and **C-** CO_2 concentration upon sorption (closed symbols) and desorption (open symbols) as function of pressure, for ODPA-P1, BTDA-P1, BPDA-P1 and PMDA-P1.

The swelling degrees are in the order PMDA-P1>ODPA-P1>BPDA-P1>BTDA-P1. The ODPA-P1 swelling degree is similar as compared to the results from Simons et al., underlining the high measurement reproducibility of spectroscopic ellipsometry.[11] For all samples, the relative refractive index shows a steep increase at the first pressure step from vacuum to 1.5 bar CO_2 pressure. This jump in the refractive index can be associated with the filling of EFV, where void (n = 1.000) is replaced by CO_2 (liquid CO_2 is estimated at $n \approx$ 1.23 [8,22,27,28]). The largest jump can be observed for PMDA-P1 and BPDA-P1, suggesting that these samples have the highest EFV accessible for the CO_2. This is in contrast with the EFV measurements by TEA that show an opposite trend. This can be attributed to the fact that the sorption is also affected by the distinct characteristics of the different polymer backbones, and the affinity of the sorbing gas for the polymers. At higher pressures, the relative refractive index decreases due to the dilation of the polymer matrix by CO_2, while most EFV has been filled in the first pressure increment to 1.5 bar CO_2. All PEIs have a strong hysteresis in the relative refractive index, similar to the swelling degree hysteresis. In particular PMDA-P1 and ODPA-P1 show pronounced refractive index hysteresis as compared to BTDA-P1 and BPDA-P1. When returning to vacuum upon desorption, all the relative refractive indices fall below 1, indicating that the polymer matrix remains slightly dilated after CO_2 sorption. This effect is typical for the sorption-desorption behavior of glassy polymers. The CO_2 concentrations follow the same order as the swelling degrees, from high to low, PMDA-P1>ODPA-P1>BPDA-P1>BTDA-P1. The similarity in the swelling degree and CO_2 isotherms is due to the limited contribution of the EFV to the total CO_2 sorption; additional CO_2 sorption is therefore accompanied by polymer dilation and a drop in the relative refractive index.

Figure 4.3 shows the swelling, relative refractive index and CH_4 concentration as function of CH_4 pressure. The swelling degrees are in the order PMDA-P1>ODPA-P1>BPDA-P1>BTDA-P1. The swelling degrees and CH_4 concentrations follow the same order as those found for sorption experiments in CO_2, albeit with lower values. CH_4 sorption does not result in pronounced hysteresis effects, in contrast to the CO_2 sorption data. The absence of hysteresis can be due to the limited dilation of the matrix in the time-scale of the pressure increments. The relative refractive index data reveals that there is only little EFV filling by CH_4, which is in agreement with rather low methane solubility (Figure 4.3C).

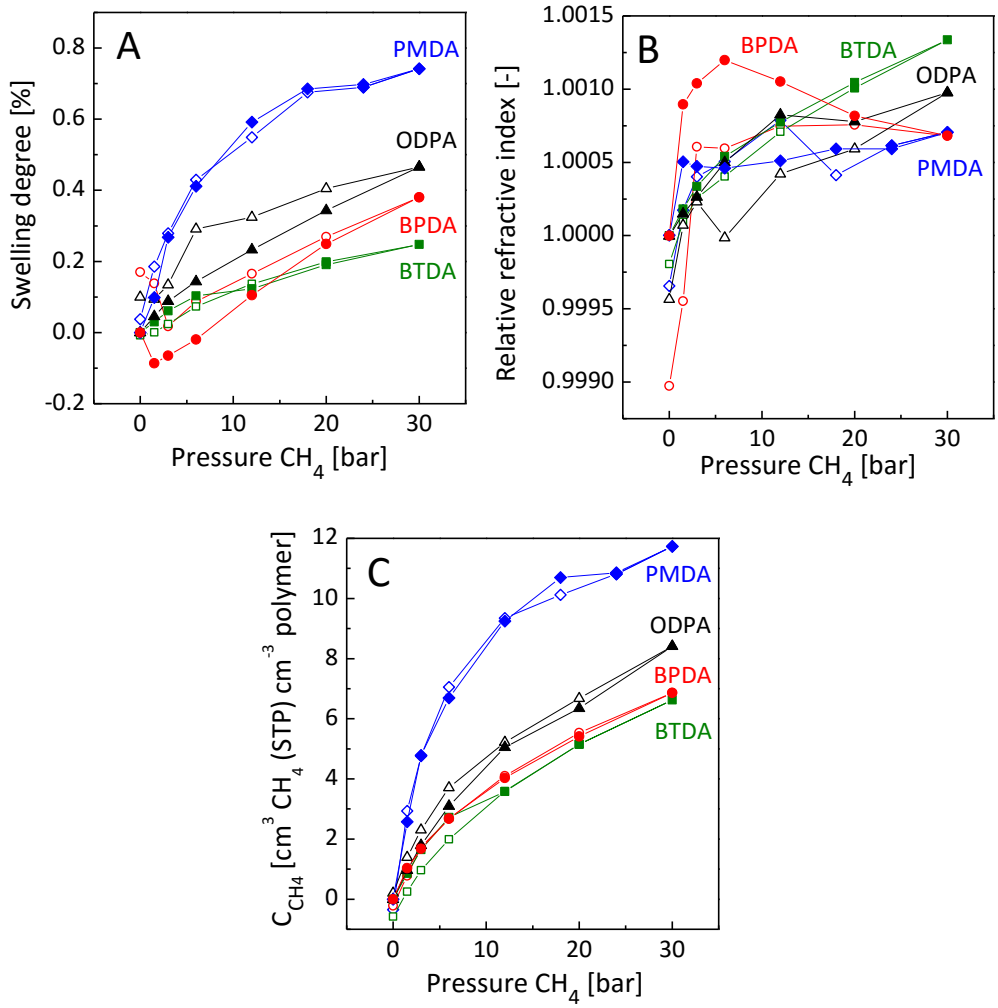

Figure 4.3. A- swelling, **B-** relative refractive index, and **C-** CH_4 concentration upon sorption (closed symbols) and desorption (open symbols) as function of pressure, for ODPA-P1, BTDA-P1, BPDA-P1 and PMDA-P1.

4.5.3 High-pressure gas sorption: sorbed gas molar volume

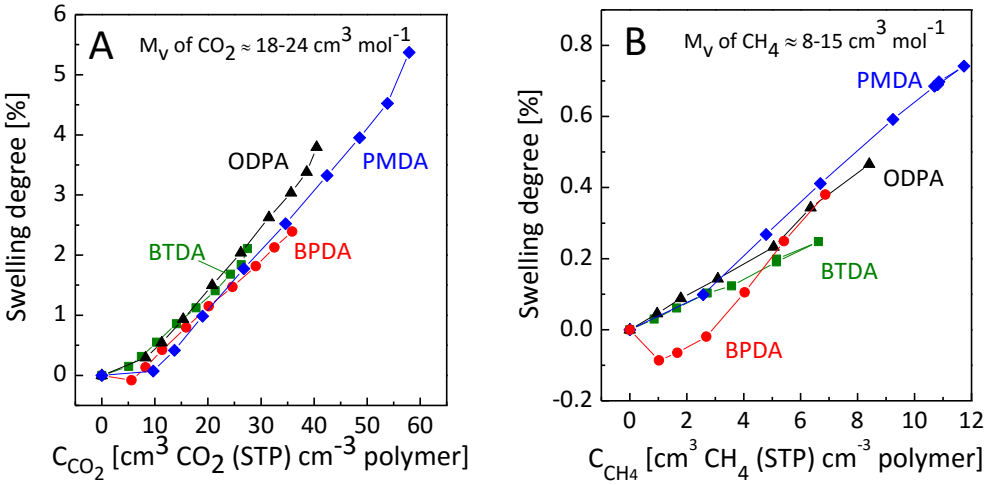

Figure 4.4. Swelling as function of **A-** CO_2 concentration and **B-** CH_4 concentration of ODPA-P1, BTDA-P1, BPDA-P1 and PMDA-P1. The slopes of the swelling degree versus the CO_2 and CH_4 concentrations have been fitted by a linear least squares fit. The first data at vacuum have been omitted in the fit to eliminate the contribution of EFV filling.

Figure 4.4 shows the dilation as function of CO_2 and CH_4 concentrations, for all PEI samples. For all PEIs, the dilation as function of CO_2 concentrations follows the same trend. An initial concentration increase is observed without any substantial swelling. The absence of swelling is due to the predominant filling of EFV in the lower pressure range, as was observed from the relative refractive index data in Figure 4.2. Only at pressures above 1.5 bar, the data show a linear trend. For PMDA-P1 and ODPA-P1, the slope inclines at the last measurement point (60 bar CO_2), indicating that plasticization of the matrix induces further dilation. The partial molar volume (V_m) of the sorbing molecule can be calculated from the slope of the dilation versus concentration. For the linear regions in the graph, the partial molar volumes of CO_2 are: 23.6 cm^3 mol^{-1} (PMDA-P1), 18.2 cm^3 mol^{-1} (BPDA-P1), 23.7 cm^3 mol^{-1} (ODPA-P1), and 18.7 cm^3 mol^{-1} (BTDA-P1). This range, 18-24 cm^3 mol^{-1}, is similar to the values derived from SE data on thin films [11] or from bulk dilation and sorption isotherm data (21-27 and 20-30 cm^3 mol^{-1}).[29–31] The CH_4 concentration in the polymers is much lower as compared to CO_2. The partial molar volumes are: 15.9 cm^3 mol^{-1} (PMDA-P1), 18.5 cm^3 mol^{-1} (BPDA-P1), 12.6 cm^3 mol^{-1} (ODPA-

P1), and 8.4 cm^3 mol^{-1} (BTDA-P1). The smaller apparent molar volumes of sorbed CH_4, as compared to CO_2, might be related to the differences in V_m of the liquid state as well as condensability of the two gases. The V_m of liquid CH_4 is around 37 cm^3 mol^{-1}, while the V_m of liquid CO_2 is around 46 cm^3 mol^{-1}.[32] Due to filling of EFV the apparent V_m could be lower than the actual penetrant V_m. The higher condensability of CO_2, and the higher affinity of this gas for the polymer, results in larger sorbed concentrations. Already at lower pressures a considerable part of the EFV is filled by CO_2. In the case of CH_4 far lower concentrations are present in the polymer at lower pressures. This implies that for CH_4 the relative contribution of EFV filling to total sorption is larger as compared to CO_2, in the entire pressure range studied. Consequently, the apparent V_m of CH_4 is relatively low.

4.5.4 High-pressure gas sorption: gas solubility selectivities

The membrane gas selectivity is a product of the gas solubility selectivity and diffusivity differences. The solubility selectivity can be estimated from the sorption isotherms of the individual gases. Figure 4.5 shows the ideal CO_2/CH_4 solubility selectivities of all PEIs, calculated from the sorption isotherms given in Figures 4.2 and 4.3. The calculations do not take into account competitive sorption effects, and therefore the CO_2/CH_4 solubility effects in a mixed gas separation process might deviate from those calculated from pure gases. The solubility selectivity is higher at low pressures, as has also been observed for PPO.[33] The decrease in solubility is related to the shape of the sorption isotherms. Whereas CO_2 fills the EFV and displays high sorption at low pressures, CH_4 only marginally sorbs at low pressures. At higher pressures, the relative contribution of the EFV to the sorption capacity becomes smaller (Henry mode sorption dominates over Langmuir mode sorption at higher pressures).

For Henry sorption a linear proportionality is expected between the swelling (or concentration) and the pressure. The sorption selectivity is in that case equal to the ratio of the parameters of proportionality of the two gases, and is independent of the pressure. Indeed, in Figure 4.5 the sorption selectivities become more or less independent of pressure, with values in the range 3-4. The slight increase in selectivity for PDMA-P1 at high pressure is due to the large plasticization of this polymer at high CO_2 pressures.

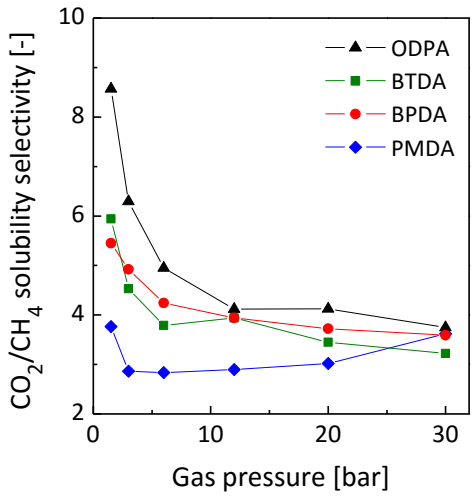

Figure 4.5. Ideal CO_2/CH_4 solubility selectivity at 35 °C, calculated from the sorption isotherms of the pure gases.

4.5.5 High-pressure gas sorption: penetrant-induced relaxations

The gas separation properties of glassy membranes depend on the dilation of the polymer. If the dilation becomes larger, the sorption capacity for a gas increases. Moreover, the dilation might results in enlarged diffusivity of the components. In the worst case, the diffusivity of the larger component increases most, ruining the selectivity of the membrane.[34] To predict whether stable membrane performance can be expected, it is essential to know the (long-term) dilation dynamics of the membrane as function of pressure. The dilation dynamics can be studied via the evolution of the thickness after a pressure increment. Such a pressure increment induces chemical-potential-gradient controlled (primary) relaxations and polymer chain (secondary) relaxations (Figure 4.6).

The primary relaxations are attributed to the fact that the polymer needs to dilate to be able to accommodate penetrant molecules that diffuse into the polymer, in order to reduce the gradient in their chemical potential. The secondary relaxations are attributed to slow rearrangements of the polymer chains that are induced by the altered state of the polymer upon sorption of penetrant molecules. During the secondary relaxations, the chemical potential of the penetrant inside and outside of the polymer are almost equal but relaxations of the polymer allow a larger extent of sorption. As such, these secondary relaxations are related to the macromolecular mobility of the swollen system.

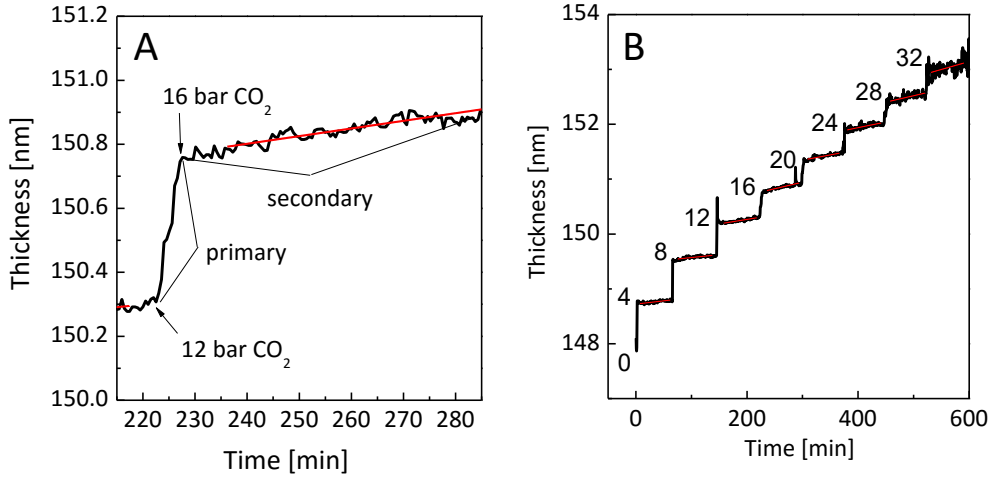

Figure 4.6. Thickness of ODPA-P1 as function of time for changes in CO_2 pressure **A-** from 12 to 16 bar, and **B-** from vacuum to 32 bar with increments of 4 bar. The primary increase in thickness occurs more or less directly upon the pressure increment. The secondary increase in thickness gradually occurs in the time after the pressure increment.

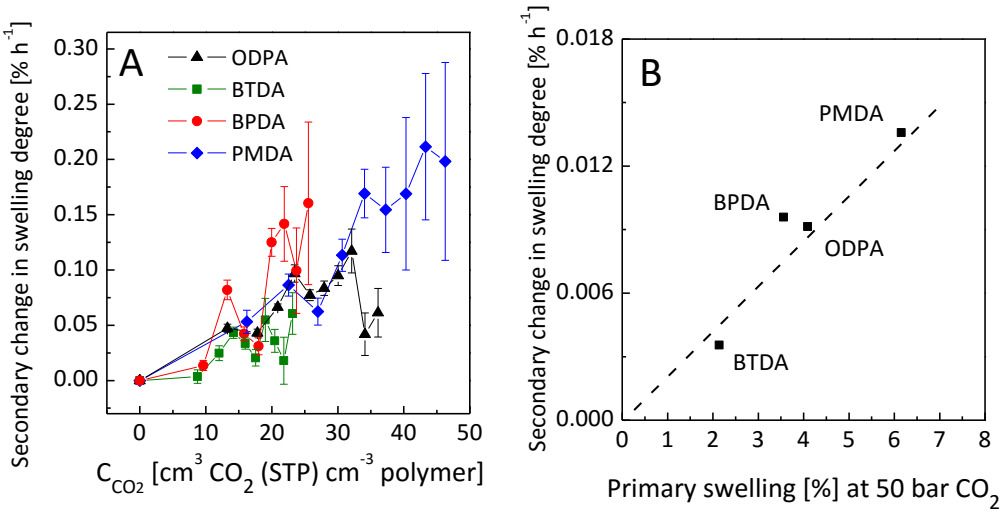

Figure 4.7. A- The change in swelling degree of the PEIs as function of the CO_2 concentration. Error bars correspond to a 95% confidence interval around the slope of the thickness versus time. **B-** The change in swelling degree of the PEIs as function of the primary swelling degree after an incremental change from vacuum to 50 bar of CO_2. The dotted line is drawn as a guide for the eye.

Figure 4.7A shows the magnitudes of the secondary relaxations as a function of CO_2 concentration. The values are calculated from the slope of swelling versus time, after each pressure step. The data show a general increase in macromolecular mobility with increasing CO_2 concentration. The broad scatter in the data and the relatively large error bars imply that, for a given concentration of sorbed CO_2, no significant differences are observed between the macromolecular mobility's of the different polymers. Figure 4.7B shows the rate of secondary relaxation of each PEI layer as function of the magnitude of the primary relaxations, after an incremental change from vacuum to 50 bar of CO_2. The rates of the secondary relaxations are much smaller as compared to those observed when the pressure is increased in a stepwise manner to 30 bar (Figure 4.7A).

The small rates indicate that, at the pressure of 50 bar, the polymers are heavily plasticized and no longer exhibit distinct rigid glassy characteristics.[35] The data also indicate a strong positive correlation between primary and secondary relaxations. The correlation between the swelling degree and long-term effects predicts that the stability of the membrane at high pressures is in the order, from good to poor, BTDAP1>ODPA-P1>BPDA-P1>PMDA-P1.

4.6 Conclusions

In conclusion, the sorption capacities of CO_2 and CH_4 depend to great extent on the polymer backbone of the PEI. PMDA-P1shows the highest sorption of both CO_2 and CH_4. For low pressures, the ideal sorption selectivity reduces with pressure. This is because for CH_4 in this pressure range the contribution of EFV filing to the total sorption is relative large. At higher pressures, the relative contribution of EFV filling decreases and the sorption selectivity becomes constant for all polymers.

For CO_2, in the pressure range 0 to 30 bar, the penetrant sorption is accompanied by primary and secondary polymer relaxations. A strong positive correlation between the two types of relaxations exists; at increasing pressure the magnitudes of both the primary and secondary relaxations increase. A correlation between the two types of relaxations persists when the polymers are exposed to an incremental change in CO_2 pressure from 0 to 50 bar, but the rate of the secondary relaxations is much smaller than in the pressure range up to 30 bar. This indicates that, at 50 bar, the polymers have lost their distinct glassy characteristics.

For ODPA-P1, the highest sorption selectivity can be obtained, while it shows little long-term relaxations at CO_2 pressures up to 25 bar. This study can serve as a benchmark for further systematic studies on the sorption behavior of glassy PEIs for gas separation applications.

4.7 Appendix: TEA results

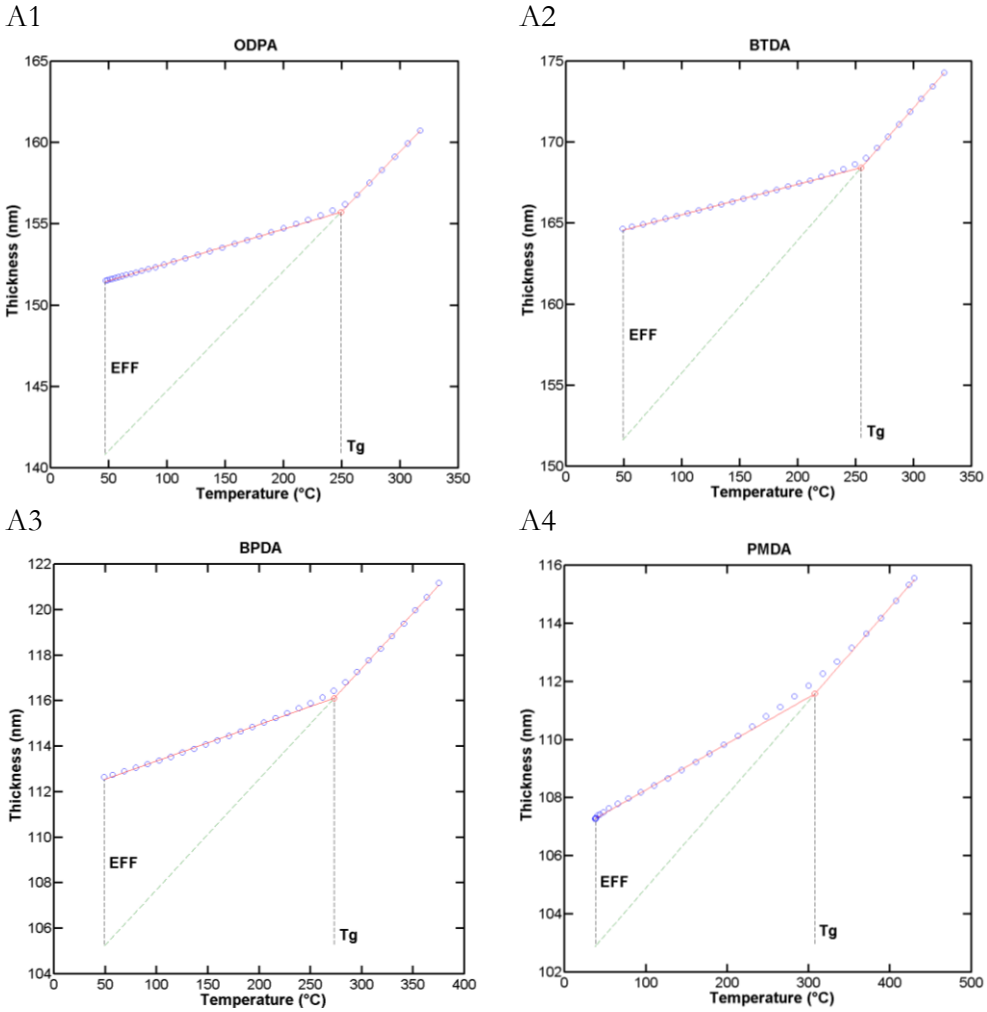

Figure A. The film thickness as a function of temperature derived from the TEA data for PEIs based on **A1-** ODPA, **A2-** BTDA, **A3-** BPDA and **A4-** PMDA.

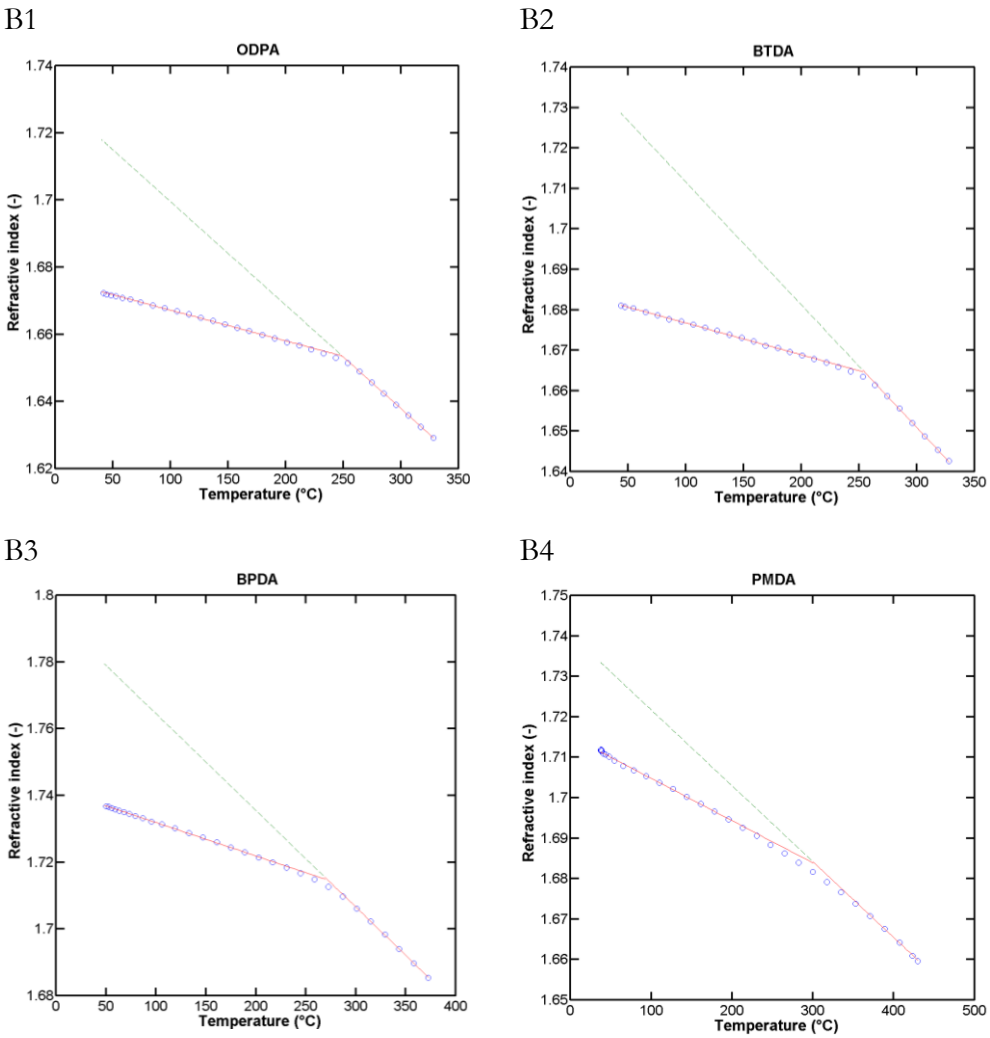

Figure B. The refractive index as a function of temperature derived from the TEA data for PEIs based on **B1-** ODPA, **B2-** BTDA, **B3-** BPDA and **B4-** PMDA.

4.8 References

[1] R. W. Baker, *Ind. Eng. Chem. Res.* **2002**, *41*, 1393.

[2] C. Staudt-Bickel, W. J. Koros, *J. Membr. Sci.* **1999**, *155*, 145.

[3] J. D. Wind, D. R. Paul, W. J. Koros, *J. Membr. Sci.* **2004**, *228*, 227.

[4] R. W. Baker, Chapter 8 in: *Membrane Technology and Applications*, 2nd ed., John Wiley & Sons, Chichester, UK, **2004**, 301.

[5] R. D. Raharjo, B. D. Freeman, E. S. Sanders, *Polymer* **2007**, *48*, 6097.

[6] M. Wessling, M. L. Lopez, H. Strathmann, *Sep. Purif. Technol.* **2001**, *24*, 223.

[7] T. Visser, N. Masetto, M. Wessling, *J. Membr. Sci.* **2007**, *306*, 16.

[8] J. D. Wind, S. M. Sirard, D. R. Paul, P. F. Green, K. P. Johnston, W. J. Koros, *Macromolecules* **2003**, 6433.

[9] M. Wessling, H. Strathmann, A. Bos, I. G. M. Pu, *J. Membr. Sci.* **1999**, *155*, 67.

[10] L. M. Robeson, *Curr. Opin. Solid State Mater. Sci.* **2000**, *4*, 549.

[11] K. Simons, K. Nijmeijer, J. G. Sala, H. van der Werf, N. E. Benes, T. J. Dingemans, M. Wessling, *Polymer* **2010**, *51*, 3907.

[12] R. A. Pethrick, F. Santamaria-Mendia, *J. Polym. Sci. Part B Polym. Phys.* **2015**, *53*, 1654.

[13] W. Ogieglo, H. Wormeester, K. Eichhorn, M. Wessling, N. E. Benes, *Prog. Polym. Sci.* **2015**, *42*, 42.

[14] J. D. Wind, S. M. Sirard, D. R. Paul, P. F. Green, K. P. Johnston, W. J. Koros, *Macromolecules* **2003**, 6442.

[15] N. R. Horn, D. R. Paul, *Macromolecules* **2012**, *45*, 2820.

[16] B. W. Rowe, B. D. Freeman, D. R. Paul, *Macromolecules* **2007**, *40*, 2806.

[17] N. Ritter, I. Senkovska, S. Kaskel, J. Weber, *Macromolecules* **2011**, 976.

[18] W. J. Koros, A. H. Chan, D. R. Paul, *J. Membr. Sci.* **1977**, *2*, 165.

[19] W. J. Koros, D. R. Paul, A. A. Rocha, *J. Polym. Sci. Polym. Phys. Ed.* **1976**, *14*, 687.

[20] B. Kraftschik, W. J. Koros, *Macromolecules* **2013**, *46*, 6908.

[21] W. Ogieglo, H. Wormeester, M. Wessling, N. E. Benes, *Polymer* **2014**, *55*,

1737.

[22] S. M. Sirard, P. F. Green, K. P. Johnston, *J. Phys. Chem. B* **2001**, *105*, 1385.

[23] R. Feynman, R. Leighton, M. Sands, Chapter 32 in: *The Feynman Lectures on Physics,* Addison-Wesley Publishing Company, Inc., Reading, MA, USA, **1964**.

[24] E. J. Kappert, M. J. T. Raaijmakers, W. Ogieglo, A. Nijmeijer, C. Huiskes, N. E. Benes, *Thermochimica Acta* **2015**, *601*, 29.

[25] Pressure Equipment Directive, European Commission, retrieved Sep 8 2015 from: http://ec.europa.eu/growth/sectors/pressure-gas/pressure-equipment/guidelines/index_en.htm.

[26] C. M. Herzinger, B. Johs, W. A. McGahan, J. A. Woollam, W. Paulson, *J. Appl. Phys.* **1998**, *83*, 3323.

[27] S. M. Sirard, K. J. Ziegler, I. C. Sanchez, P. F. Green, K. P. Johnston, *Macromolecules* **2002**, *35*, 1928.

[28] S. M. Sirard, H. Castellanos, P. F. Green, K. P. Johnston, *J. Supercrit. Fluids* **2004**, *32*, 265.

[29] D. Punsalan, W. J. Koros, *Polymer* **2005**, *46*, 10214.

[30] P. Gotthardt, A. Gruger, H. G. Brion, R. Plaetschke, R. Kirchheim, *Macromolecules* **1997**, *30*, 8058.

[31] Y. Mi, S. Zhou, S. A. Stern, *Macromolecules* **1991**, *24*, 2361.

[32] S. Fuks, J.-C. Legros, A. Bellemans, *Physica* **1965**, *31*, 606.

[33] B. J. Story, W. J. Koros, *J. Membr. Sci.* **1992**, *67*, 191.

[34] A. Bos, I. G. M. Pünt, M. Wessling, H. Strathmann, *Sep. Purif. Technol.* **1998**, *14*, 27.

[35] W. Ogieglo, M. Wessling, N. E. Benes, *Macromolecules* **2014**, *47*, 3654.

CHAPTER 5

Oxadiazole-based PI membranes for separating CO_2/CH_4 gas mixtures

In this chapter we will discus how the PI backbone geometry and the presence or absence of a strong electrostatic dipole moment governs gas transport and the ability to separate CO_2/CH_4 gas mixtures. To this end, two polar (μ = 3D) 1,3,4-oxadiazole diamines, ODD and mODD, and one non-polar *m*-terphenyl diamine were synthesized and coupled with 3 selected dianhydrides, *i.e.* 6FDA, ODPA and ODDA. In all 6FDA-based membranes CO_2 permeabilities (P_{CO2}) are the highest of the series, reaching a maximum of 33 Barrer (at 6 bar) for 6FDA-TPD, which is 6 times higher than P_{CO2} observed for Matrimid®. The 6FDA-ODD membrane shows excellent membrane performance with high P_{CO2} values at all feed pressures. More specifically, this membrane has a P_{CO2} of 16 Barrer at 3 bar making it 3 times more permeable than Matrimid®. This study yielded important design rules with respect to PI backbone design. In terms of permeability, we found that the backbone geometry dominates, whereas the presence of an electrostatic dipole moment governs selectivity. Up to 12 bar none of the membranes reaches their plasticization pressure.

5.1 Introduction

The development of polyimide (PI) gas separation membranes has been hindered by their inherent trade off relationship between the gas permeability and the separation selectivity.[1,2] New membranes need to exhibit high permeability as well as high selectivity. The way to achieve this, in all-aromatic polyimides as dense glassy membranes, is through a careful structure/property optimization process. The gas separating properties of dense glassy polymeric membranes are very sensitive to the chemical structure of the repeating units, with permeability coefficients of CO_2 in different polymer classes varying greatly from 0.0003 Barrer [3] to 27,000 Barrer [4].[5]

Theoretical and empirical studies have shown that by incorporating bulky pendant groups both permeability and selectivity can be simultaneously increased.[6–8] Bulky pendant groups such as trimethylsilyl, fluorenyl, phenyl or t-butyl groups inhibit chain packing efficiency consecutively increasing free volume and therefore enhancing permeability, while maintaining high selectivity.[6,9] One such example is a PMDA-TBAPB polyimide membrane [10] shown in Figure 5.1A. The most permeable glassy polymers are those which possess high free volumes (intermolecular voids within a material).[11,12] Free volume can be trapped in the solid state during membrane preparation when the polymer backbone contains bulky pendant groups or groups that introduce steric hindrance and frustrate chain packing thereby increasing the average interchain spacing. One well-known modification is the hexafluoro propane linker $-C(CF_3)_2-$, present in 2,2'-bis(3,4-carboxylphenyl)hexafluoropropane dianhydride (6FDA). This dianhydride has been a popular monomer in many polyimide membrane studies.[9,13–16]

Another method to introduce more free volume is with thermally rearranged (TR) polymers.[17,18] When aromatic polyimides with hydroxyl functional groups in the *ortho*-position are heated to high temperatures (350–450 °C) they thermally rearrange to form poly(benzoxazole)s.[19] This process results in a rigid high T_g polymer backbone comprised of interconnected heterocyclic rings. The cavity size and free volume element distribution in these polymers is favorable for CH_4 separation. TR polymer 6FDA-HAB, Figure 5.1B, shows CO_2 permeabilities that are 30 times higher than for the precursor polyimide.[19]

A

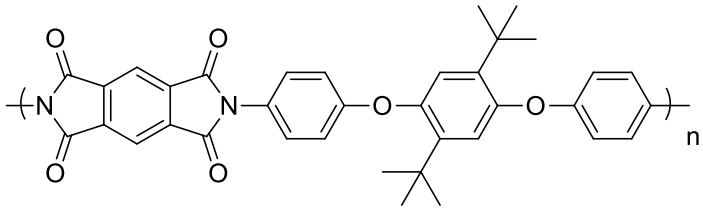

T_g = 329 °C P_{CO2} = 141 Barrer $\alpha_{CO2/CH4}$ = 18

B

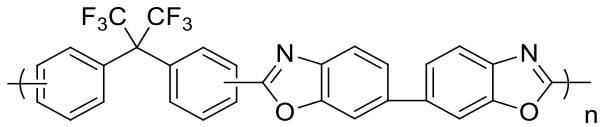

T_g = 271 °C P_{CO2} = 570 Barrer $\alpha_{CO2/CH4}$ = 29

C

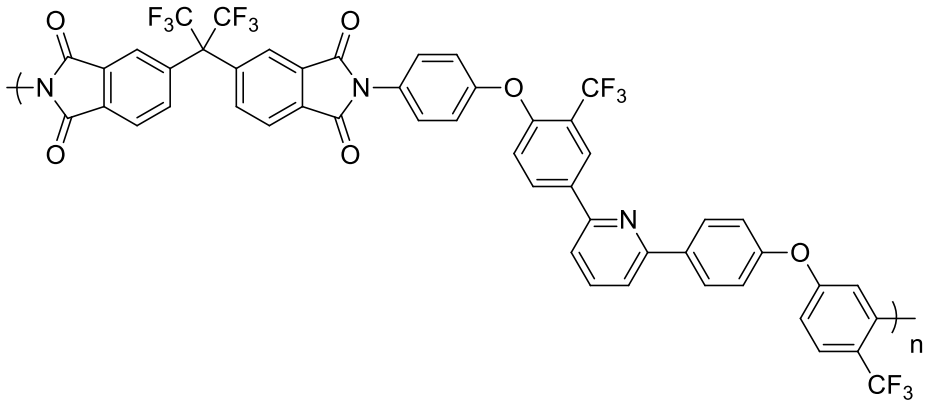

T_g = 264 °C P_{CO2} = 52 Barrer $\alpha_{CO2/CH4}$ = 27

Figure 5.1. Selected examples of several bulky polymer structure modifications. **A**- PMDA-TBAPB[10] is a PEI membrane with bulky pendant t-butyl groups, **B**- TR(6FDA-HAB)[20] is a thermally rearranged 6FDA-based polyimide membrane and **C**- 6FDA-BAPy[15] is a PEI with a pyridine heterocycle in the backbone. Key gas separation parameters and T_gs are listed below each example.

Having this in mind, another aspect we set off to investigate in this study is the role of heterocyclic (heteroaromatic) rings in the polyimide backbone. Even though a great deal of research has been done on the role which the polyimide main chain structure has on gas separation, what seems to be lacking is an understanding of the role of the heterocycles in these processes. Heterocycles are inherent to the backbone of aromatic polyimides, but in order to further increase their content, Sen *et al.*[15] included pyridine and thiophene in the polyetherimide (PEI) backbone. Their results show that the enhanced polarity of heterocyclic groups (*e.g.* pyridine and thiophene) in the PEI backbone

increases the permeability of CO_2 by 60% for the pyridine-containing PEI and by 36% for the thiophene-containing PEI, while maintaining a similar CO_2/CH_4 selectivity as found in the linear PEI analogs.

The studies summarized above motivated us to look into another method towards inducing free volume in all-aromatic PIs. In this chapter we will present a new series of PIs, in which we have increased the complexity of the polyimide backbone design by exploring diamine monomers that introduce both non-linearity (prevent crystallization) and increase the concentration of electrostatic dipole moments per polymer repeat unit. The synthesis and membrane CO_2 permeability and CO_2/CH_4 selectivity of this series of high T_g PIs based on 3-ring boomerang-shaped diamines will be discussed.

5.2 Polymer design

Expanding on the poly(etherimide)s introduced in Chapters 2 and 3, we want to explore the possibility to increase the free volume and diffusivity of our polymers by introducing non-linear (boomerang-shaped) 3-ring diamine monomers. Therefore we have synthesized a series of 9 polyimides with systematic backbone modifications that enabled us to compare membrane performance, interpret the effect of each moiety and extract further design rules.

All three diamines chosen for this study were based on a 3-ring boomerang-shaped structure with different cores in the center of the kink. They are 2,5-bis(4-aminophenyl)-1,3,4-oxadiazole (ODD), 2,5-bis(3-aminophenyl)-1,3,4-oxadiazole (mODD) and 4,4''-diamino-*m*-terphenyl (TPD), see Figure 5.2. Both ODD and mODD have an oxadiazole core but they differ in the relative position of the amine groups, they are *para*-positioned in ODD and *meta*-positioned in mODD. Oxadiazole was the chosen heterocycle due to the specific properties displayed by poly(oxadiazole)s and oxadiazole-based polymer membranes such as high CO_2/CH_4 selectivity, high T_g (low intersegmental mobility) and chemical stability.[8,15] As a reference we have synthesized a *meta*-terphenyl diamine, TPD. Doing so allows us to contrast the difference in gas separation performance between the polar 1,3,4-oxadiazole-based PIs and the non-polar *m*-terphenyl-based PIs without drastically changing the overall polymer geometry. The 1,3,4-oxadiazole heterocycle has an electrostatic dipole moment of 3 D whereas the central 1,3-phenyl unit in TPD has no dipole moment.[21] Changing the exocyclic bond angle in these 3-ring diamines, from 134° for ODD and mODD to 120° for TPD subtly modifies

the backbone to a more bend or kinked conformation. The advantage of working with kinked 3-ring diamines is that they frustrate the chain-chain packing preferences, which in turn inhibits polymer crystallization.

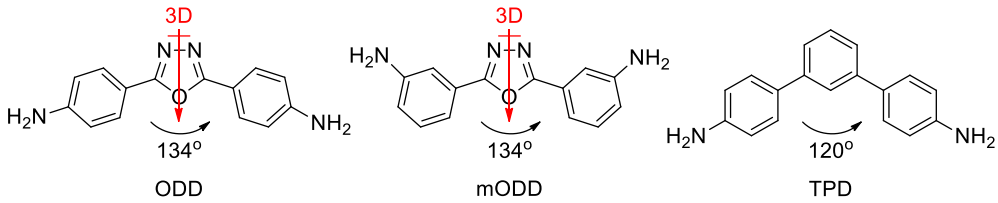

Figure 5.2. Chemical structures of the 3-ring diamines. Diamines with an oxadiazole core have an exocyclic bond angle of 134° whereas the terphenyl diamine has the exocyclic bond angle of 120°. In terms of molecule polarity, the oxadiazole core provides a dipole moment of 3 Debye in ODD and mODD. TPD is the non-polar reference monomer.

Three dianhydride moieties that are selected for this study are 3,3',4,4'-oxydiphthalic dianhydride (ODPA), 4,4'-(1,3,4-oxadiazole-2,5-diyl)diphtalic anhydride (ODDA) and 2,2'-bis(3,4-carboxylphenyl)hexafluoropropane dianhydride (6FDA) (Figure 5.3).

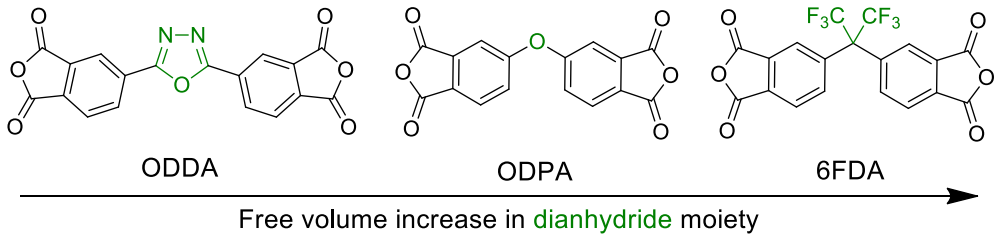

Figure 5.3. Chemical structures of the selected dianhydride moieties. Expected increase in free volume due to the core structure.

6FDA is a dianhydride commonly used for making the PI chains bulkier. It is a rather inflexible monomer as CF_3 groups inhibit rotation, which increases chain rigidity and free volume thus increasing permeability as well as selectivity.[9,15] Contrary to 6FDA, ODPA has flexible ether linkages and our previous research (presented in Chapters 2 and 3) has shown that ODPA is a good candidate for CO_2/CH_4 gas separation membranes. We have chosen to synthesize and use ODDA since it allows us to prepare a kinked PI chain with two strong lateral dipole moments, in combination with ODD and mODD diamines, loading the heterocyclic content in every monomer unit. This way we have systematically tailored the segmental mobility and steric hindrance induced by pendant groups

thereby changing the non-equilibrium free volume in this series of polyimides. Due to 6FDA's bulkiness and ODPA's flexibility, the expected free volume increase is in the order 6FDA>ODPA>ODDA.

5.3 Gas permeation

The gas separation experiments of this novel series PI-based membranes were performed at the Catalysis Engineering Department of the TU-Delft. The setup used will be described in more detail in section 5.4.5.

The gas separating performance was defined again with the gas permeability (P) of the components and the gas separating factor, the mixed gas selectivity (α). The permeability for a component (P_i) was calculated following Eq. (5.1):

$$P_i = S_i \times D_i \tag{5.1}$$

According to the solution-diffusion model, the permeability coefficient is the product of a solubility coefficient (S_i) and a diffusivity coefficient (D_i) of the *i*-component.

The mixed gas selectivity of a membrane for one gas over the other arises due to differences either in the solubility coefficient (S_i/S_j) or in the diffusivity coefficient (D_i/D_j). Therefore the ability of a polymer membrane to separate two gases (*e.g.*, i and j) is the ideal selectivity $\alpha_{i/j}$ (Eq. (5.2)).

$$\alpha_{i/j} = \frac{P_i}{P_j} = \left(\frac{D_i}{D_j}\right) \times \left(\frac{S_i}{S_j}\right) \tag{5.2}$$

For our binary gas mixture, the selectivity was calculated as the ratio of the permeability of the more permeable compound (CO_2) to the permeability of the less permeable compound (CH_4). This is a value that is less commonly reported, as it is not a material property since it depends on operating conditions, such as the feed composition.

5.4 Experimental

5.4.1 Materials

Monomers 4,4''-diamino-*m*-terphenyl (TPD) and 4,4'-(1,3,4-oxadiazole-2,5-diyl)diphtalic anhydride (ODDA) were synthesized according to literature

procedures, and described in detail in section 5.4.3. Monomers 2,5-bis(4-aminophenyl)-1,3,4-oxadiazole (ODD) and 2,5-bis(3-aminophenyl)-1,3,4-oxadiazole (mODD) were previously synthesized according to [22]. All other start materials were purchased from commercial sources and used as received unless stated otherwise. Dianhydrides 6FDA and ODPA were purchased from TCI Co. Ltd. and dried prior to use overnight in a vacuum oven at 60 °C. N-Methyl-2-pyrrolidinone (NMP) was obtained from Acros Organics. Matrimid® 5218 was supplied by Huntsman Advanced Materials in the form of a soluble fully imidized polyimide powder.

5.4.2 Characterization

The structures of the TPD and ODDA monomers were confirmed by ^{1}H NMR (Agilent-400 MR DD2, 400 MHz) and ^{13}C NMR (Agilent-400 MR DD2, 100 MHz). All samples were dissolved in dimethyl sulfoxide-d6 and the recorded spectra were referenced to the solvent (DMSO-d6: ^{1}H 2.50 and ^{13}C 39.5 ppm) relative to TMS. For GC/MS analysis of TPD, a Shimadzu GCMS-QP2010S gas chromatograph mass spectrometer was used coupled with the GL Sciences Optic 3 high-performance injector. Separation of the evolved gases was achieved using a 30 m × 0.025 mm SGE forte BPX-5 capillary column operated at a He flow rate of about 1 ml/min. Software ATAS Evolution Workstation (ATAS GL International) controlled heating of the injection port of the GC from 50 °C to 300 °C in 5 min. The GC column oven was programmed from 50 °C, with a heating rate of 20 °C/min, to 300 °C (held for 30 min). LabSolutions data system, GCMSsolutions (Shimadzu) Postrun analysis software was used to integrate the peaks. Melting points were determined by differential scanning calorimetry (DSC) using a PerkinElmer Sapphire DSC. A heating rate 20 °C/min was used for all melting point measurements.

Gel permeation chromatography (GPC) measurements of the polyamic acids were performed on a Shimadzu Prominence GPC system equipped with two Shodex LF-804 columns. N-Methyl-2-pyrrolidone (NMP) with 5 mM of LiBr was used as eluent at a flow rate of 0.5 mL/min at 60 °C. Data analyses were performed with LabSolutions software using the refractive index detector data. Quantification was made based on polystyrene standard calibration. All polyamic solutions were filtered through a 0.45 μm PTFE filter prior to a GPC run.

The thermal properties of the PEI films were determined by DSC using a PerkinElmer Sapphire DSC. Samples were heated at a rate of 20 °C/min under a nitrogen atmosphere. Thermogravimetric analysis (TGA) was performed on a Perkin Elmer Pyris diamond TG/DTA under a nitrogen atmosphere and a scan rate of 10 °C/min. Polymer thin films were investigated using a dynamic mechanical thermal analyzer (DMTA) in the temperature range 0 °C to 400 °C, at a heating rate of 2.5 °C/min and at a frequency of 1 Hz, under a nitrogen atmosphere. Approximate dimensions of films were 20 × 4 × 0.03 mm. All samples were dried in a vacuum oven at 60 °C for 1 h prior to testing.

To investigate the morphology of the PI films (19–38 μm), XRD experiments were conducted using a Bruker AXS D8 Advance X-ray diffractometer in reflection mode (Bragg Brentano geometry), with cobalt as the radiation source and LynxEye as the detector. For every PI film, three layers were fixed onto a silicon wafer support with Scotch tape. All experiments were performed at room temperature in the 2θ range from 5° to 50°, with step size of 0.04° at 0.8 seconds per step.

5.4.3 Monomer synthesis

Terphenyl diamine (TPD) was synthesized using Suzuki-Miyara aryl-aryl coupling conditions, the synthesis is a modified procedure of what was reported by Sinclair and Sherburn [23]. Our two-step procedure is shown in Scheme 5.1 and the synthetic details are described in more detail bellow.

4,4"-dinitro-m-terphenyl. A 1000 mL three-neck round-bottomed flask, equipped with an argon gas inlet tube, a reflux condenser, and a magnetic stirrer, was charged with 5 g (0.030 mol) of 1,3-benzenediboronic acid, 12.19 g (0.060) of 1-bromo-4-nitrobenzene, 60 mL of 2M K_2CO_3 solution and 300 ml of THF. This mixture was stirred under a slight argon over pressure. After 1 h, 0.349 g (1 mol%) of tetrakis(triphenylphospine)palladium catalyst was added, and 10 min later the gas inlet tube was removed and a gentle flow of argon was introduced on top of the condenser. This mixture was heated to reflux for 24 h. When the reaction was complete, the now dark colored mixture was cooled down to 25 °C and precipitated in 600 mL of ice water. A yellow precipitate was filtered off and washed with ethanol. The solid crude product was recrystallized twice from DMF. Pale yellow crystals were obtained and dissolved in DCM with charcoal to remove any remaining impurities, this mixture was filtered over celite and silica and the product was obtained as a white powder. Yield 5.33 g (55%); TLC:

(9/1 hexane/ethyl acetate) t_r = 0.622 (one spot). GC/MS m/z (relative intensity) t_R = 22.2 min, 320 (100%).

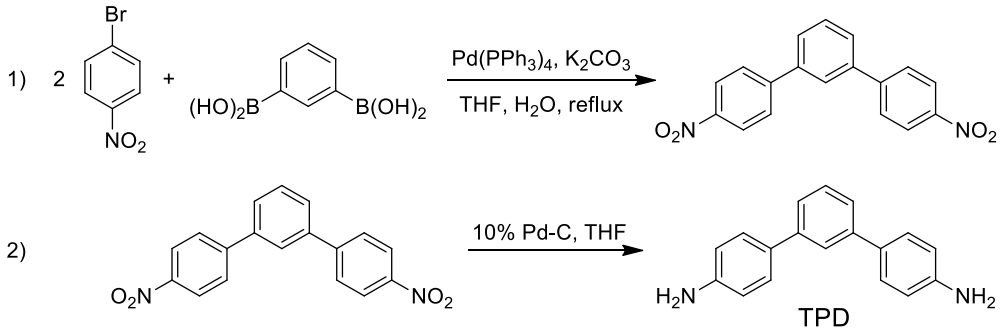

Scheme 5.1. Synthesis of 4,4"-diamino-*m*-terphenyl (TPD).

4,4"-diamino-m-terphenyl (TPD). A 250 mL hydrogenation bottle was charged with 5.33 g (0.017 mol) of 4,4"-dinitro-*m*-terphenyl, 150 mL of dry THF, and 0.29 g of 10% palladium on carbon. After degassing with argon for 20 minutes, the bottle was placed in a Parr hydrogenator, and the nitro groups were reduced under hydrogen atmosphere at 50 psi for 2 h at room temperature, then the shaker was turned off and the mixture was left under the same conditions of pressure and temperature overnight. The solution was filtered over celite and the THF was removed by rotary evaporation. Pure TPD was obtained after two recrystallizations from ethanol/water (90/10) as pale brown crystals. Yield: 2.8 g (52%); mp: T_{onset} = 151 °C, T_{max} = 161 °C. TLC (9/1 hexane/ethyl acetate) t_r = 0 (one spot). ^{1}H NMR (DMSO-d6, 400 MHz) δ (ppm): 7.64 (s, 1H), 7.41 (d, 4H, J = 8 Hz), 7.37 (t, 1H, J = 4 Hz), 7.36 (d, 2H, J = 4 Hz), 6.65 (d, 4H, J = 8 Hz), 5.21 (s, 4H); ^{13}C NMR (DMSO-d6, 100MHz) δ (ppm): 114.63, 122.96, 123.33, 127.73, 128.16, 129.51, 141.57, 168.48. GC/MS m/z (relative intensity) t_R = 18.35 min, 260 (100%).

Diphtalic anhydride with an 1,3,4-oxadiazole core (ODDA) was synthesized according to a method found in a patent by Palaniswamy *et al.*[24] Here, benzenetricarboxylic anhydride is reacted with hydrazine, forming a heterocyclic 1,3,4-oxadiazole ring (Scheme 5.2).

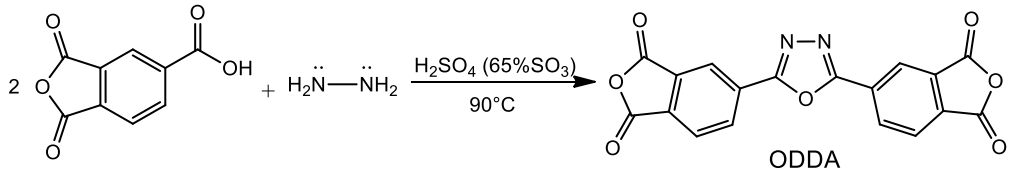

Scheme 5.2. Synthesis of 4,4'-(1,3,4-oxadiazole-2,5-diyl)diphtalic anhydride (ODDA).[24]

4,4'-(1,3,4-oxadiazole-2,5-diyl)diphtalic anhydride (ODDA). A 250 mL three-neck round-bottom flask, equipped with a stirring bar, condenser and a nitrogen inlet, was charged with 29.62 g of 1,2,4-benzenetricarboxylic anhydride (154 mmol) and 80 mL of fuming sulfuric acid (65% free SO_3). This suspension was heated to 80 °C and stirred under nitrogen until all solid were dissolved, after which 9.56 g (73 mmol) of hydrazine sulfate salt was added in portions. The reaction mixture was heated and stirred at 90 °C for 4 hours. The reaction mixture was poured onto crushed ice and the white precipitate was filtered off. White sticky solids were washed with water and filtered several times until the pH was neutral. The white solids were combined in a flask containing 50 mL of toluene so that the residual water could be removed by azeotropic distillation. The solids were dried for 48 h in a vacuum oven at 60 °C, after which recrystallization from acetic anhydride (50 mL/g) yielded the desired product as pure white crystals. Yield: 7.91 g (26.7%); mp: T_{onset} = 322 °C, T_{max} = 326 °C (326 °C).[24] ^{1}H-NMR (DMSO-d6, 400MHz) δ (ppm): 8.32 (d, 2H, J = 8 Hz), 8.70 (d, 2H, J = 6.8 Hz), 8.92 (s, 2H); ^{13}C NMR (DMSO-d6, 100MHz) δ (ppm): 123.29, 123.47, 126,29, 129.54, 132.72, 133.82, 162.37, 162.44, 163.50.

5.4.4 Polymer synthesis

Polyamic acids of high molecular weight were prepared from the dianhydride and diamine monomers, in equimolar quantities, as 15 wt.% solutions in NMP at 25 °C.

Preparation of ODDA-ODD 15 wt.% polymer film (representative procedure, Scheme 5.3): A dry 50 mL one-neck round-bottom flask was charged with 0.634 g (2.51 mmol) of 2,5-bis(4-aminophenyl)-1,3,4-oxadiazole (ODD) and 8 mL of dry NMP (water content < 0.005%) was added. This solution was then stirred for 5 min, under a dry nitrogen flow, at room temperature with a magnetic stirrer at 120 rpm until the diamine monomer was dissolved. After this step the polymerization was initiated by adding 0.910 g (2.51 mmol, an equimolar

amount) of 4,4'-(1,3,4-oxadiazole-2,5-diyl)diphtalic anhydride (ODDA), and the walls of the flask were washed with 2 mL of NMP. Polymerization was allowed to continue for 24 h. under a nitrogen atmosphere, stirring at 90 rpm.

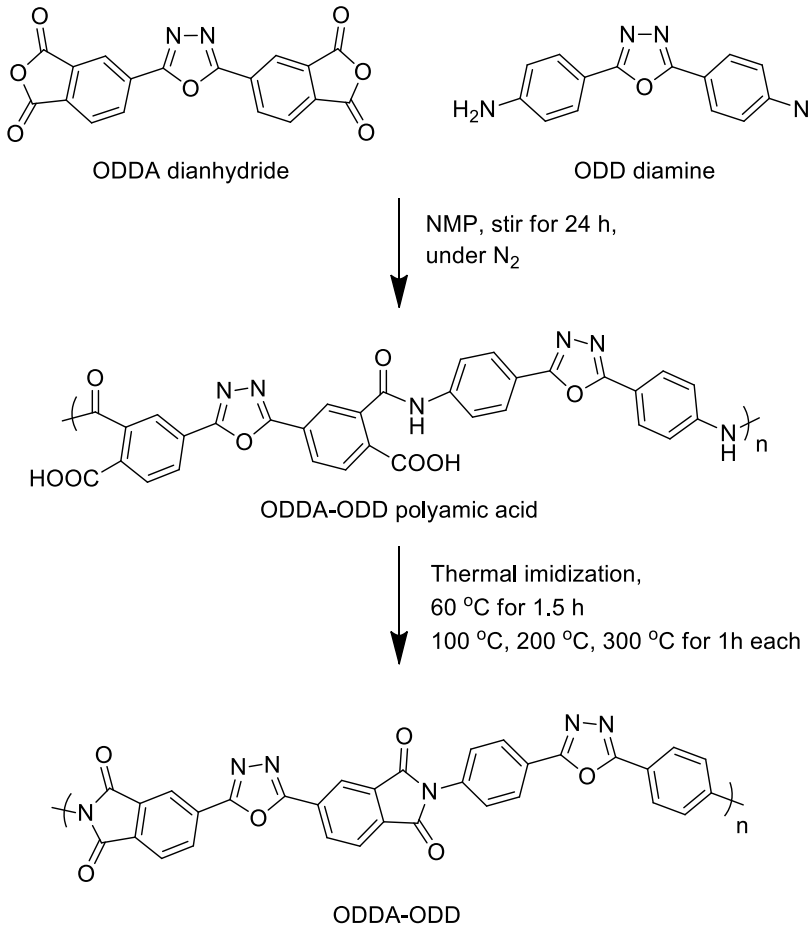

Scheme 5.3. Polymerization procedure used to prepare an ODDA-ODD free-standing membrane.

Film preparation. In order to remove any solid particles, the polyamic acid solution was filtered using a Sartorius pressure filter. The resulting filtered solution was degassed to remove bubbles and then cast with a doctor-blade onto a clean, dry glass plate (film thickness ~0.6 mm) and placed in a clean vacuum oven at 60 °C for 1.5 h. Films were thermally imidized by heating to 100 °C for 1 h, 200 °C for 1 h, and 300 °C for 1 h. After an overnight cooling to

25 °C, the film was released from the glass plate by placing it in lukewarm water. All PIs were obtained as free-standing films using this procedure.

Matrimid® film preparation. 0.62 g of Matrimid® powder was dissolved in 4 mL of NMP, this solution was cast with a doctor-blade onto a clean, dry glass plate and it was subjected to the same thermal program as described above for other polymers of this series. A free-standing film was obtained and used for gas permeation measurements as a reference material.

5.4.5 Gas permeation measurements

Gas permeation experiments were performed using an in-house built setup depicted in Scheme 5.4. An equimolar CO_2:CH_4 mixture was used as feed (50 mL/min of CO_2 and 50 mL/min of CH_4), while helium (67.7 mL/min) was used as sweep gas for the permeate flow. The trans-membrane pressure was set in the range of 3 bar to 12 bar using a back-pressure controller at the retentate side. The temperature in the permeation module was kept constant and equal to 35 °C. The composition of the permeate flow was periodically measured using an on-line gas chromatograph (Interscience Compact GC) equipped with a packed Carboxen 1010 PLOT (30 m × 0.32 mm) column, a thermal conductivity detectors (TCD) and a flame-ionization detector (FID). Digital flow meters measured the gas flows.

Separation selectivity and gas permeability values are reported after a steady operating regime was reached. Experiments were performed at 4 different pressures, at 3, 6, 9 and 12 bar. Permeability coefficients were calculated from the steady-state pressure increase $\Delta P_p/\Delta t$ with Eq. (5.3):

$$P_i = \frac{\varphi_{ni} \times \delta}{\Delta P_i \times A} \tag{5.3}$$

where φ_{ni} is the molar flow rate of the *i*-component, δ is the thickness of the membrane, ΔP_i is the partial pressure difference of the *i*-component across the membrane and A is the membrane area. The SI unit for the permeability is mol s^{-1} m^{-1} Pa^{-1}. Still, permeabilities are commonly reported in non-SI unit Barrer, where 1 Barrer = 3.35×10^{-16} mol s^{-1} m^{-1} Pa^{-1}.

Selectivity (α) was calculated as the ratio of permeabilities of two components, with Eq. (5.4):

$$\alpha_{CO_2/CH_4} = P_{CO_2} \,/\, P_{CH_4} \tag{5.4}$$

where P_{CO2} and P_{CH4} are permeabilities of CO_2 and CH_4, respectively.

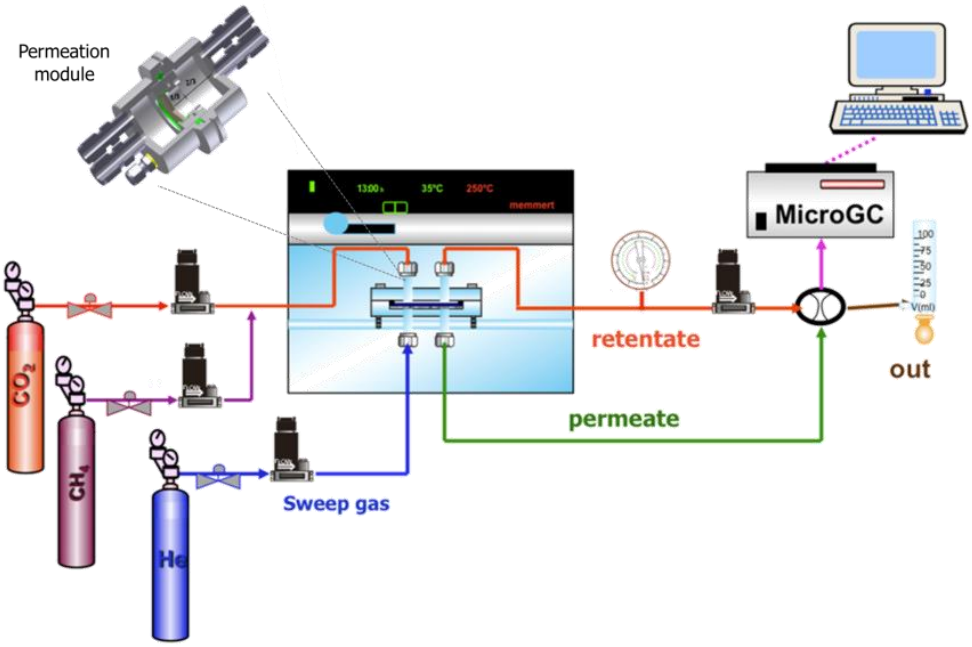

Scheme 5.4. Schematic representation of the permeation setup and the membrane module. Scheme adapted with permission from the Catalysis Engineering group, TU Delft.

All membranes were cut to fit the module, their area determined to be 4.16 cm^2. However, a promising membrane 6FDA-TPD was showing leaks due to small cracks. In order to circumvent this issue a smaller membrane was used (area ~ 1 cm^2). Since the dimensions of the module are fixed, this smaller membrane was sandwiched between two layers of aluminum tape and the edges were sealed with a cold-setting resin (EpoFix™). To determine whether this approach is comparable to the experimental set-up used for larger membranes, we measured two other 6FDA-based membranes (6FDA-ODD and 6FDA-mODD) using similar sample dimensions. A mixed feed pressure of 3 bar pressure was used to confirm consistency.

5.5 Results

5.5.1 Gel permeation chromatography measurements

The molecular weights of the polyamic acid intermediates, measured using GPC, are listed in Table 5.1. The actual GPC curves are shown in Appendix (Figure A). High molecular weight polyamic acids could be prepared without difficulties, with number average molecular weights in the range of ~33,000 to ~110,000 g/mol and polydispersities (PDI) typical for step-growth polymers. All GPC curves show a unimodal molecular weight distribution (Figure A, see Appendix).

Table 5.1. Molecular Weight data of the polyamic acids as determined by GPC.

Polymer	M_n (g/mol)	M_w (g/mol)	PDI=M_w/M_n
6FDA-TPD	42,000	64,000	1.5
6FDA-ODD	59,000	110,000	1.9
6FDA-mODD	62,000	150,000	2.4
ODPA-TPD	110,000	319,000	2.9
ODPA-ODD	33,000	61,000	1.9
ODPA-mODD	50,000	116,000	2.3
ODDA-TPD	101,000	229,000	2.2
ODDA-ODD	76,000	143,000	1.9
ODDA-mODD	47,000	93,000	2.0

Tough, flexible and easy-to-handle PI films were obtained after thermal imidization. 6FDA gives very clear pale-yellow films, while ODPA and ODDA give darker yellow color to the films, respectively. The almost colorless transparency of 6FDA-based series indicates other application potential of these high-performance polyimides. All polyamic acids were prepared at 15 wt.% solids. With the exception of ODDA-mODD, all polymerizations went without difficulty and yielded high molecular weight polyamic acids. The issue with ODDA-mODD was that monomers wouldn't readily dissolve in NMP. Two modifications were made, firstly mODD was sonicated in NMP for 2 hours after which the dianhydride was added and the solution was warmed with a heat gun at 100 °C for 1 minute in order to dissolve ODDA. This resulted in high molecular weight polymer. Despite these adjustments, ODDA-mODD films

turned out to be very brittle in nature, had to be handled with care and did not make a good membrane.

5.5.2 Dynamic thermogravimetric analysis

The thermal stability of all 9 PI films was investigated by dynamic thermogravimetric analysis. Sample films were cleaned and degreased with ethanol and dried at 60 °C for 2 hours. All films were investigated under inert (nitrogen) conditions using a heating rate of 10 °C/min. This provided information with respect to the polymer decomposition temperature, the temperature at which a weight loss of 5% occurs ($T_{5\%}$) as well as the char yield at 585 °C. The resulting thermograms, showing polymer weight as a function of temperature, are shown in Figure 5.4 and the values for $T_{5\%}$ and char yield are listed in Table 5.2.

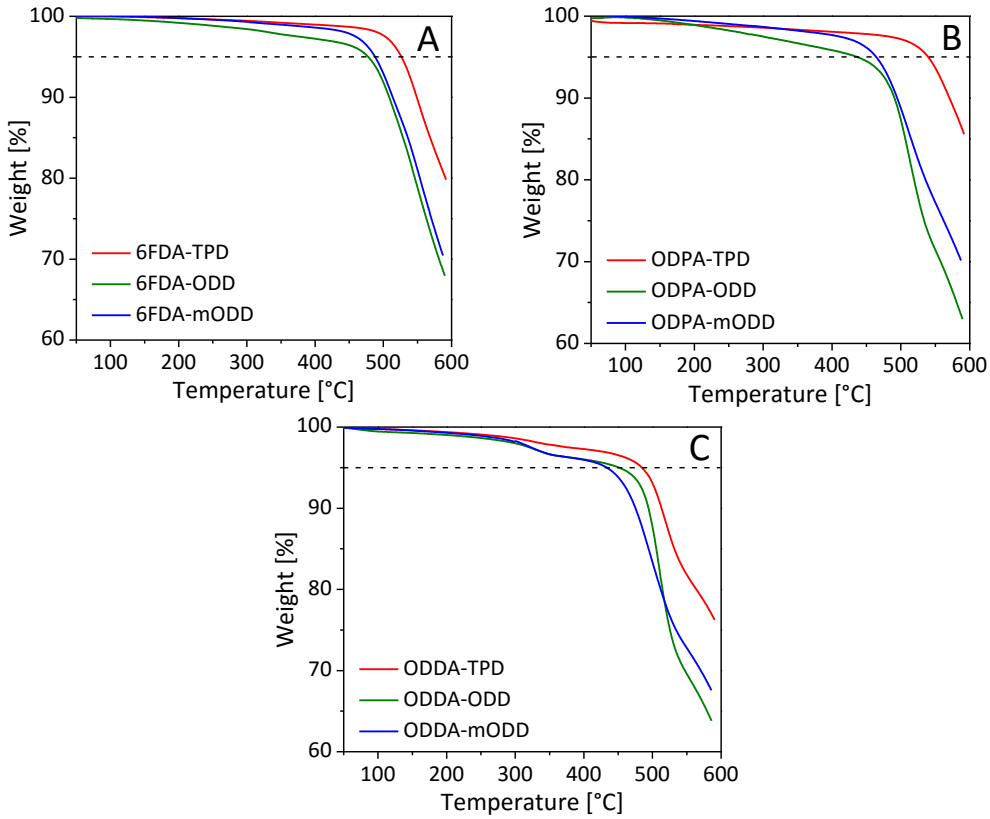

Figure 5.4. TGA thermograms of the PI films. **A**- 6FDA-series, **B**- ODPA-series and **C**- ODDA-based PI series; heating rate 10 °C/min in (N_2 atmosphere). The dotted line marks the 5% weight loss point.

All 9 PIs in this series show a gradual decrease in weight as a function of temperature up to ~450 °C, see Figure 5.4. The weight loss below 450 °C is due to outgassing of low molecular weight species such as solvent (NMP). Above 450 °C, the PI films degrade due to thermal decomposition. ODDA-based PIs display a weight-loss stage at ~320 °C. This temperature is consistent with the degradation of the ODDA monomer and can be attributed to the oxadiazole ring deterioration. The highest thermal stability is displayed by ODPA-TPD and 6FDA-TPD. TPD is an all-aromatic (phenylene-based) monomer and hence exhibits superior thermal stability. The values reported in Table 5.2 are typical for all-aromatic PEIs and PIs containing heterocycles.[25–27] As the PI-based membranes will operate at or slightly above 25 °C the thermal stability of this series will not be an issue.

Table 5.2. Dynamic thermogravimetric analysis results of the polyimide films. Heating rate 10 °C/min and nitrogen atmosphere.

Polymer	TGA	
	5% weight loss (°C)	char yield at 585 °C (%)
6FDA-TPD	527	81
6FDA-ODD	478	69
6FDA-mODD	488	71
ODPA-TPD	540	87
ODPA-ODD	437	64
ODPA-mODD	465	71
ODDA-TPD	484	77
ODDA-ODD	452	64
ODDA-mODD	434	68

5.5.3 Differential scanning calorimetry (DSC)

The thermal properties of the PI films were determined by DSC using a PerkinElmer Sapphire DSC. Samples were heated at a rate of 20 °C/min under a nitrogen atmosphere to ~400 °C, depending on the thermal stability of the sample as determined by TGA. The DSC curves, first heats only, are shown in Figure 5.5 and the T_g values are summarized in Table 5.3.

We were unable to detect a T_g for ODPA-ODD as well as the ODDA-based series by DSC.

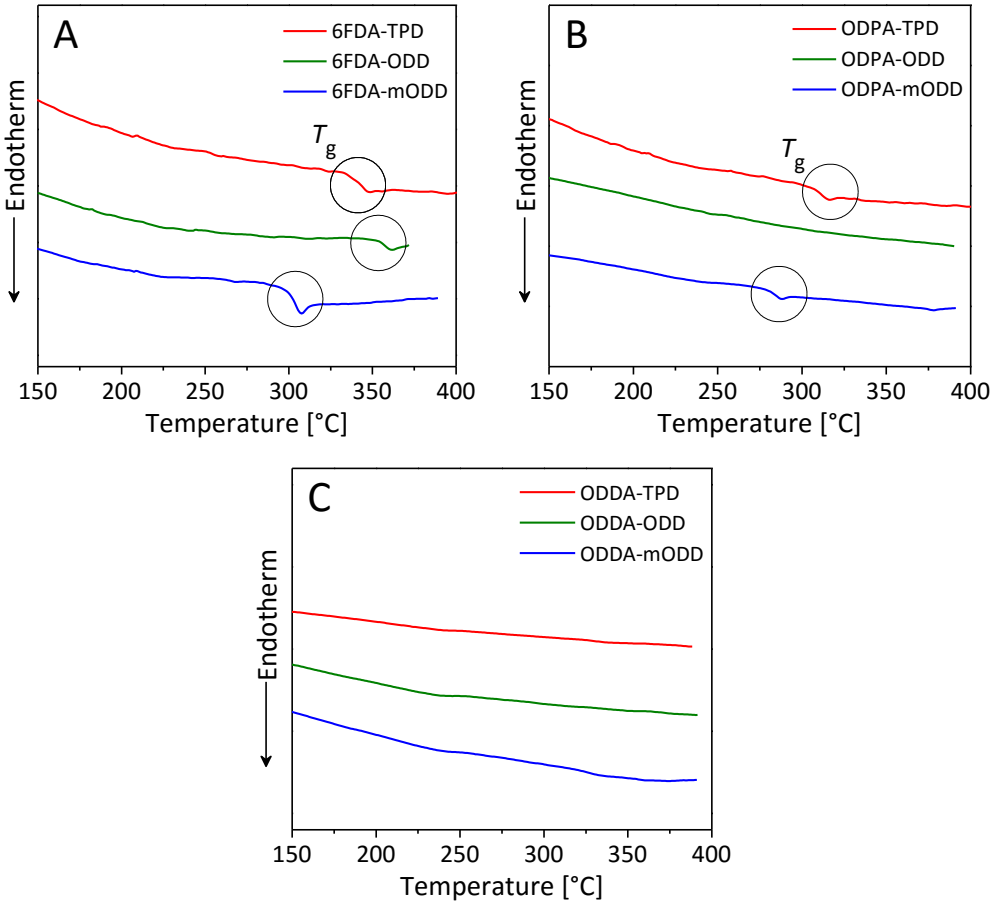

Figure 5.5. DSC curves showing the T_g events as a function of temperature. **A**- 6FDA-series, **B**- ODPA-series and **C**- ODDA-based PI series. First heat, recorded in N_2 atmosphere at 20 °C/min. All curves have been normalized to sample weight and translated vertically for sake of clarity.

Based on the DSC experiments it would appear that all 9 PIs are amorphous. This is in line with what has been reported for 6FDA- and ODPA-based PI's and PEIs.[25,28] However, we proceeded with X-ray diffraction studies to definitely determine the morphology, described later.

For the 6FDA-based series we observed the following trend in T_g: mODD<TPD<ODD. Other trends in T_g could not be observed as it was difficult to determine the T_g for ODDA-based series and ODPA-ODD. Since the 6FDA moiety introduces the most significant chain packing disruption, with stiff CF_3 groups hindering chain rotation, this leads to the largest free volume content and results in PIs with the highest T_gs. This can be very beneficial for

membrane performance. We discuss nature of ODPA-ODD later on in Section 5.5.5.

Table 5.3. Thermal and mechanical properties of the polyimides.[a]

Polymer	DSC	DMTA	
	T_g (°C)[b] DSC	T_g (°C)[c] DMTA	*E'* (GPa, 30 °C)
6FDA-TPD	338	336	3.5
6FDA-ODD	356	352	4.7
6FDA-mODD	303	300	5.0
ODPA-TPD	311	310	4.9
ODPA-ODD	-	276	4.3
ODPA-mODD	283	282	4.4
ODDA-TPD	-	335	4.4
ODDA-ODD	-	320	4.2
ODDA-mODD	-	-[d]	4.0

[a] DSC (first heating) and DMTA data were collected using a heating rate of 20 and 2.5 °C/min, respectively. [b] T_g is reported at the inflection point. [c] T_g is determined at the maximum of the loss modulus (E"). [d] film failed before T_g event.

5.5.4 Dynamic mechanical thermal analysis (DMTA)

The DMTA results show the values for the storage modulus (E') and T_g as determined at the maximum of the loss modulus (E") (Table 5.3). All PI membrane films show storage moduli (E') in the range of 3.5-5 GPa, which is typical for all-aromatic PIs.[25,29] The T_g values determined by DMTA correspond very well with ones observed by DSC. All DMTA curves are shown in Figure 5.6. With the exception of ODDA-mODD, a film that failed before the T_g event could be observed, all films show clear T_g events (as determined at the max of E"). The same is true for the β-transitions, with peak maxima clearly observed between 80 and 150 °C for all 9 films and the β-transitions seem to be independent of the diamine used. This can be explained by the dependence of the β-transition temperature and T_g on the rotation around the bond joining the dianhydride core and the phthalimide moieties.[29,30]

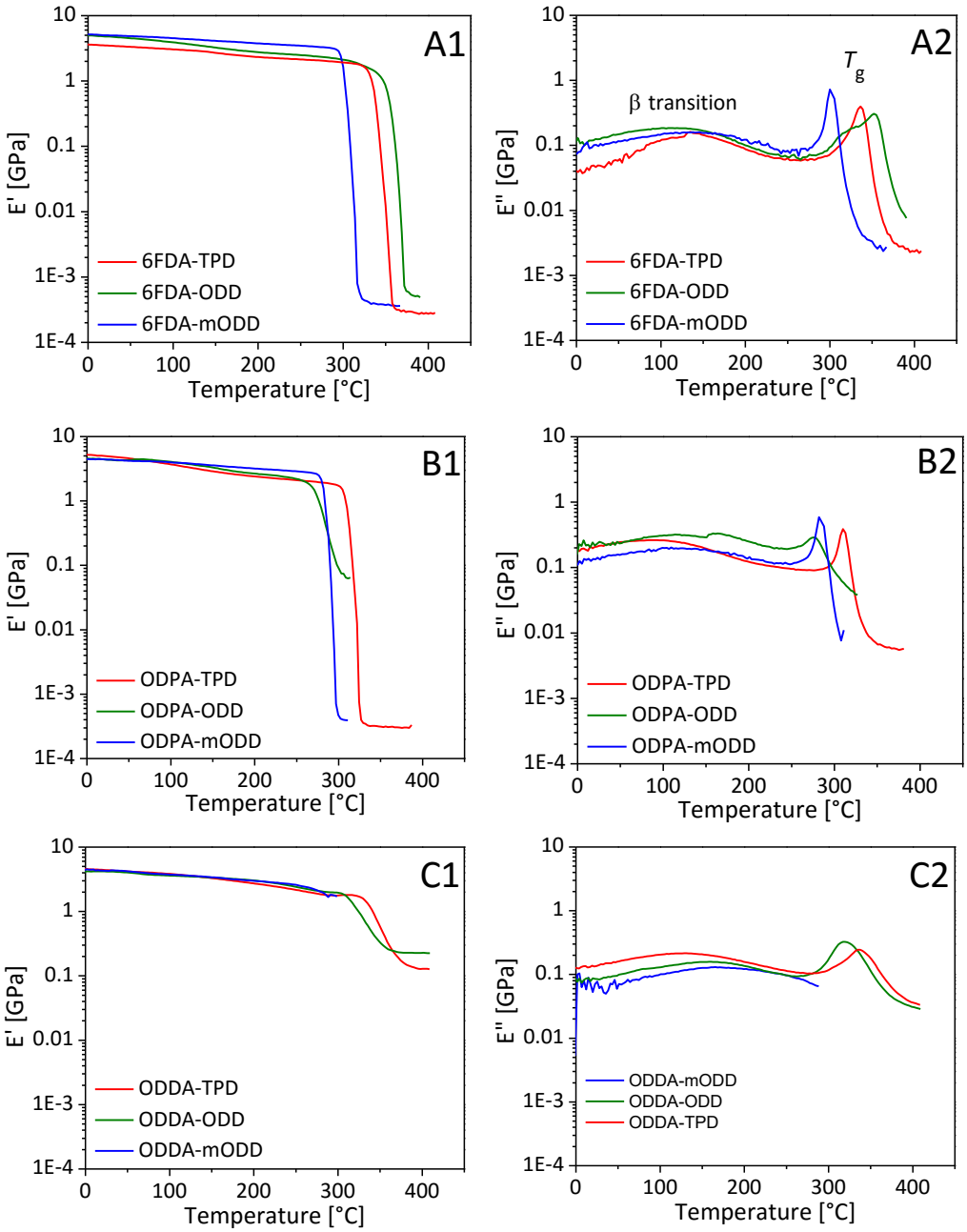

Figure 5.6. DMTA results of the PI films. The storage moduli (E') and loss moduli (E'') were recorded as a function of temperature (N_2 atmosphere at a frequency of 1 Hz and a heating rate of 2.5 °C/min). **A**- 6FDA-series, **B**- ODPA-series and **C**- ODDA-based PI series.

5.5.5 Film morphology, X-ray diffraction (XRD)

XRD analysis was performed on all 9 PI films (19–38 μm) and the results are shown in Figure 5.7. All 6FDA- and ODDA-based films are fully amorphous and in the ODPA-based series only ODPA-ODD is a semi-crystalline film (Figure 5.7B), with the degree of crystallinity 14%, while other two ODPA-based films are amorphous. The degree of crystallinity in the film was quantified by comparing the ratio of the area under the crystalline peaks to the total area of the curve. The melting endotherm and T_m of this semi-crystalline are not observed in our DSC scans up to 400 °C (Figure 5.5), it is assumed that the melting point lays well above the polymer degradation temperature.

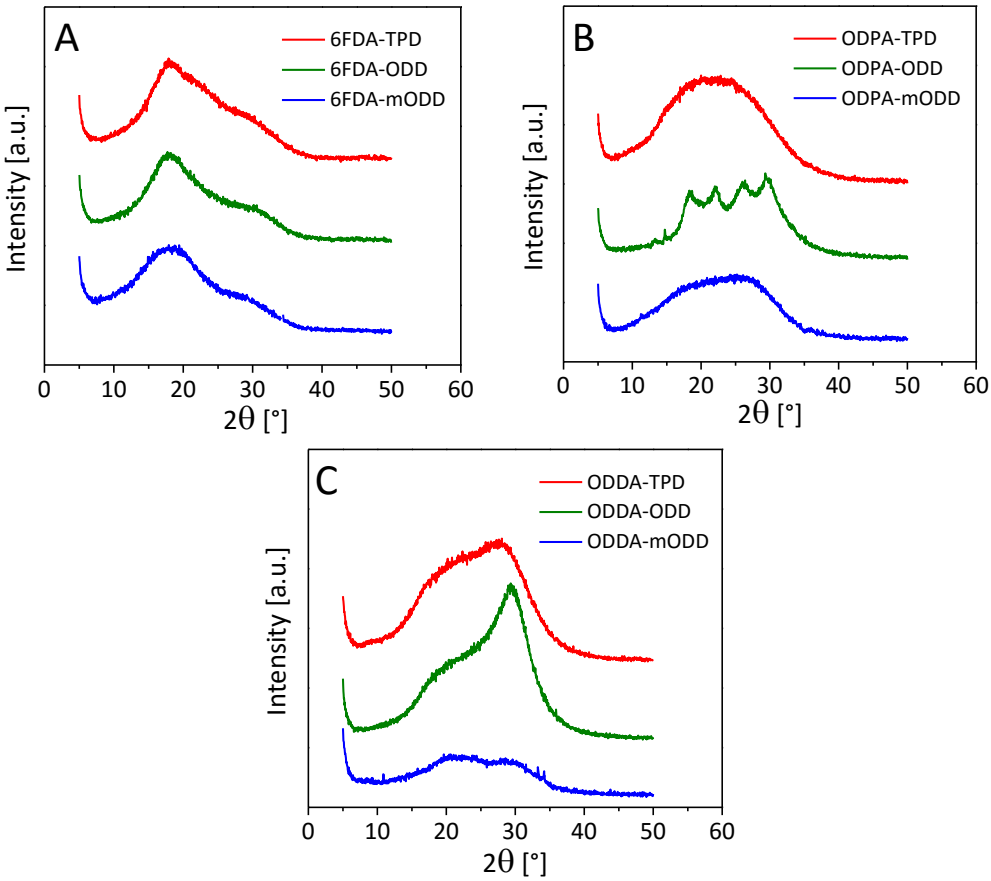

Figure 5.7. XRD results of the fully imidized PI films. The intensity is plotted as a function of the scattering angle. All curves have been translated vertically for sake of clarity. **A**- 6FDA-series, **B**- ODPA-series and **C**- ODDA-series.

5.5.6 Gas separation membranes

The gas separating capabilities of this polyimide membrane series (including the reference material Matrimid®) have been assessed with permeation experiments performed at 3, 6, 9 and 12 bar of equimolar CO_2/CH_4 feed at 35 °C. Values for CO_2 permeability and mixed gas selectivity are reported after a steady operating regime was reached. Polyimide ODDA-mODD was brittle and had too many cracks throughout the film thus could not be tested as a gas separation membrane. Attempts were made to test the film but significant leaks were observed and therefore those results were omitted.

Due to some small cracks on the film's surface, 6FDA-TPD couldn't be measured properly. Having in mind the excellent performance displayed by 6FDA-based membranes in the past (and confirmed by our measurements of 6FDA-ODD, 6FDA-mODD and to some extend also ODPA-TPD) it was imperative for us to find a way to measure the gas separating performance of 6FDA-TPD as well. We therefore resorted to using a smaller film ($A \approx 1$ cm^2 compared to $A \approx 4$ cm^2 for all other membranes) without visible defects. For comparison purposes, we also prepared small membranes ($A \approx 1$ cm^2) of the 3 6FDA-based films. In order for the films to fit in the module, these smaller membranes were placed between two layers of aluminum tape and the edges were sealed with a cold-setting resin (EpoFix™). Permeation experiments of 6FDA-ODD and 6FDA-mODD prepared using this method yielded remarkably similar P_{CO2} values with errors between 1.8 and 2.9 %. These values are presented in Table 5.4. With these encouraging results, confirming that our modified approach is valid, we carried out the permeation study of the 6FDA-TPD membrane.

Table 5.4. Comparison of permeability values for larger and smaller membranes. Permeability measured at 35 °C and a CO_2/CH_4 (50/50 vol.%) mixed feed pressure of 3 bar.

Polymer	CO_2 permeability (Barrer)		Error (%)
	4 cm^2 membrane	1 cm^2 membrane	
6FDA-ODD	16.09	15.17	2.94
6FDA-mODD	3.60	3.73	1.77

Figure 5.8 shows the CO_2 permeabilities of 8 PI membranes and Matrimid® as a function of the mixed feed pressure at 35 °C. The data is grouped by dianhydride moiety for sake of clarity.

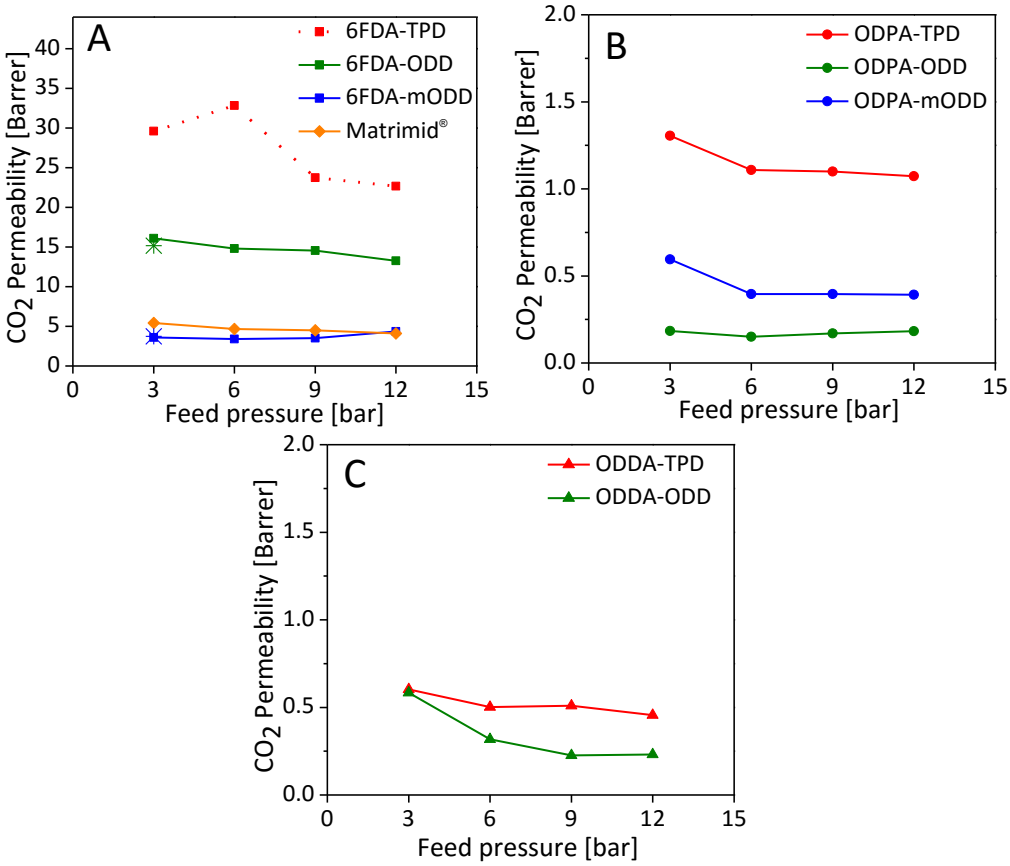

Figure 5.8. CO_2 permeability as a function of the mixed feed pressure at 35 °C. **A**- Matrimid® and 6FDA-series (star symbols represent reference values for small (1 cm^2) membranes 6FDA-ODD (green) and 6-FDA-mODD (blue)), **B**- ODPA-series and **C**- ODDA-based membrane series. Feed mixed gas: CO_2/CH_4 (50/50 vol.%). Note the different scale of the *y*-axis in plot A. 6FDA-TPD is measured with a smaller membrane area.

It is well known in the membrane field that the introduction of a $-C(CF_3)_2-$ bridge into the polyimide backbone effectively improves permeability as well as selectivity for different gas pairs.[9,15] As expected, our permeation experiments show that all three 6FDA-based PIs have the highest permeabilities in this whole series. CO_2 permeability coefficients as a function of feed pressure for 6FDA-based PIs are shown in Figure 5.8A alongside commercially used membrane Matrimid®. It has to be noted, that these values are even more

impressive when one realizes that the values for all 6FDA-based PIs had to be plotted on an extend *y*-axis scale (40 Barrer max.) vs 2.0 Barrer for the ODPA- and ODDA-PIs.

The 6FDA-ODD membrane shows excellent membrane performance with high CO_2 permeability values at all feed pressures. With P_{CO2} of 16 Barrer at 3 bar it is 300% more permeable than the commercial reference Matrimid®. 6FDA-mODD has a lower CO_2 permeability than Matrimid® at lower pressures but they are comparable at higher pressures of 9 and 12 bar. For both 6FDA-ODD and Matrimid® P_{CO2} decreases steadily with feed pressure increase. It is expected that P_{CO2} would reach a minimum at a certain pressure *i.e.* the plasticization pressure (described in more detail in Chapter 2). The downward trend of mixed gas selectivity confirms this (Figure 5.9A). In case of 6FDA-mODD plasticization pressure is around 9 bar. The effect of 6FDA moiety in PI backbone on the increase in gas permeability is clear; nevertheless, it is apparent that a subtle change introduced in the diamine structure amounts to a large P_{CO2} difference as well. The only modification between ODD and mODD diamine moieties is the position of the terminal amine groups. The more bent-shaped structure of ODD, with amine groups in *para*-position, yields a membrane with 4.5 times larger P_{CO2} than its mODD counterpart, with amine groups in *meta*-position. Throughout the pressure range 6FDA-TPD displays superior performance in CO_2 permeability. With respect to the other two 6FDA-based membranes, at 3 bar of mixed feed 6FDA-TPD has a CO_2 permeability of 30 Barrer, almost 2 times that of 6FDA-ODD, 8 times that of 6FDA-mODD and 6 times that of commercial Matrimid®. With an increase in feed pressure, 6FDA-TPD shows a somewhat unexpected behavior with an initial P_{CO2} increase (33 Barrer at a feed pressure of 6 bar), followed by a drop to 23 Barrer.

Both ODPA- and ODDA-based membranes have significantly lower CO_2 permeabilities than the 6FDA-series. In the ODPA-based series (Figure 5.8B) the TPD diamine has a great effect on P_{CO2}. Above 3 bar the permeability drops slightly but remains constant with further pressure increase. At 3 bar of feed pressure the difference in P_{CO2} between ODPA-ODD and ODPA-mODD is trifold, which is in contrast with the same diamines in combination with 6FDA. Remarkably both ODDA-based membranes display the same property at 3 bar, shown in Figure 5.8C, with ODDA-TPD remaining somewhat steady throughout the measurement range and ODDA-ODD dropping to a minimum around 10 bar. This indicates that plasticization occurred and an increase in

permeability together with a drop in selectivity is to be expected at higher pressures. A trend that is observed for all diamines is that P_{CO2} decreases in the order 6FDA>ODPA≥ODDA. Performance of ODPA-ODD and ODDA-ODD somewhat resembles that of the PEI series described in Chapter 2.

The gas separating performance of our new PI membranes and Matrimid® is summarized in Figure 5.9. The values for CO_2/CH_4 selectivities as a function of the partial pressure of gas at 3, 6, 9 and 12 bar are presented and grouped by the dianhydride moiety for sake of clarity.

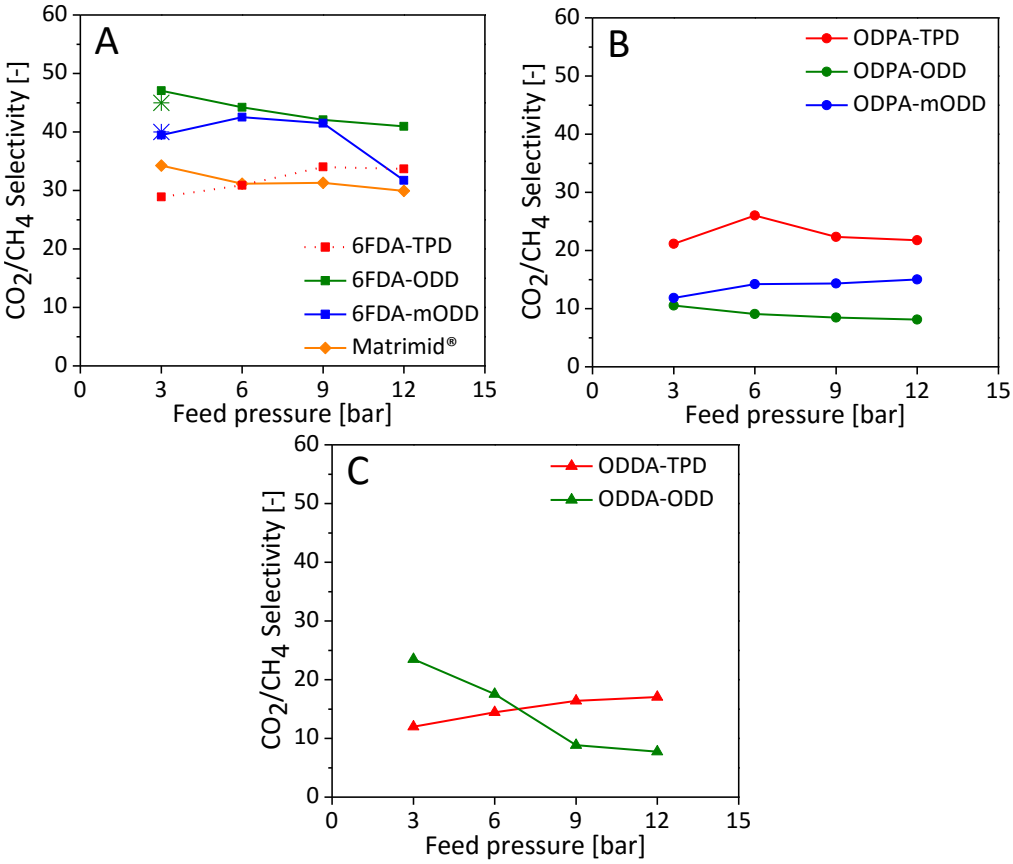

Figure 5.9. CO_2/CH_4 selectivity as a function of feed pressure. **A**- Matrimid® and 6FDA-series (star symbols represent reference values for small membranes 6FDA-ODD (green) and 6-FDA-mODD (blue)), **B**- ODPA-series and **C**- ODDA-based membrane series. Feed mixed gas: CO_2/CH_4 (50/50 vol.%). 6FDA-TPD is measured with a smaller membrane area of 1 cm^2 vs 4 cm^2 for all other membranes.

Both 6FDA-ODD and 6FDA-mODD membranes display very desirable selectivity values, both are higher than that of Matrimid® (Figure 5.9A). The

highest values are observed for 6FDA-ODD with a CO_2/CH_4 selectivity of 47 at 3 bar of mixed feed; it decreases steadily to 40 at 12 bar. At the feed pressure of 3 bar, 6FDA-ODD is 40% more selective than Matrimid®. 6FDA-ODD and Matrimid® show a slight downward slope indicating imminent plasticization pressure around 12 bar or higher. The shape of the 6FDA-mODD curve suggests plasticization behavior, with the pressure of plasticization being at 9 bar. From that point on the selectivity drops as the permeability for both gases increases. The optimum pressure for the application of 6FDA-mODD as a gas separating membrane is around 6 bar, where it shows P_{CO2} of 3.5 Barrer and CO_2/CH_4 selectivity of 43. In terms of separating ability, 6FDA-TPD membrane is comparable to Matrimid® with stable values for selectivity around 30 throughout the whole pressure range.

Unlike the ODPA-based PEIs as reported in Chapter 2, which exhibit selectivities between 50 and 70, these 3 ODPA-based membranes show unusually low selectivities for PI membranes. ODPA-TPD is two times more selective than its oxadiazole containing counterparts, but these values are still only around 20 for the entire pressure range. On the other hand, ODDA-TPD displays interesting behavior in terms of maintaining permeability with increasing selectivity upon an increase in feed pressure. Unfortunately, the selectivity values are as low as 21 to 26 and further investigation of this membrane would not be of any interest. A sudden drop in selectivity for ODDA-ODD is in line with the approaching plasticization pressure announced by a drop in P_{CO2} (Figure 5.8C).

5.6 Conclusions

We have designed, synthesized and characterized a new series polyimides (PIs) with the aim to understand how backbone geometry and the presence of (local) electrostatic dipole moments govern gas transport properties in this promising class of membranes. All PIs synthesized exhibit high glass transition temperatures (T_g > 270 °C), high thermal stability ($T_{5\%}$ > 450 °C) and excellent mechanical properties (E' ~ 4 GPa at 30 °C). All 6FDA-based membranes showed high CO_2 permeability values, ranging from 4 to 30 Barrer. The best performing membrane of the series is 6FDA-TPD. Compared to other two 6FDA-based membranes, at 3 bar of mixed feed 6FDA-TPD has a CO_2 permeability of 30 Barrer, which is almost 2 × that of 6FDA-ODD, 8 × that of 6FDA-mODD and 6 × that of commercially available Matrimid®. With respect

to selectivity, 6FDA-TPD is still comparable to Matrimid®, demonstrating values of around 30 throughout the applied pressure range. The optimum pressure for the application of 6FDA-TPD and 6FDA-ODD as a gas separating membranes would be between 3 and 6 bar, where they shows P_{CO2} of 33 and 15 Barrer respectively, and CO_2/CH_4 selectivity of 31 and 44 respectively. With respect to permeability and selectivity, 6FDA-ODD and Matrimid® demonstrate parallel behavior. Still, 6FDA-ODD is 3 × more effective than Matrimid® at selectively permeating CO_2 while also maintaining 40% higher separating selectivity with increasing feed pressure. Unlike single gas permeation experiments, our mixed feed tests unequivocally demonstrate that our membranes are able to operate using a 50/50 vol.% CO_2/CH_4 feed. As anticipated, introducing the 6FDA dianhydride moiety appears to be beneficial for gas separation performance and important design rules can be extracted regarding the effect of the diamine structure. When paired with 6FDA, both kinked TPD and ODD monomers are superior in permeability in comparison to mODD, which adopts a more linear geometry when incorporated into the PI backbone. However, when we contrast the selectivity performance of the polar 1,3,4-oxadiazole PI series (ODD and mODD) with the non-polar *m*-terphenyl (TPD) PI series, we can conclude that the strong dipole moment associated with the 1,3,4-oxadiazole heterocycle (3D) governs the high selectivity in the ODD- and mODD-based PI series. Therefore, in terms of permeability, we found that the backbone geometry dominates, whereas the presence of an electrostatic dipole moment governs selectivity. Even though telltale signs of plasticization are observed in some of the membranes, none of the membranes display the typical plasticization behavior up to 12 bar of mixed feed.

5.7 Appendix A: GPC curves

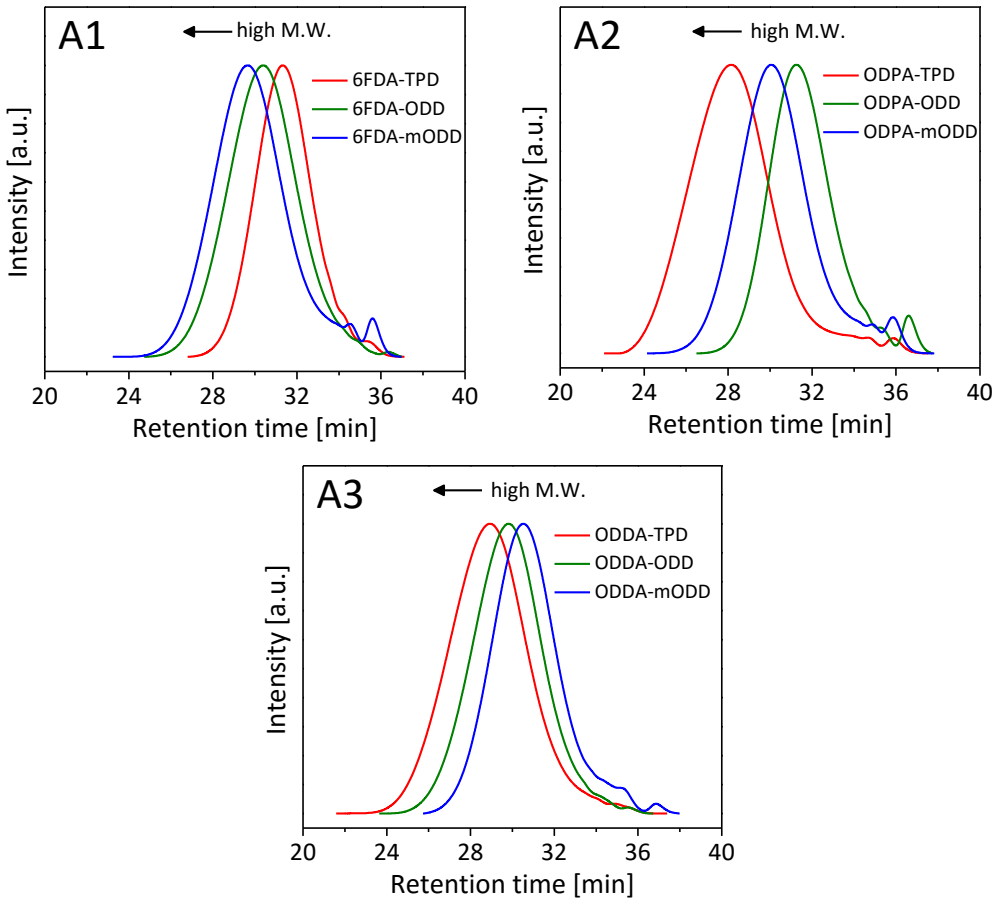

Figure A. GPC curves obtained for polyamic acid intermediates. **A1**- 6FDA-series, **A2**- ODPA-series and **A3**- ODDA-based series. The removal of any possible solids in the polyamic acids, prior to a GPC run, is done by filtration of the polyamic solution through a 0.45 μm PTFE filter.

5.8 References

[1] L. M. Robeson, *J. Membr. Sci.* **1991**, *62*, 165.

[2] L. M. Robeson, *J. Membr. Sci.* **2008**, *320*, 390.

[3] S. M. Allen, M. Fujii, V. Stannett, H. B. Hopfenberg, J. L. Williams, *J. Membr. Sci.* **1977**, *2*, 153.

[4] T. C. Merkel, V. I. Bondar, K. Nagai, B. D. Freeman, I. Pinnau, *J. Polym. Sci. Part B Polym. Phys.* **2000**, *38*, 415.

[5] Y. Yampolskii, *Macromolecules* **2012**, *45*, 3298.

[6] D. Ayala, *J. Membr. Sci.* **2003**, *215*, 61.

[7] B. D. Freeman, *Macromolecules* **1999**, *32*, 375.

[8] S. A. Stern, *J. Membr. Sci.* **1994**, *94*, 1.

[9] M. R. Coleman, W. J. Koros, *J. Membr. Sci.* **1990**, *50*, 285.

[10] M. Calle, A. E. Lozano, J. de Abajo, J. G. de la Campa, C. Álvarez, *J. Membr. Sci.* **2010**, *365*, 145.

[11] P. M. Budd, N. B. McKeown, D. Fritsch, Y. Yampolskii, V. Shantarovich, Chapter 2 in: Y. Yampolskii, B. D. Freeman (Eds.), *Membrane Gas Separation*, John Wiley & Sons, Chichester, UK, **2010**, 29.

[12] M. Cecopieri-Gomez, J. Palacios-Alquisira, J. Dominguez, *J. Membr. Sci.* **2007**, *293*, 53.

[13] D. F. Sanders, Z. P. Smith, R. Guo, L. M. Robeson, J. E. McGrath, D. R. Paul, B. D. Freeman, *Polymer* **2013**, *54*, 4729.

[14] C.-J. Chang, R.-L. Chou, Y.-C. Lin, B.-J. Liang, J.-J. Chen, *Thin Solid Films* **2011**, *519*, 5013.

[15] S. K. Sen, B. Dasgupta, S. Banerjee, *J. Membr. Sci.* **2009**, *343*, 97.

[16] J. R. Fried, N. Hu, *Polymer* **2003**, *44*, 4363.

[17] H. B. Park, C. H. Jung, Y. M. Lee, A. J. Hill, S. J. Pas, S. T. Mudie, E. Van Wagner, B. D. Freeman, D. J. Cookson, *Science* **2007**, *318*, 254.

[18] R. W. Baker, B. T. Low, *Macromolecules* **2014**, *47*, 6999.

[19] D. F. Sanders, Z. P. Smith, C. P. Ribeiro, R. Guo, B. D. Freeman, D. R. Paul, J. E. McGrath, S. Swinnea, *J. Membr. Sci.* **2012**, *415–416*, 558.

[20] Y. Jiang, F. T. Willmore, D. Sanders, Z. P. Smith, C. P. Ribeiro, C. M. Doherty, A. Thornton, A. J. Hill, B. D. Freeman, I. C. Sanchez, *Polymer* **2011**, *52*, 2244.

[21] M. Lehmann, J. Seltmann, A. A. Auer, E. Prochnow, U. Benedikt, *J. Mater. Chem.* **2009**, *19*, 1978.

[22] M. Dabiri, P. Salehi, M. Baghbanzadeh, M. Bahramnejad, *Tetrahedron Lett.* **2006**, *47*, 6983.

[23] D. J. Sinclair, M. S. Sherburn, *J. Org. Chem.* **2005**, *70*, 3730.

[24] G. Palaniswamy, F. Hannour, T. J. Dingemans, R. Bouwer, Patent number WO2014 000850 A1, **2014**.

[25] T. J. Dingemans, E. Mendes, J. J. Hinkley, E. S. Weiser, T. L. StClair, *Macromolecules* **2008**, *41*, 2474.

[26] M. Grucela-Zajac, M. Filapek, L. Skorka, K. Bijak, K. Smolarek, S. Mackowski, E. Schab-Balcerzak, *Synth. Met.* **2014**, *188*, 161.

[27] Y. Mansoori, M. Ghanbari, *Polym. Adv. Technol.* **2015**, *26*, 658.

[28] Z. P. Smith, D. F. Sanders, C. P. Ribeiro, R. Guo, B. D. Freeman, D. R. Paul, J. E. McGrath, S. Swinnea, *J. Membr. Sci.* **2012**, *415–416*, 558.

[29] M. Ding, *Prog. Polym. Sci.* **2007**, *32*, 623.

[30] S.-H. Hsiao, G.-S. Liou, S.-H. Chen, *J. Polym. Sci. Part A Polym. Chem.* **1998**, *36*, 1657.

CHAPTER 6

Free volume in oxadiazole-based polyimides measured by positron annihilation Doppler broadening (PADB)

Positron annihilation Doppler broadening (PADB) was used to characterize the free volume of novel non-linear "boomerang-shaped" all-aromatic PI membranes. Membranes based on ODPA- and ODDA-dianhydrides exhibit the lowest *S* parameter, whereas the 6FDA-based samples all lie on the higher *S* side of the *S*-*W* plot, with 6FDA-TPD really standing out. The combination of a low *W*-parameter and high *S*-parameter indicates that the highest free volume content in the series is observed for 6FDA-TPD. Incorporating diamines based on 2,5-substituted oxadiazole heterocycles in the PI backbone increases the free volume when compared to the ether-linked 3-ring diamines discussed in previous chapters (P1, M1 and O1). However, the largest increase in free volume comes from TPD, a 3-ring *meta*-substituted diamine with an exocyclic bond angle of 120°. Our results show that on an *S*-*W* map this polymer series tend to group according to their dianhydride as well as their diamine moieties. The trend in free volume was confirmed using permeability studies and we confirmed again that PADB is an excellent tool for assessing the free volume characteristics of PI-based membranes.

6.1 Introduction

In Chapter 5 we presented a novel series of polyimides with a non-linear backbone design and either polar or non-polar aromatic moieties. With this series, shown in part in Figure 6.1, we studied the effects of chain linearity (effect on polymer morphology) and how the presence or absence of strong lateral electrostatic dipoles affects the gas separation performance. In this Chapter we will investigate the free volume characteristics of 6 non-linear PIs using PADB. We used PIs based on polar 2,5-bis(4-aminophenyl)-1,3,4-oxadiazole (ODD) and its non-polar analog 4,4''-diamino-*m*-terphenyl (TPD). Both diamines are *para*-substituted with respect to the central ring, and ODD brings a strong lateral dipole moment of 3 Debye with its central oxadiazole ring. Changing the exocyclic bond angle in these 3-ring diamines, from 134° for ODD to 120° for TPD subtly modifies the (non-polar) geometry to a more bent or kinked conformation, which is likely to increase the free volume in the polymers.

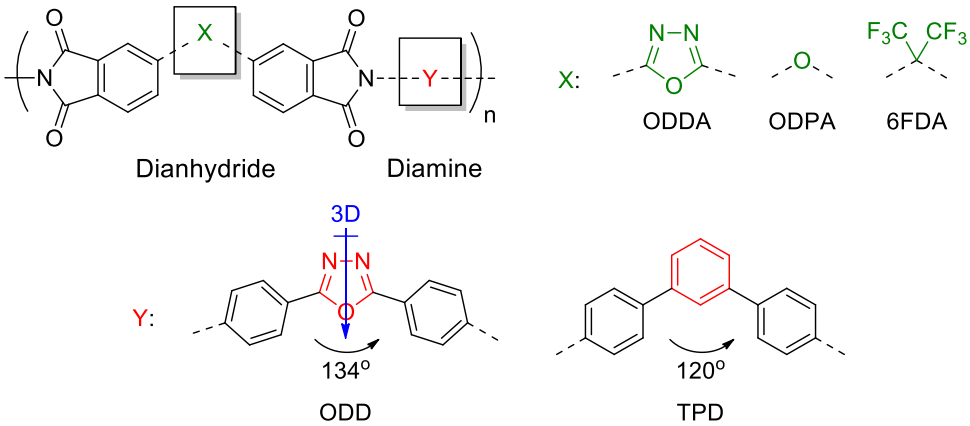

Figure 6.1. Chemical structures of the non-linear polyimides. Structures of the dianhydrides are in green. The core structures of diamines are in red, with the oxadiazole core having an exocyclic bond angle of 134° whereas the terphenyl diamine has an exocyclic bond angle of 120°. The oxadiazole core in ODD has a transverse dipole moment of 3 Debye. TPD is non-polar.

With respect to the dianhydrides, we have selected 2,2'-bis(3,4-carboxylphenyl)hexafluoropropane dianhydride (6FDA) as a well-known dianhydride with excellent gas separation performance. 6FDA is a rather stiff monomer, its -CF_3 groups inhibit rotations thereby increasing rigidity and free volume. Furthermore, we investigate 3,3',4,4'-oxydiphthalic dianhydride

(ODPA), which has shown promising membrane performance in the previous series (see Chapters 2 through 4). Contrary to 6FDA, ODPA has flexible ether bridge and is expected to have a lower free volume content. In previous measurements (Chapter 3) ODPA-based PEIs, specifically ODPA-P1, exhibited the highest *S* parameter values in that series making it an interesting monomer for further studies. We have synthesized 4,4'-(1,3,4-oxadiazole-2,5-diyl)diphthalic anhydride (ODDA), in order to learn more about non-linear PIs with two strong lateral dipole moments in the polymer backbone (ODDA-ODD). A Matrimid® membrane was used as a reference material. The thermal and mechanical properties of this series are summarized in Table 6.1.

Table 6.1. Thermal and mechanical properties of the non-linear polyimides as reported in Chapter 5.

Polymer	DSC[a]	DMTA[a]	
	T_g (°C)[b] DSC	T_g (°C)[c] DMTA	*E'* (GPa, 30 °C)
6FDA-TPD	338	336	3.5
6FDA-ODD	356	352	4.7
ODPA-TPD	311	310	4.9
ODPA-ODD	-	276	4.3
ODDA-TPD	-	335	4.4
ODDA-ODD	-	320	4.2

[a] DSC (first heating) and DMTA data were collected using a heating rate of 20 and 2.5 °C/min, respectively. [b] T_g is reported at the inflection point. [c] T_g is determined at the maximum of the loss modulus (E").

In Chapter 5 we have shown how the inclusion of the 6FDA dianhydride disrupts chain packing of the polyimides and yields higher free volume content and CO_2 diffusivity, in fact, the highest within the series. We also observed that the kink in the polymer backbone structure, which we varied with 3-ring boomerang-shaped diamines, had a significant effect in terms of CO_2 permeability. Based on these observations we decided that we needed to further explore the free volume characteristics of these membranes.

The two most frequently used techniques to probe open volume defects in materials are positron annihilation Doppler broadening (PADB) and positron annihilation lifetime spectroscopy (PALS).[1–6] In Chapter 3 the reader can find an in-depth description of the free volume in polymer membranes and how both techniques can be used. Moreover, Chapter 3 establishes that we were able

to successfully correlate findings from PADB to PALS. We showed that there is a correlation between the *S* parameter obtained by PADB and the o-Ps fraction determined by PALS, which is in line with what has been reported by other research groups.[7,8]

Generally, PALS requires bulk polymer to surround the positron annihilation source with enough material (Chapter 3, Figure 3.4) in order to ensure that a minimum of 93% of positrons from the source annihilate within the sample.[3,6,9] For our measurements at the Charles University in Prague, this measurement requirement amounted to approximately 0.6 mm thick stacks of polymer on each side of the positron annihilation source. This meant that a defect-free membrane surface of approximately 120 cm^2 was needed. This can be presented as a major drawback of the PALS technique, as high quality films are not always available.

On the other hand, PADB suffers from a lack of exposure in the field of polymeric materials. PADB is a very valuable and recognized tool for analyzing metals and ceramics [10–12], while not so often used for polymer characterization. It is a tool for characterizing defects at different depths from the surface, observing defect evolution, monitoring damaging processes such as corrosion *et cetera*.[10,12,13]

Now, in the field of polymers, the story changes, PADB gives way to PALS as the preferred method for characterization of voids.[14–16] Even though the importance of characterizing the free volume in membranes is understood, there seems to be a discrepancy between the need for these measurements and their occurrence in published research. We aim to demonstrate that PADB is a technique suitable for a quick initial assessment of the difference in free volume between related polymer membranes.

Our previous findings, specifically the performance of ODPA-P1 (Chapters 2 and 3), inspired us to further investigate the role of free volume in PEI-based membrane materials. We chose to look into more detail at how bulky groups and heterocyclic building blocks affect the free volume and thus the gas transport properties (Chapter 5). With the 6FDA-TPD membrane outperforming commercial membrane Matrimid® with 600% higher CO_2 permeability, it was clear we needed to characterize the free volume of this membrane series.

As discussed in Chapter 3 (Figures 3.6 and 3.7) there is a correlation between the *S* parameter and the radius of the free volume elements. To this end we have extended the use of PADB towards the analysis of our novel series non-linear 'boomerang-shaped' polyimides. This series allows us to control the geometry and to systematically tailor the segmental mobility and steric hindrance induced by pendant groups, thereby changing the non-equilibrium free volume in the polyimides. In this Chapter we will discuss the PADB-measured free volume characteristics of this membrane series in relation to their gas separation properties.

6.2 Experimental

6.2.1 Materials

We have synthesized a series of 6 polyimides with systematic backbone modifications and we have prepared a Matrimid® film as a reference membrane material. Their synthesis and properties are introduced and described in detail in the previous chapter (Chapter 5).

6.2.2 PADB measurements

PADB experiments were performed with the Delft Variable Energy Positron beam (VEP). Positrons emitted from a radioactive ^{22}Na source are, after moderation to thermal energies and subsequent acceleration, injected in the PI films with a kinetic energy ranging from 100 eV to 25 keV. The beam intensity is about 10^4 positrons per second and the beam diameter at target is about 8 mm.

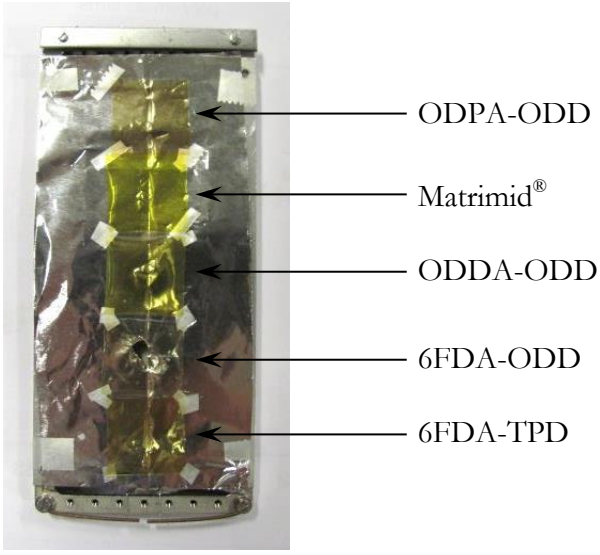

Figure 6.2. Sample holder with 5 PI membranes.

The *S* parameter was calculated as the ratio of the counts registered in a fixed central momentum window ($|p_{//}| < 3.5\times10^{-3}$ m_oc) to the total number of counts in the photo peak. This choice of the momentum window makes the *S* parameter sensitive to annihilations with low momentum valence electrons or as p-Ps. Similarly, the *W* parameter is obtained from the high momentum regions (W_{left} and W_{right}) (10×10^{-3} $m_oc < |p_{//}| < 26\times10^{-3}$ m_oc) and accounts for annihilations with high momentum core electrons. The energy resolution of the detector setup is 1.2 keV at 511 keV. All PADB measurements were performed at 25 °C.

All membranes were cut into single square sheets of 20 × 20 × 0.03 mm and mounted on a sample holder (shown in Figure 6.2) which was then placed in the chamber. Five different samples were mounted each time, only two separate runs were required for measuring all 7 samples.

6.3 Results

PADB measurements on our 7 polyimide films were performed with the Delft Variable Energy Positron beam. After analysis, data are presented in an *S*-*W* map as shown in Figure 6.3.

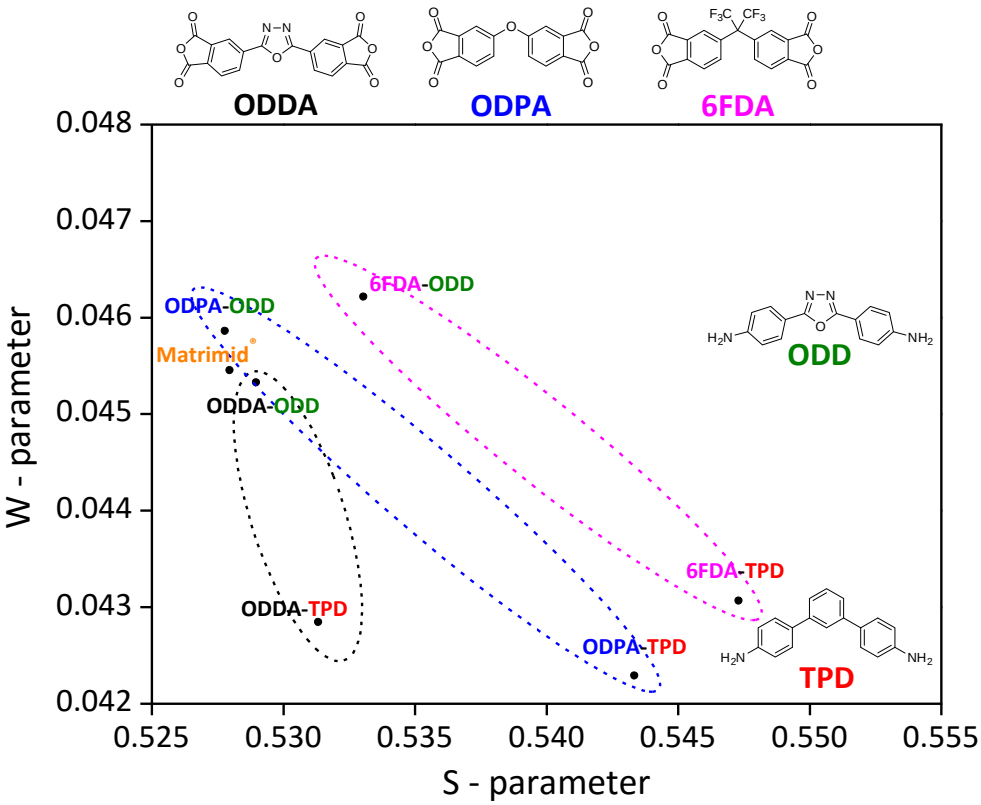

Figure 6.3. *S-W* plot constructed from PADB measurements showing the Doppler broadening parameters of all 7 polyimide film samples. For sake of clarity, the ODDA-based samples are shown within a black ellipse, the ODPA-based samples within a blue ellipse and 6FDA-based samples within a pink ellipse.

The *S* parameter was calculated as the ratio of the counts registered in a fixed central momentum window to the total number of counts in the photo peak. This choice of the momentum window makes the *S* parameter sensitive to annihilations with low momentum valence electrons or as p-Ps. The *W* parameter is obtained from the high momentum regions and accounts for annihilations with high momentum core electrons.

In work by Sato *et al.* [7] a linear relation between the *S* parameter and o-Ps fraction was found both for the low-momentum range of valence electron contributions, as described by the *S* parameter, as well as the high-momentum range of core electron contributions, as described by the *W* parameter. We observed the same in our work presented in Chapter 3. Since positron annihilation in open volumes typically leads to a decrease in *W* and an increase

in *S* parameter, we can expect a polymer with a higher free volume content to reside on the lower right quadrant of the *S*-*W* map.[17]

From the data, it is immediately obvious that the *W* parameters of the TPD-based polymers are the lowest of the series, *W* (ODD) > *W* (TPD). The *W* parameter values of around 0.043 for these three polymers are even significantly lower than for the entire PEI series discussed in Chapter 3. Since this parameter is sensitive to annihilations with the high momentum core electrons of elements (as opposed to valence electrons), it is higher for a defect-free material and lower for more open volumes. Considering only the *W* parameter it is clear that the major differentiator is the core of the 3-ring boomerang-shaped diamine moiety. The oxadiazole core giving higher *W* values vs. the 1,3-phenyl core, which gives lower *W* values. Decreased values of *W* parameter indicate open volumes, which corresponds well to our findings presented in Chapter 5. There, we observed higher CO_2 gas permeabilities every time a TPD diamine replaced an oxadiazole-based diamine. This is very interesting, but to gain a better understanding of the free volume of these materials we will focus our discussion on interpreting the *S* parameter values.

Within our series, the 6FDA-TPD membrane really stands out. In terms of gas transport properties, this membrane showed the highest CO_2 permeability of the entire series and, as expected, this membrane showed the highest *S* parameter value, indicating the increased free volume, confirming the highest free volume within the series.

Looking at the diamine moiety, the trend in *S* values is TPD > ODD, meaning that by substituting the central oxadiazole ring for a 1,3-phenyl ring in the 6FDA-based series results in a significant free volume increase (S = 0.533 to S = 0.547, which correlates to an increase in the void radius from 2 to ~ 4.5 Å, see Figure 6.4). Introducing non-linear, or boomerang-shaped, 3-ring diamines increases the free volume when compared to the ether-linked 3-ring diamine monomers as discussed in the previous chapters (P1, M1 and O1). The exocyclic bond angle in these 3-ring diamines changes from 134° for ODD to 120° for TPD thereby creating a more prominent kink in the backbone, which frustrates the chain-chain packing preferences and results in high T_g amorphous PIs with increased free volume and a high selectivity. An increase in free volume makes for a more permeable membrane.

When observing the differences in free volume brought on by the change in the dianhydride moiety, the resulting *S* parameter values follow the sequence: 6FDA>ODPA>ODDA. Because a high *S* value is associated with a narrow momentum distribution (i.e. low momentum annihilations either via direct annihilation with valence electrons or through p-Ps decay) this sequence can be interpreted as reflecting an increase in free volume, either by size, free bond rotation (ODPA) or both (6FDA).

In Chapter 3 we have successfully linked findings from PADB to PALS. We showed that there is a correlation between the *S* parameter obtained by PADB and the o-Ps fraction determined by PALS. Certainly, we have used a small data set, yet we believe we have created a database that can be the basis for an initial assessment and for molecular modelling efforts. However, the latter is outside the scope of this thesis.

Based on two PADB *S*-*W* maps, the first one presented in Chapter 3 (Figure 3.6) and the second one being Figure 6.3, we can say that the end-point of the *S*-*W* map in Figure 3.6 corresponds to the starting point of the *S*-*W* map in Figure 6.3. Specifically, values for the *S* and *W* parameters of ODPA-O1 (Figure 3.6) match those of ODPA-ODD (Figure 6.3). Consequently, we expect the void size of this entire PI series to be higher than that of the previously investigated PEI series.

As a result of the extensive PADB study performed on both the PEI and PI series, as reported in this thesis, we combined all data from both *S*-*W* maps in Figure 6.4. The Doppler broadening parameters of all 19 PEI and PI film samples reported in this thesis are plotted and grouped by dianhydride moiety for sake of clarity.

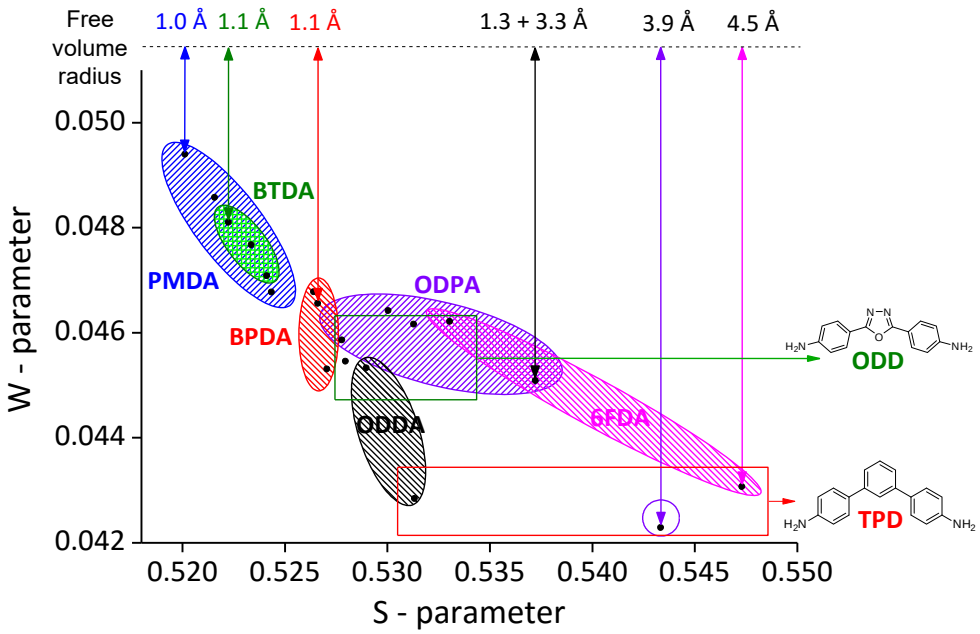

Figure 6.4. Summarized *S*-*W* plot constructed from all 19 PEI and PI film samples as reported in this thesis. For sake of clarity, samples based on the same dianhydride are shown within an ellipse, with the PMDA-series in blue, the BTDA-series in green, the BPDA-series in red, the ODPA-series in purple, the ODDA-series in black and the 6FDA-series in pink. Data points associated with the ODD-series occupy the green rectangle, whereas all data points associated with the TPD-series are captured within the red rectangle. The free volume, as represented by the PADB *S* parameter (quantified by PALS for 4 samples – Chapter 3) was extrapolated in order to predict the R_2 value of the free volume radius for the ODPA-TPD and 6FDA-TPD samples.

Based on the PALS method, ODPA-P1 was the only material in the PEI series with a free volume that could be described by both smaller and larger free volume elements, the smaller ones being R_1 = 1.3 Å and the larger ones being R_2 = 3.3 Å. With this in mind it is fair to state that the free volume voids of ODPA-TPD and 6FDA-TPD have radii above 3 Å. Since this cannot be quantified using PADB experiments alone, data was estimated by a linear fit of radii (obtained by PALS experiments of the P1, M1 and O1 PEI series) as a function of the *S* parameter, given in the Appendix. Values for radii of ODPA-TPD and 6FDA-TPD were obtained by extrapolation. In case of ODPA-P1 the larger void radius, R_2, was used (Table 3.1).

The effect of introducing a TPD moiety in the PI backbone is quite pronounced in ODPA-based series. The extrapolated free volume radius of 3.9 Å is larger than for all other ODPA-based samples, which most likely originates from the TPD moiety, nonetheless it is still in the range observed by others for ODPA-based PIs.[18,19] For example, Bas *et al.* observed radii of 2.75 Å for ODPA-based polyimides and copolyimides.[18] The same can be said for 6FDA-TPD, which has a cavity radius of 4.5 Å and is our best performing membrane with the highest free volume content. The extrapolated free volume is slightly higher than observed by others who explored similar, but more simple, PI/PEI backbones based on 6FDA.[18,20] In work by Askari *et al.* [20] 6FDA-based copolyimides have radii of 3.6-3.8 Å.

6.4 Conclusions

We have investigated the free volume of new series non-linear, boomerang-shaped, all-aromatic polyimides using positron annihilation (PADB). The major differentiator is the core of the 3-ring boomerang-shaped diamine moiety, with the 2,5-oxadiazole core having higher *W* value and the 1,3-phenyl core having lower *W* value. Lower values for the *W* parameter indicate open volumes, which in turn corresponds to higher CO_2 gas permeabilities. The *W* parameters of TPD-based polymers were the lowest of the series, which is in agreement with the CO_2 gas permeability as measured for this series (Chapter 5). The *W* parameter follows the trend: ODD>TPD. Based on the diamine moiety, the *S* parameter follows the trend: TPD>ODD, which correlates to the trend for the *W* parameter. Looking at the dianhydride moiety, the *S* parameter follows the trend 6FDA>ODPA>ODDA. This sequence can be interpreted as an increase in free volume. CF_3 groups from 6FDA inhibit chain rotations, therefore, the rigidity and free volume, as well as permeability are increased.

PADB proved to be a fast and convenient method to assess the differences in free volume of all-aromatic PI-and PEI-based membranes. The *S* parameter is sensitive to open volume defects and the *W* parameter is sensitive to the chemical surrounding at the annihilation site. In Chapter 3 we established that there is a correlation between the *S* parameter obtained by PADB and the o-Ps fraction determined by PALS. Based on these findings, we concluded that PADB can be used to qualitatively assess differences in free volume content of PI- and PEI- based membranes whereas PALS is a better choice for quantifying the free volume. We believe that the work presented in this chapter makes a

strong case for using PADB as an initial and fast exploratory technique for probing the free volume of PI/PEI-based membranes. We also believe that PADB can be extended to other polymer-based membranes.

6.5 Appendix: Extrapolation

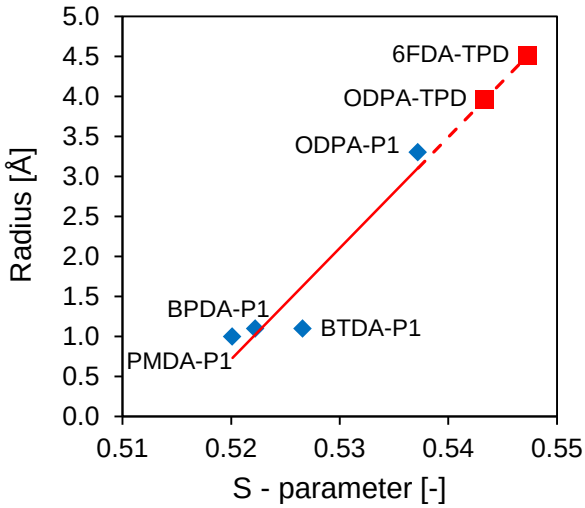

Figure A. Estimation of radii for ODPA-TPD and 6FDA-TPD based on the linear extrapolation of P1-based data and *S* parameter of said two samples. Blue markers signify the experimental data from P1-based series, while the red markers represent the estimated radii based on *S* parameter for ODPA-TPD and 6FDA-TPD. Linear fit was used as follows: $R^2 = 0.894$, $Radius = 138.88 \times (S\ \text{parameter}) - 71.504$.

6.6 References

[1] B. W. Rowe, S. J. Pas, A. J. Hill, R. Suzuki, B. D. Freeman, D. R. Paul, *Polymer* **2009**, *50*, 6149.

[2] M. Calle, C. M. Doherty, A. J. Hill, Y. M. Lee, *Macromolecules* **2013**, *46*, 8179.

[3] R. Zhang, J. Robles, J. Kang, H. Samha, H. M. Chen, Y. C. Jean, *Macromolecules* **2012**, *45*, 2434.

[4] C. A. Quarles, J. R. Klaehn, E. S. Peterson, J. M. Urban-Klaehn, *AIP Conf. Proc.* **2011**, *1336*, 513.

[5] G. C. Eastmond, J. H. Daly, A. S. McKinnon, R. A. Pethrick, *Polymer* **1999**, *40*, 3605.

[6] W. Xie, H. Ju, G. M. Geise, B. D. Freeman, J. I. Mardel, A. J. Hill, J. E. McGrath, *Macromolecules* **2011**, *44*, 4428.

[7] K. Sato, K. Ito, K. Hirata, R. S. Yu, Y. Kobayashi, *Radiat. Phys. Chem.* **2007**, *76*, 112.

[8] G. Choudalakis, A. D. Gotsis, H. Schut, S. J. Picken, *Eur. Polym. J.* **2011**, *47*, 264.

[9] Y. Yampolskii, V. Shantarovich, *Positron Annihilation Lifetime Spectroscopy and Other Methods for Free Volume Evaluation in Polymers*, in: Y. Yampolskii, I. Pinnau, B.D. Freeman (Eds.), *Materials Science of Membranes for Gas and Vapor Separation*, John Wiley & Sons, Chichester, UK, **2006**, 191.

[10] M. L. Ruiz-Ripoll, H. Schut, N. H. Van Dijk, R. C. Alderliesten, S. Van Der Zwaag, R. Benedictus, *J. Phys. Conf. Ser.* **2011**, *262*, 12052.

[11] R. I. Grynszpan, W. Anwand, G. Brauer, P. G. Coleman, *Ann. Chim. Sci. des Matériaux* **2007**, *32*, 365.

[12] Y. C. Wu, T. Zhai, P. G. Coleman, *Metall. Mater. Trans. A* **2012**, *43*, 2823.

[13] I. Prochazka, J. Cizek, O. Melikhova, T. E. Konstantinova, I. A. Danilenko, I. A. Yashchishyn, *J. Am. Ceram. Soc.* **2014**, *97*, 982.

[14] A. J. Hill, B. D. Freeman, M. Jaffe, T. C. Merkel, I. Pinnau, *J. Mol. Struct.* **2005**, *739*, 173.

[15] G. Dlubek, F. Borner, R. Buchhold, K. Sahre, R. Krause-Rehberg, K.-J. Eichhorn, *J. Polym. Sci. Part B Polym. Phys.* **2000**, *38*, 3062.

[16] V. P. Shantarovich, T. Suzuki, C. He, V. W. Gustov, *Radiat. Phys. Chem.* **2003**, *67*, 15.

[17] Y. C. Jean, P. E. Mallon, D. M. Schrader, (Eds.), *Principles and Applications of Positron and Positronium Chemistry*, World Scientific, Singapore, **2003**, 236.

[18] C. Bas, C. Bernard, C. Dauwe, *J. Membr. Sci.* **2010**, *349*, 25.

[19] R. A. Pethrick, F. Santamaria-Mendia, *J. Polym. Sci. Part B Polym. Phys.* **2015**, *53*, 1654.

[20] M. Askari, M. L. Chua, T.-S. Chung, *Ind. Eng. Chem. Res.* **2014**, *53*, 2449.

SUMMARY

Efficient and cost-effective technologies that will enable separation and capture of CO_2 are needed. The development of high-performance all-aromatic poly(ether)imide (P(E)I) membranes is attractive as they offer a large degree of design freedom and they are cheap to operate. However, the molecular design rules towards P(E)I membranes that exhibit high selectivity and high permeability with no or little CO_2 plasticization are still largely unknown. The main objective of the research presented in this thesis is to understand the structure-property relationships of all-aromatic polyimide- and polyetherimide-based gas separation (CO_2/CH_4) membranes. In particular, the role of backbone design and how this affects the free volume and gas separation performance of the final membranes.

In **Chapter 2** a homologous series of 12 PEI membranes is presented, based on 4 different aromatic dianhydrides, *i.e.* ODPA, BPDA, BTDA and PMDA and 3 aromatic *ortho* (O1), *meta* (M1) and *para* (P1) substituted diamines. All membranes were tested using a mixed feed of CO_2/CH_4 at different pressures. Within the ODPA-based series, the CO_2 permeability values decrease in the order P1>O1>M1 and remains steady up to mixed feed pressures of 40 bar. All three M1-based membranes suffer from plasticization. Two from the 12 membranes show promising selectivities: The OPDA-P1 membrane, which also exhibits resistance to plasticization up to 40 bar and the BPDA-O1 membrane.

In order to quantify the free volume of the PEI-based membranes presented in the previous chapter, we employed positron annihilation lifetime spectroscopy (PALS) and positron annihilation Doppler broadening (PADB) and our findings are presented in **Chapter 3**. The semi-crystalline PMDA-based PEI samples exhibit the lowest free volume, whereas the amorphous ODPA-based samples exhibit the highest free volume. ODPA-P1 is notable as this membrane exhibits voids with a radius of ~3.3 Å. The lowest free volume within this series was measured for BPDA-M1, which has voids of 0.7 Å. We also observed a good correlation between the *S* parameter, as determined by PADB, and the free volume content as quantified by PALS.

In **Chapter 4** we described the spectroscopic ellipsometry experiments that were performed to study the sorption of compressed CO_2 and CH_4 in four thin PEI films based on the P1 diamine with ODPA, BPDA, BTDA and PMDA dianhydrides. We observed how the sorption capacity depends to a great extent on the PEI backbone composition. PMDA-P1 shows the highest CO_2 sorption, while ODPA-P1 shows the highest sorption selectivity. This study can serve as a benchmark for further systematic studies on the sorption behavior of glassy PEIs for gas separation applications.

In **Chapter 5** we introduced novel non-linear 3-ring diamines based on a polar 1,3,4-oxadiazole heterocycle (ODD) and a non-polar 1,3-phenylene (TPD) central core. This design allowed us to introduce strong transverse dipole moments (~3 D) and increase the free volume without significant polymer crystallization. Polymer chain packing could be disrupted even further by selecting 6FDA as the corresponding dianhydride. The 6FDA-ODD and 6FDA-TPD membranes showed excellent membrane performance with high P_{CO2} values at all feed pressures, reaching a maximum of 33 Barrer (at 6 bar). In terms of permeability, we found that the backbone geometry dominates, whereas the presence of an electrostatic dipole moment governs selectivity. Up to 12 bar, none of the membranes reached their plasticization pressure, this is an important feature for industrial application.

In **Chapter 6** the PADB free volume characterization of the PI-based membranes, introduced in Chapter 5, will be described. We found that the S, W parameter pairs for these polymers tend to group according to their dianhydride and diamine moiety. On one end, ODPA- and ODDA-based PI samples exhibit the lowest S parameter, while on the other end the 6FDA-based samples exhibit the highest S parameter, which correlates to a higher free volume content. When contrasted with the ether-linked 3-ring monomers (P1, M1 and O1), as discussed in the previous chapters, we demonstrated that non-linear "boomerang-shaped" all-aromatic structures contribute to increasing the free volume of PIs. Our findings on the free volume correlate well with our permeability studies, presented in Chapter 5, where we showed that TPD-based PIs have the highest permeabilities. Again, we'll show that PADB is an excellent tool to assess the free volume characteristics of PI-based membranes.

SAMENVATTING

Efficiënte en kosteneffectieve technologieën zijn nodig om CO_2 gas te scheiden en op te vangen. Het is aantrekkelijk om geheel aromatische poly(ether)imide (P(E)I) membranen te ontwikkelen, omdat deze membranen een grote ontwerpvrijheid hebben en goedkoop zijn in het gebruik. De moleculaire ontwerpregels van P(E)I membranen met een hoge selectiviteit, een hoge permeabiliteit en die geen of weinig last hebben van CO_2 plastisering zijn echter grotendeels onbekend. Het hoofddoel van het onderzoek, zoals gepresenteerd in deze thesis, is inzicht krijgen in de structuureigenschappen van geheel aromatische polyimide- en polyetherimide-gebaseerde (CO_2/CH_4) gasscheidingsmembranen. Speciale nadruk zal worden gelegd op het ontwerpen van de polymeerketen en hoe deze het vrije volume en de gasscheidingseigenschappen beïnvloeden.

In **Hoofdstuk 2** wordt een homologe serie van 12 PEI membranen geïntroduceerd gebaseerd op 4 verschillende dianhydrides, te weten ODPA, BPDA, BTDA and PMDA, en 3 aromatisch *ortho*- (O1), *meta*- (M1) and *para*- (P1) gesubstitueerde diamines. Alle membranen zijn getest met een CO_2/CH_4 gasmengsel bij verschillende partiële drukken. Als we naar de ODPA-gebaseerde serie kijken dan zien we dat de CO_2 permeabiliteit daalt in de volgorde P1 >O1 >M1 en de permeabiliteit stabiel blijft tot een CO_2/CH_4 gasdruk van 40 bar. Alle drie M1-gebaseerde membranen hebben last van CO_2-geïnduceerde plastisering. Twee van de 12 membranen zijn veelbelovend qua selectiviteit; zowel het ODPA-P1 membraan als het BPDA-O1 membraan blijken stabiel te zijn tegen CO_2-geïnduceerde plastisering tot 40 bar.

Om het vrij volume van de PEI-membranen te kwantificeren hebben we Positron Annihilation Lifetime Spectroscopy (PALS) en Positron Annihilation Doppler Broadening (PADB) ingezet. Onze bevindingen presenteren we in **Hoofdstuk 3**. De semi-kristallijne PMDA-gebaseerde PEI- membranen hebben het laagste vrije volume, en de amorfe ODPA-gebaseerde membranen hebben het hoogste vrije volume. ODPA-P1 is opmerkelijk omdat dit membraan volume elementen heeft met een radius van ~3.3 Å. Het laagste vrije volume in

deze serie werd gemeten voor BPDA-M1. Dit membraan heeft volume elementen van ~0.7 Å. Als we naar de PADB en PALS resultaten kijken, dan zien we een hoge correlatie tussen de gemeten *S* parameter (PADB) en het vrije volume (PALS).

In **Hoofdstuk 4** beschrijven we de spectroscopische ellipsometrie experimenten die zijn uitgevoerd om het hogedruk CO_2 en CH_4 sorptie gedrag te meten in 4 dunne PEI-films gebaseerd op ODPA-P1, BPDA-P1, BTDA-P1 en PMDA-P1. De sorptie capaciteit blijkt in grote mate afhankelijk te zijn van de samenstelling van de PEI-polymeerketen. PMDA-P1 laat de hoogste CO_2 sorptie zien, terwijl ODPA-P1 de hoogste sorptie selectiviteit laat zien. Deze studie kan als benchmark dienen voor toekomstige studies naar het sorptie gedrag van glasachtige PEIs voor gasscheidingstoepassingen.

In **Hoofdstuk 5** introduceren we een nieuwe serie niet-lineaire 3-ring diamines welke gebaseerd zijn op polaire heterocyclische 1,3,4-oxadiazolen (ODD) en een apolair 1,3-phenyleen (TPD) monomeer. Met deze monomeren zijn we in staat om sterke dipoolmomenten (~3 D) te introduceren die dwars op de polymeerketen staan en die tegelijkertijd polymeerkristallisatie tegen gaan. Polymeerkristallisatie kan zelfs nog verder verhinderd worden door deze niet-lineaire diamines te polymeriseren met het 6FDA-dianhydride. De 6FDA-ODD en 6FDA-TPD membranen blijken excellente membranen te zijn met hoge P_{CO2}-waarden bij alle test druk waarden, met een maximum van 33 Barrer (bij 6 bar). Als we naar de permeabiliteit van deze serie kijken dan zien we dat de geometrie van de polymeerketen de permeabiliteit bepaald en de aanwezigheid, dan wel afwezigheid, van een dipoolmoment de selectiviteit bepaald. De membranen zijn tot 12 bar getest en geen van deze membranen heeft de plastiseringsdruk bereikt. Dit is een belangrijke eigenschap voor toekomstige industriële toepassingen.

In **Hoofdstuk 6** beschrijven we het vrije volume, bepaald middels PADB, van de PI-gebaseerde membranen die we in Hoofdstuk 5 hebben geïntroduceerd. De *S* en *W* parameters voor deze PIs zijn te groeperen aan de hand van de gebruikte dianhydride en diamine monomeren. Aan één eind van het spectrum zien we ODPA- en ODDA-gebaseerde PI membranen met lage *S* parameter waardes en aan het ander eind zien we 6FDA-gebaseerde membranen met hoge *S* parameter waardes. Een hoge *S* parameter correleert met een hoger vrij volume. Wanneer we de non-lineaire PIs contrasteren met de 3-ring ether diamines (P1, M1 en O1) blijkt dat de non-lineaire "boomrangvormige"

aromatische structuren het vrije volume van de PIs vergroten. Onze bevindingen met betrekking tot het vrije volume correleren goed met de permeabiliteitstudies, zoals gepresenteerd in Hoofdstuk 5, waar we hebben laten zien dat de TPD-gebaseerde PIs de hoogste permeabiliteit hebben. Tenslotte blijkt uit onze resultaten wederom dat PADB een excellente methode is om het vrije volume van PI-gebaseerde membranen te beoordelen.

CURRICULUM VITTAE

Željka Madžarević was born on May 7th 1988 in Belgrade, Serbia. After finishing "Sveti Sava" gymnasium in 2006, she started her Bachelor studies at the University of Belgrade. In 2010 she obtained her Bachelor degree from the Faculty of Technology and Metallurgy with the thesis "*Production of thermoplastic polymer composite materials by pressure molding*". A year later she acquired her Master degree at the same Faculty after defending the thesis titled "*Removal of cationic dye from water solution by adsorption on hydrogel composites based on poly(methacrylic acid) and zeolites*" in July. In October 2011 Željka joined the Novel Aerospace Materials group, Faculty of Aerospace Engineering at the Delft University of Technology under the supervision of prof.dr. Theo Dingemans. Her Ph.D. project was funded by the Dutch Polymer Institute and she collaborated with the Positron Annihilation group (Charles University in Prague), the Membrane Science and Technology research group (University of Twente), Reactor Institute Delft and the Catalysis Engineering group (TU Delft). The results of her Ph.D. research on all-aromatic polyimide membranes are presented in this thesis.

Since September 2016 Željka is employed as a Scientist in Aliancys Quality Resins, focusing on material science in the R&D department in Zwolle.

ACKNOWLEDGEMENTS

"If I have seen further, it is by standing on the shoulders of giants"

Isaac Newton

In the next few pages I will try to summarize the remarkable effects of everybody that has been there, in one way or another, to guide me in this journey and also all those that have lifted me in my personal life. And, since there is a thin line between your dissertation and your personal life when you are a PhD student, those who did both.

Prof.dr. Theo Dingemans gave me the opportunity to begin my PhD journey. **Theo**, first of all thank you for trusting me with this task, believing in me, being committed to this project and sending me around the world to grow. Not only have you stayed true to your plan to *"make a chemist"* out of me you've also made me a better writer, a more critical thinker, a true scientist and a more confident presenter. I am grateful to you for reacting with wisdom and support in my weak moments and giving me a strong hug when celebrating the good moments.

Sybrand van der Zwaag, thank you for accepting me into the NovAM group, or better yet the NovAM family. Thank you for the guidance, support, and for the wonderful Christmas parties. I already miss the fun scientific environment you created within NovAM. Thanks to you, this group has changed my life forever.

I would like to acknowledge Dutch Polymer Institute for the financial support and fruitful interactive meetings and discussions.

I would like to thank my **promotion committee** for contributing to the improvement of this thesis. It is my honour that you agreed to be part of my defence day.

During my PhD research I had the opportunity to collaborate with many great people and research groups. Especially important was the collaboration I had with the Membrane Science and Technology research groups (University of Twente). **Nieck** Bennes, thank you for all the support and inspiration in this research, it was a pleasure working with you, **Wojciech** Ogieglo and **Michiel**

Raaijmakers. **Kitty** Nijmeijer, thank you for allowing me to use the facilities at your group and for the work we did together with **Salman** Shahid.

Generosity of **Jorge** Gascon and **Beatriz** Seoane, from the Catalysis Engineering group (TU Delft), has made it possible for me to do gas separation measurements in Delft. Thank you for our collaboration, your hospitality and giving me access to the permeation setup.

My special gratitude goes to **Henk** Schut from the Reactor Institute Delft for introducing me to the wonderfully complex world of positrons, for his patience in teaching, and for our various discussions. Thank you for introducing me to **Jakub** Čížek and the Positron annihilation group (Charles University in Prague). We have done some amazing work together Jakub, your hospitality and PALS measurements are highly appreciated.

To **Johan** Bijleveld, thank you for stepping up for me so much in the final months, for lending a helping hand with the final experiments, it wouldn't have been possible without you. To **Frans** and **Lijing**, thank you for your readily available help and support. To **Ruud** Hendrikx and **Ben** Norder for their help in characterizing my materials with XRD.

To my TMF colleagues and mentors, to professor **Katarina** Jeremić who is responsible for igniting this whole PhD adventure and my mentor **Sava** Veličković (*in memoriam*) for his advice and constant encouragement.

To my unforgettable NovAM family… thank you! To **Mina**, for working so well with me, for your patience with me, for becoming my friend in less than one month. To **Ranjita**, for being an example of calm and success, for all of our culinary adventures, for teaching me so much. To **Michiel**, for being my brilliant officemate, for all the support, the silly discussions including nail polish, the gossips, our playlist and our memories. I will always remember my first day in Delft, and the first drinks in *Doerak* after the job interview, you said "choose us!" and I did. It was the best decision ever! To **Maruti**, for being the craziest, the original postman, the "just one more beer" guy, the genius, the guru. To **Hongli**, for being a really nice officemate, I am thankful for all your help and our fun conversations. To **Srikanth**, for supporting me, for *still* being my colleague, you are so good at that! To **Wouter** a.k.a. Birdy for being so positive and upbeat, for your koalaty puns, for kastanje, for making the most boring meetings bearable. To **Martino**, for bringing the crazy energy and genuine cheerfulness to our group. To **Kevin**, for all your accents, your contagious

silliness. To **Nora**, for being my first student and for your incredible laugh. To **Daniella** & **Jelmer**, for being inspirational, for being relatable, for your honesty and amazing food. To **Maria**, you *cualquiera*, thank you for becoming my friend, I am grateful for your playfulness, wisdom and accepting attitude. I also wish to thank **Shanta** for all her help, **Casper**, **Hamideh, Wouter P, Arijana, Renee, Qingbao**, **Jimmy**, **Ricardo**, **Jasper**, **Mladen**, **Andert**, **Jie**, **Jesus**, **Marek**, **Ugo**, **Nijesh**, **Jianwei**, **Qi**, **Jason**, **Xiaojun**, **Hussein**, **Nan**, **Antonio**, **Marianella**, **Jibran**, **The Ostriches**, **Christian**, **Paul**, **Jeromy**, **Jeroen**, **Fre**, **Frederick**, **Ruben**, **Bananamen** and the rest of my colleagues for making NovAM, hands down, the best group in the world. I am also grateful for my new friends from TU/e, **Paola** & **Miran**, **Shohreh**, **Michiel** & **Maaike**, **Lara**, **Frans**, **Dulce** and **Emila**.

The Serbian crew: **Dara** & **Sale**, **Laki** & **Danka**, **Ivana** & **Mare**, **Maja** & **Deki**, **Nataša** & **Alex**, **Viki** & **Tobi**, you all made it easy to live here. Having friends like you is more than I could have asked for.

Želim da se zahvalim i svima onima zbog kojih je teško biti u Holandiji… **Vule** i **Vaniću**, hvala vam na savetima, ventilima za izduvavanje i smehu. Mojim TMF drugarima (a posebno **Jassy**, **Anji**, **OHTPI** ekipi), hvala vam što ste i dalje uz mene. Zahvalna sam posebno mojim prijateljicama i kumama, **Bojani** i **Marijani** i mojoj sestri **Nataši**.

Boki, jer je čista duša koja neizmerno voli. Jer odrastamo zajedno već 15 godina, moje duhovno dete i ja, uvek je tu da me sasluša i bude na mojoj strani. **Makici**, jer je najposvećenija osoba koju poznajem. Jer će dati sebe 100% za ljude i povode koji su njoj vredni. I ja se osećam srećnom što sam među njima. **Naletu**, jer znam da na nju mogu da se oslonim u kakvoj god situaciji da se nađem, znam da bi me i iz zatvora izvukla! Jer smo iz godine u godinu sve više slične i sve više bliske, dve veštice kojima je 2000 km razdaljine sitnica.

Takođe sam zahvalna i mojoj rodbini koja je uvek pokazivala interesovanje za ono čime se bavim, čak i ako nekad ne bi sasvim razumeli šta ja to radim. **Jagodi** i **Ceci** što su me srdačno primile u Joviće. **Mladenu**, **Ivanu**, **Bojani**, **Seki** i **Nataši** što uskoče kad god mi treba njihov savet ili pomoć. Baba **Branki** na brizi, ujki **Miši** na podršci u obrazovanju - možda nisam čokolatijer, ali sam doktor nauka koji ume da pravi slatkiše! Za ovih 6 godina u inostranstvu ostala sam bez previše dragih osoba, od kojih mi mnogo nedostaju deda **Miloš**, baba **Rita** i deda **Drago**. Mili moji, znam da me čuvate.

Jedina dva bića koja me vole onoliko dugo koliko već postojim su moji **mama** i **tata**. Hvala vam što me volite, podržavate, tešite i bodrite, srećna sto ste me baš vi vaspitali!

Mama, hvala ti što si me naučila da se pakujem kao da igram Tetris, ali da ako pokušam da se uklopim onda ću nestati u masi, baš kao u tetrisu… Ponosna sam ko sam postala zahvaljujući tvojim životnim lekcijama. Voli te tvoja mrvica.

Tajo, hvala ti na nesebičnoj podršci, na razgovorima do kasno u noć, na savetima, brizi, ljubavi i karamelu! Od tebe sam naučila da budem plemenita i strpljiva, voli te tvoja ćera-sin!

Ova teza je posvećena mom **Boletu**, koji nikada neće prestati da mi nedostaje, da bude sastavni deo moje duše i da me motiviše da budem još bolja.

I najslađe za kraj. **Slaviša**, za vreme ovog doktorata promenio si ulogu iz momka u verenika (*beyoncé*) u muža, a u svakom pojedinačnom trenutku bio si mi najveći oslonac, partner, doktor, motivator i najbolji moj officemate! Beskrajno sam ti zahvalna na razumevanju i ljubavi. Volim te → ∞ *and beyond!*

Sincerely yours / Zauvek vaša,

Željka

Utrecht, June 2017.

LIST OF PUBLICATIONS AND PRESENTATIONS

Journal articles

W. Ogieglo, **Z. P. Madzarevic**, M. J. T. Raaijmakers, T. J. Dingemans, N. E. Benes – High-pressure sorption of carbon dioxide and methane in all-aromatic poly(etherimide)-based membranes, J. Polym. Sci., Part B: Polym. Phys. 54 (2016), 986 – 993.

M. J. T. Raaijmakers, **Z. P. Madzarevic**, W. Ogieglo, E. J. Kappert, T. J. Dingemans, N. E. Benes – In-situ analysis of the thermal imidization of thin film polyamic acids to poly(etherimide)s, *To be submitted.*

Z. P. Madzarevic, S. Shahid, D. C. Nijmeijer, T. J. Dingemans – Systematic changes in the backbone structure of a series poly(etherimide)s and the effects on CO_2/CH_4 gas separation performance, *In preparation.*

Z. P. Madzarevic, H. Schut, J. Cizek, T. J. Dingemans – Free volume in PEI membranes measured by positron annihilation lifetime spectroscopy and positron annihilation Doppler broadening, *To be submitted.*

Z. P. Madzarevic, B. Seoane, H. Schut, J. C. Bijleveld, J. Gascon, T. J. Dingemans – Free volume in oxadiazole-based PI membranes for separating CO_2/CH_4 gas mixtures, *In preparation.*

R. J. Varley, J. Wiggins, **Z. P. Madzarevic**, W. Vogel, M. Marchetti, T. J. Dingemans, B. Dao, S. Tucker, S. Christensen – Reaction Kinetics and Structure Property Relationships of Isomeric Tri-phenyl Ether Linked Diamines Cured with Bisphenol F Epoxy, *In preparation.*

V. V. Panic, **Z. P. Madzarevic**, T. Volkov-Husovic, S. J. Velickovic – Poly(methacrylic acid) based hydrogels as sorbents for removal of cationic dye basic yellow 28: Kinetics, equilibrium study and image analysis, Chem. Eng. J. 217 (2013), 192 – 204.

Selected oral presentations:

Z. P. Madzarevic, H. Schut, B. Seoane, J. Cizek, J. Gascon, T. J. Dingemans, Oxadiazole-based polyimides for separating CO_2/CH_4 gas mixtures, Oral presentation, European Polymer Federation Congress, 2015, Dresden, Germany.

Z. P. Madzarevic, S. Shahid, H. Schut, J. Cizek, K. Nijmeijer, T. J. Dingemans, The role of polyetherimide backbone composition on CO_2/CH_4 gas separation performance, Oral presentation, Dutch Polymer days, 2015, Lunteren, The Netherlands

Z. P. Madzarevic, S. Shahid, H. Schut, J. Cizek, K. Nijmeijer, T. J. Dingemans The role of polyetherimide backbone composition on CO_2/CH_4 gas separation performance, Oral presentation, International Congress on Membranes and Membrane Processes (ICOM), 2014, Suzhou, China